



US Army Corps
of Engineers®
Engineer Research and
Development Center

Environmental Quality and Installations Program

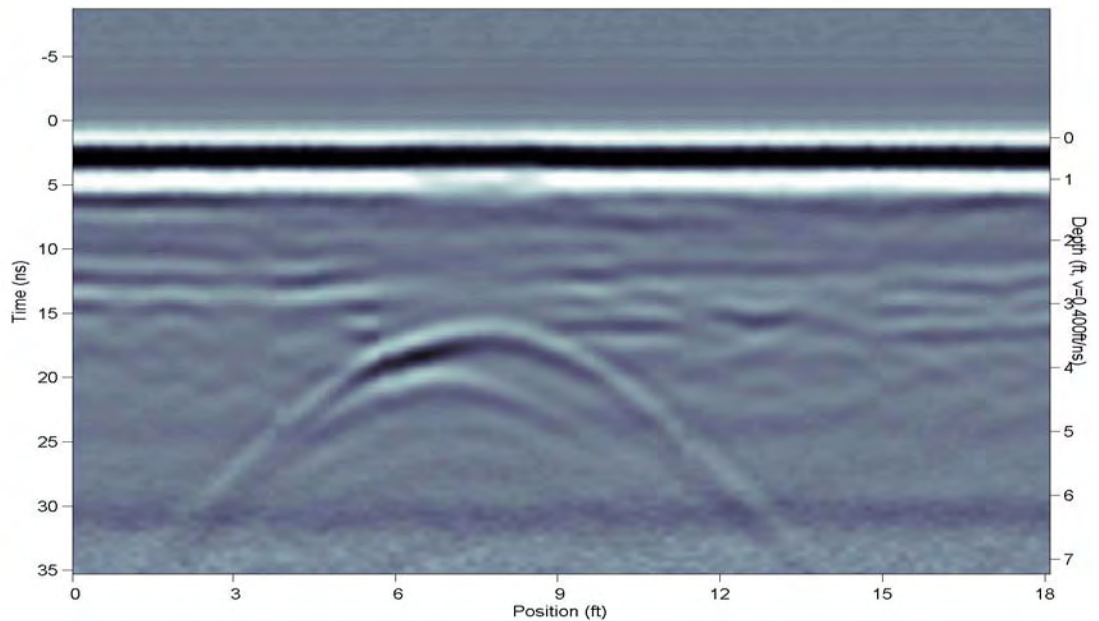
UXO Characterization: Comparing Cued Surveying to Standard Detection and Discrimination Approaches

Report 2 of 9

Ground Penetrating Radar for Unexploded Ordnance Characterization; Fundamentals

Stephen D. Billings and Kevin Kingdon

September 2008



UXO Characterization: Comparing Cued Surveying to Standard Detection and Discrimination Approaches

Report 2 of 9

Ground Penetrating Radar for Unexploded Ordnance Characterization; Fundamentals

Stephen D. Billings and Kevin Kingdon

Sky Research, Inc.

445 Dead Indian Memorial Road

Ashland, OR 97520-9706

Report 2 of 9

Approved for public release; distribution is unlimited.

Prepared for Headquarters, U.S. Army Corps of Engineers
Washington, DC 20314-1000

Monitored by Environmental Laboratory
U.S. Army Engineer Research and Development Center
3909 Halls Ferry Road, Vicksburg, MS 39180-6199

Abstract: The objective of project W912HZ-04-C-0039, “UXO Characterization: Comparison of Cued Surveying to Standard Detection and Standard Discrimination Approaches,” was to research, develop, optimize, and evaluate the efficiencies of different modes of unexploded ordnance (UXO) characterization and remediation as a function of the density of UXO and associated clutter. This report, one of nine written for the project, focused on an overview of the fundamentals of ground penetrating radar (GPR) with specific emphasis on the detection and discrimination potential of the technology. Part A (Chapters 1–6) includes a brief overview of general GPR concepts, data, and survey procedures. Factors that determine the site-specific applicability of GPR are identified and existing tools for assessing the applicability of GPR to a particular site are reviewed. Part B (Chapters 7–10) describes the types of GPR instrumentation and reviews previous UXO and landmine specific work involving GPR.

In both Parts A and B, GPR concepts introduced are discussed and illustrated with data acquired at the Sky Research Ashland (Oregon) test plot using commercial off the shelf (COTS) GPR sensors. In Part A, single GPR profiles over a row of emplaced UXO targets acquired using a single-channel 250-megahertz (MHz) COTS GPR system are displayed. Further examples illustrate how multiple survey lines collected in a grid can be combined to create two-dimensional (2D) and three-dimensional (3D) visualizations of the subsurface and the targets contained therein. In Part B, examination of GPR data collected at the Ashland test site continues, but in this case, focuses on a range of frequencies (250, 500, 1000 MHz) and the comparative information that can be obtained from these respective frequencies. Discussion of the results observed from these initial measurements, limitations of the methods used, and a proposal for use of GPR in a cued-interrogation mode along with the types of information that are obtainable are presented.

DISCLAIMER: The contents of this report are not to be used for advertising, publication, or promotional purposes. Citation of trade names does not constitute an official endorsement or approval of the use of such commercial products. All product names and trademarks cited are the property of their respective owners. The findings of this report are not to be construed as an official Department of the Army position unless so designated by other authorized documents.

DESTROY THIS REPORT WHEN NO LONGER NEEDED. DO NOT RETURN IT TO THE ORIGINATOR.

Contents

Figures and Tables	v
Preface	viii
Unit Conversion Factors	ix
Acronyms	x
General Introduction and Background	xi
1 GPR Basics –Introduction	1
1.1. GPR basics – the data.....	2
1.2. GPR basics – time slice images and 3-dimensional (3D) volumes.....	5
1.3. GPR basics – extending to UXO case.....	7
2 GPR Survey Site Considerations	9
2.1. Determining the applicability of GPR.....	10
2.2. Consulting the GPR suitability map.....	11
2.3. Target depth.....	11
2.4. Target electrical properties.....	11
2.5. GPR resolution.....	12
2.6. Effects of water.....	12
2.7. External factors.....	13
3 Survey Design	15
3.1. Selecting the survey grid.....	15
3.2. Determining the GPR footprint.....	15
3.3. Antenna orientation.....	16
3.4. Positioning.....	17
4 Modeling of Typical UXO Targets	18
5 Practical Processing of GPR Data: A Case Study from the Ashland Test Site	24
5.1. Targets.....	25
5.2. Editing data.....	26
5.3. Dewow filter.....	26
5.4. Time gains.....	27
5.5. Additional processing.....	30
5.5.1. Filtering.....	30
5.5.2. Background subtraction.....	31
5.5.3. Migration.....	32
5.5.4. Enveloping.....	33
5.6. Extending the picture: Adjacent survey lines.....	34
5.7. 2D plan map images.....	35

5.8. 3D volume images.....	38
5.8.1. Interpretation of 3D animation.....	38
5.8.2. Known targets versus unknown clutter	40
5.8.3. Deeper targets.....	43
5.9. Discussion.....	45
6 Future Work.....	46
7 Overview	47
8 GPR Equipment	48
9 Previous Work.....	52
9.1. UXO-specific work.....	52
9.2. Landmine-specific work.....	54
9.3. Options for interpreting data	56
10 Ashland Test Plot – Multiple Frequency GPR Data	57
10.1. 250-MHz data	58
10.2. 500-MHz data.....	63
10.3. 1000-MHz data.....	65
10.4. Detailed grids for a single target using multiple frequencies	65
10.4.1. 250-MHz grid data	67
10.4.2. 500-MHz grid data.....	71
10.4.3. 1000-MHz grid data.....	75
11 Conclusions and Caveats	79
12 Strategy for Ashland Test Plot	81
References.....	84

Report Documentation Page

Figures and Tables

Figures

Figure 1. Cone-shaped nature of the GPR beam.	2
Figure 2. Single frame from an animation depicting the time snapshots of the electric field.	3
Figure 3. Hyperbolic responses are generated when crossing a linear target that is perpendicular to a survey line.	3
Figure 4. A series of parallel and perpendicular survey lines provides the best coverage in a GPR survey.	5
Figure 5. Plan map view of survey area depicting the average amplitude over the time interval between 9 and 20 ns.	6
Figure 6. Hyperbolic response for single target on survey line run perpendicular to the survey line illustrated in Figure 3.	7
Figure 7. Detection of multiple targets in close proximity using GPR measurements.	10
Figure 8. Vertical noise bands in the 250-MHz GPR data were observed from the Trimble RTK system transmitting real time updates using a radio frequency around 400 MHz.	14
Figure 9. Possible transmit and receive antenna orientations.	16
Figure 10. Cross-sectional view of the UXO targets modeled.	18
Figure 11. Modeling results for the UXO targets described in Figure 3 and Table 1 buried in a clay soil.	20
Figure 12. Modeling results for the UXO targets described in Figure 3 and Table 1 buried in a dry sandy soil.	21
Figure 13. Targets contained in the survey grid collected at the Ashland test site and used in this section as a case study for the processing of GPR data.	25
Figure 14. A GPR section with no gain or processing applied. Red arrows indicate areas where ground has subsided and air gaps are present. No UXO targets are visible.	27
Figure 15. The same GPR section illustrated in Figure 14, but with a constant gain of 70 applied.	28
Figure 16. The same GPR section illustrated in Figure 14, but with an AGC gain using a window value of 1 pulse width and maximum gain value of 400 applied.	29
Figure 17. The same GPR section illustrated in Figure 14, but with an SEC gain using a start value of 0, attenuation of 7, and maximum value of 400 applied.	30
Figure 18. The same GPR section illustrated in Figure 14, but with the average trace removed and an SEC gain using a start value of 0, attenuation of 7, and maximum value of 400 applied.	31
Figure 19. Calibrating a hyperbolic response to obtain a velocity estimate.	32
Figure 20. The same GPR section illustrated in Figure 18, but with migration applied using a velocity of 0.06 m/ns.	33
Figure 21. The same GPR section illustrated in Figure 20 with enveloping applied via a Hilbert transform.	34
Figure 22. Adjacent survey lines from top to bottom. Lines were separated by 20 cm.	36

Figure 23. Plan map view of the survey area displaying the average amplitudes over the depths of 0.3 to 0.8 m.....	37
Figure 24. Single frame of 3D animation created from the survey results.	39
Figure 25. 3D image of the survey results truncated at 0.49-m depth.	40
Figure 26. A plan view 3D image of Figure 25	40
Figure 27. Adjacent survey lines from top to bottom.....	42
Figure 28. Lines Y7 and Y8, which cross the same resonant response on perpendicular survey lines.	43
Figure 29. 3D image of the survey results truncated at 0.67-m depth.	44
Figure 30. 3D image of the survey results truncated at 0.77-m depth.	44
Figure 31. Lines Y38 and Y39, which cross the same deeper target response on perpendicular survey lines.	45
Figure 32. Lines were collected with all GPR frequencies over targets emplaced in the Ashland test plot.....	57
Figure 33. Detailed emplacement information for targets indicated in Figure 32.	59
Figure 34. Additional emplacement information for targets indicated in Figure 32.	60
Figure 35. Target responses observed over GPR survey line indicated in Figure 32 using 250-MHz frequency system.	61
Figure 36. Approximate location of GPR survey line is represented by the solid line, while the red symbols indicate the locations of UXO targets described in Figures 32–34 and summarized in Table 4.	61
Figure 37. Target responses observed over GPR survey line indicated in Figure 32 using 500-MHz frequency system.	63
Figure 38. Target responses observed over GPR survey line indicated in Figure 32 using 500-MHz frequency system without removal of an average trace.....	64
Figure 39. Target responses observed over GPR survey line indicated in Figure 32 using a 1000-MHz frequency system.....	66
Figure 40. A detailed grid was collected over a single target with all three frequencies.	66
Figure 41. Single 81-mm target over which detailed grids were collected with 250-MHz, 500-MHz, and 1000-MHz GPR systems.....	67
Figure 42. Isosurface view with only amplitudes greater than 70% of the maximum amplitude in the volume displayed.....	68
Figure 43. XY plane of volume cropped at a depth of 0.25 m.....	69
Figure 44. 250-MHz average amplitudes over the time range 9–15 ns for the XLines indicated in Figure 43.....	70
Figure 45. 250-MHz average amplitudes over the time range 9–15 ns for the YLines indicated in Figure 43.....	70
Figure 46. Isosurface view with only amplitudes greater than 70% of the maximum amplitude in the volume displayed.....	72
Figure 47. Average amplitudes over the time range 9–15 ns for the XLines8-14 from the 500-MHz data.....	72
Figure 48. Survey lines XLine9 and Xline10.....	73
Figure 49. Average amplitudes over the time range 9–15 ns for the YLines14–16 from the 500-MHz data.....	74

Figure 50. Survey line YLine15 runs parallel to the long axis of the target and generates a flat response rather than a hyperbolic response in the 500-MHz data.....	74
Figure 51. Isosurface view with only amplitudes greater than 70% of the maximum amplitude in the volume displayed.....	75
Figure 52. Average amplitudes over the time range 9–15 ns for XLines8–11 from the 1000-MHz data.	76
Figure 53. Survey lines XLine8 to Xline11 for the 1000-MHz data.	77
Figure 54. Average amplitudes over the time range 9–15 ns for YLines14–16 from the 1000-MHz data.	78
Figure 55. Survey line YLine15 in the 1000-MHz data.	78

Tables

Table 1. Position and size of targets included in the modeling computations.....	19
Table 2. Targets contained in the survey grid collected at the Ashland test site.	26
Table 3. Parameter space describing potential influences on GPR measurements of landmines.	55
Table 4. Target number, type, emplaced depth and dip and depths of responses observed in GPR measurements interpreted as UXO targets.....	62

Preface

This report was prepared as part of the Congressional Interest Environmental Quality and Installations Program, Unexploded Ordnance (UXO) Focus Area, Contract No. W912HZ-04-C-0039, Purchase Request No. W81EWF-418-0425, titled, "UXO Characterization: Comparison of Cued Surveying to Standard Detection and Standard Discrimination Approaches." Research was conducted by Sky Research, Inc., for the Environmental Laboratory (EL), U.S. Army Engineer Research and Development Center (ERDC), Vicksburg, MS. The following Sky Research personnel contributed to this report:

- Dr. Stephen Billings was the project Principal Investigator.
- Kevin Kingdon conducted all data collection, processing, and analysis presented here, and wrote this report.
- Joy Rogalla was the copy editor for this report.

This project was performed under the general supervision of Dr. M. John Cullinane, Jr., Technical Director, Military Environmental Engineering and Sciences, EL; and John H. Ballard, Office of Technical Director and UXO Focus Area Manager, EL. Reviews were provided by Ballard and Dr. Dwain Butler, Alion Science and Technology Corporation. Dr. Beth Fleming was Director, EL.

COL Gary E. Johnston was Commander and Executive Director of ERDC. Dr. James R. Houston was Director.

Unit Conversion Factors

Multiply	By	To Obtain
degrees (angle)	0.01745329	radians
feet	0.3048	meters
inches	0.0254	meters
pounds (mass)	0.45359237	kilograms

Acronyms

2D	Two-Dimensional
3D	Three-Dimensional
AGC	Automatic Gain Control
COTS	Commercial Off-the-Shelf
cm	centimeter(s)
CNR	Complex Natural Resonances
CWFM	Continuous Wave Frequency Modulation
DoD	Department of Defense
DSB	Defense Science Board
EL	Environmental Laboratory
EM	Electromagnetic
EMI	Electromagnetic Induction
ERDC	Engineer Research and Development Center
FCC	Federal Communications Commission
ft	feet
GHz	gigahertz
GPR	Ground Penetrating Radar
GPS	Global Positioning System
HSTAMIDS	Handheld Standoff Mine Detection System
JPG	Jefferson Proving Grounds
lb	pound
m	meter(s)
mm	millimeter(s)
MHz	megahertz
ns	nanosecond
RTK GPS	Real-time Kinematic Global Positioning System
RTS	Robotic Total Station
SEC	Spherical and Exponential Compensation
UXO	Unexploded Ordnance

General Introduction and Background

The clearance of military facilities in the United States contaminated with unexploded ordnance (UXO) is one of the most significant environmental concerns facing the Department of Defense (DoD). A 2003 report by the Defense Science Board (DSB) on the topic estimated costs of remediation in the tens of billions of dollars. The DSB recognized that development of effective discrimination strategies to distinguish UXO from non-hazardous material is one essential technology area where the greatest cost saving to the DoD can be achieved.

The objective of project W912HZ-04-C-0039 “UXO Characterization: Comparison of Cued Surveying to Standard Detection and Standard Discrimination Approaches,” was to research, develop, optimize, and evaluate the efficiencies of various modes of UXO characterization and remediation as a function of the density of UXO and associated clutter. Survey modes investigated in the research include:

1. Standard detection survey: All selected anomalies are excavated;
2. Advanced discrimination survey: Data collected in proximity to each identified anomaly are inverted for physics-based parameters and statistical or analytical classifiers are used to rank anomalies, from which a portion of the higher ranked anomalies are excavated;
3. Cued-survey mode: Each selected anomaly is revisited with an interrogation platform, high-quality data are collected and analyzed, and a decision is made as to whether to excavate the item, or whether to leave it in the ground.

Specific technical objectives of the research were to:

- Determine the feasibility and effectiveness of various interrogation approaches based on the cued-survey approach;
- Determine the feasibility and effectiveness of various interrogation sensors including magnetics, ground penetrating radar (GPR), and electromagnetic induction (EMI), and evaluate combinations of these sensors;
- Develop and evaluate the most promising interrogation platform designs;

- Develop optimal processing and inversion approaches for cued-interrogation platform data sets;
- Evaluate the data requirements to execute accurate target parameterization and assess the technical issues of meeting these requirements using detection and interrogation survey techniques;
- Determine which survey mode is most effective as a function of geological interference, and UXO/clutter density;
- Investigate the feasibility and effectiveness of using detailed test stand measurements on UXO and clutter to assist in the design of interrogation algorithms used in the cued-search mode.

The main areas of research involved in these coordinated activities include:

- Sensor phenomenology including GPR, EMI, and magnetometry;
- Data collection systems; platforms, field survey systems, field interrogation systems;
- Parameter estimation techniques; inversion techniques (single, cooperative, joint), forward-model parameterizations, processing strategies;
- Classification methods; thresholding, statistical models, information systems.

This report, “UXO Characterization: Comparing Cued Surveying to Standard Detection and Discrimination Approaches: Report 2 of 9 – Ground Penetrating Radar for Unexploded Ordnance Characterization; Fundamentals,” is one of a series of nine reports written as part of W912HZ-04-C-0039:

1. UXO Characterization: Comparing Cued Surveying to Standard Detection and Discrimination Approaches: Report 1 of 9 – Summary Report;
2. UXO Characterization: Comparing Cued Surveying to Standard Detection and Discrimination Approaches: Report 2 of 9 – Ground Penetrating Radar for Unexploded Ordnance Characterization; Fundamentals;
3. UXO Characterization: Comparing Cued Surveying to Standard Detection and Discrimination Approaches: Report 3 of 9 – Test Stand Magnetic and Electromagnetic Measurements of Unexploded Ordnance;
4. UXO Characterization: Comparing Cued Surveying to Standard Detection and Discrimination Approaches: Report 4 of 9 – UXO Characterization Using Magnetic, Electromagnetic and Ground Penetrating Radar Measurements at the Sky Research Test Plot;

5. UXO Characterization: Comparing Cued Surveying to Standard Detection and Discrimination Approaches: Report 5 of 9 – Optimized Data Collection Platforms and Deployment Modes for Unexploded Ordnance Characterization;
6. UXO Characterization: Comparing Cued Surveying to Standard Detection and Discrimination Approaches: Report 6 of 9 – Advanced Electromagnetic and Magnetic Methods for Discrimination of Unexploded Ordnance;
7. UXO Characterization: Comparing Cued Surveying to Standard Detection and Discrimination Approaches: Report 7 of 9 – Marine Corps Base Camp Lejeune: UXO Characterization Using Ground Penetrating Radar;
8. UXO Characterization: Comparing Cued Surveying to Standard Detection and Discrimination Approaches: Report 8 of 9 – Marine Corps Base Camp Lejeune: UXO Characterization Using Magnetic and Electromagnetic Data;
9. UXO Characterization: Comparing Cued Surveying to Standard Detection and Discrimination Approaches: Report 9 of 9 – Former Lowry Bombing and Gunnery Range: Comparison of UXO Characterization Performance Using Area and Cued-interrogation Survey Modes.

1 GPR Basics –Introduction

Ground penetrating radar (GPR) images the subsurface by emitting and detecting ultra-wideband radio waves, typically in the range of 1 to 1500 megahertz (MHz). The emitted signals penetrate into the subsurface, which is usually comprised of soil, rock or other naturally occurring geology. Radio waves are absorbed at different rates depending on the local survey environment, which results in finite, site-specific penetration depths. GPR detects subtle variations in the electromagnetic (EM) wave impedance, which result from changes in electrical permittivity, electrical conductivity, and magnetic permeability.

The application of GPR can range from imaging hundreds of meters in ice to resolving rebar and post tension cables embedded in concrete. GPR is not limited to surveying in soils and rock. Any low-loss material capable of transmitting the EM energy to reasonable depths can be imaged. For example, GPR technology is widely used in engineering applications for the investigation of roads and buildings built from concrete and asphalt. GPR has also proven to be a useful tool in many other non-standard scenarios such as freshwater lake bathymetry and sub-bottom profiling, non-destructive imaging of tree rot and root structure as well as monitoring of ice roads in the Arctic. While the applications of GPR are widely varying, this report focuses on the examination of GPR as it applies to the detection and discrimination of UXO targets.

This report includes a brief overview of general GPR concepts, data, and survey procedures. The GPR systems considered in this report are time-domain systems. The antennas are broadband and referenced by the center frequency of the emitted spectrum; for the equipment utilized, the bandwidth is approximately equal to the center frequency. A criterion is also presented for factors that determine the applicability of GPR and existing tools that should be considered in the site selection process. A comprehensive overview of GPR theory, concepts, and practical concerns can be found in Annan (2005), Daniels et al. (1988), Olhoeft (1998), and Cross (1999).

1.1. GPR basics – the data

GPR data are usually collected by making measurements at regular position intervals along a straight line. This straight line mimics a vertical slice through the subsurface when displayed as a cross section. The regular sampling interval is often controlled by an odometer wheel on a cart as is the case in Figure 1. At each point along the survey line, a trace of data is recorded that represents the reflections received from various depths for that point. When these traces for each point are placed side by side, a cross-sectional image of the subsurface is achieved. In these cross-sectional images, horizontal geological features such as soil horizons, bedrock, water table, etc., generally appear as flat lying objects. Point targets such as rocks, pipes (crossed perpendicularly), tree roots, and of particular interest to this study, UXO, will generate hyperbolic responses as shown in Figures 2 and 3.



Figure 1. Cone-shaped nature of the GPR beam.

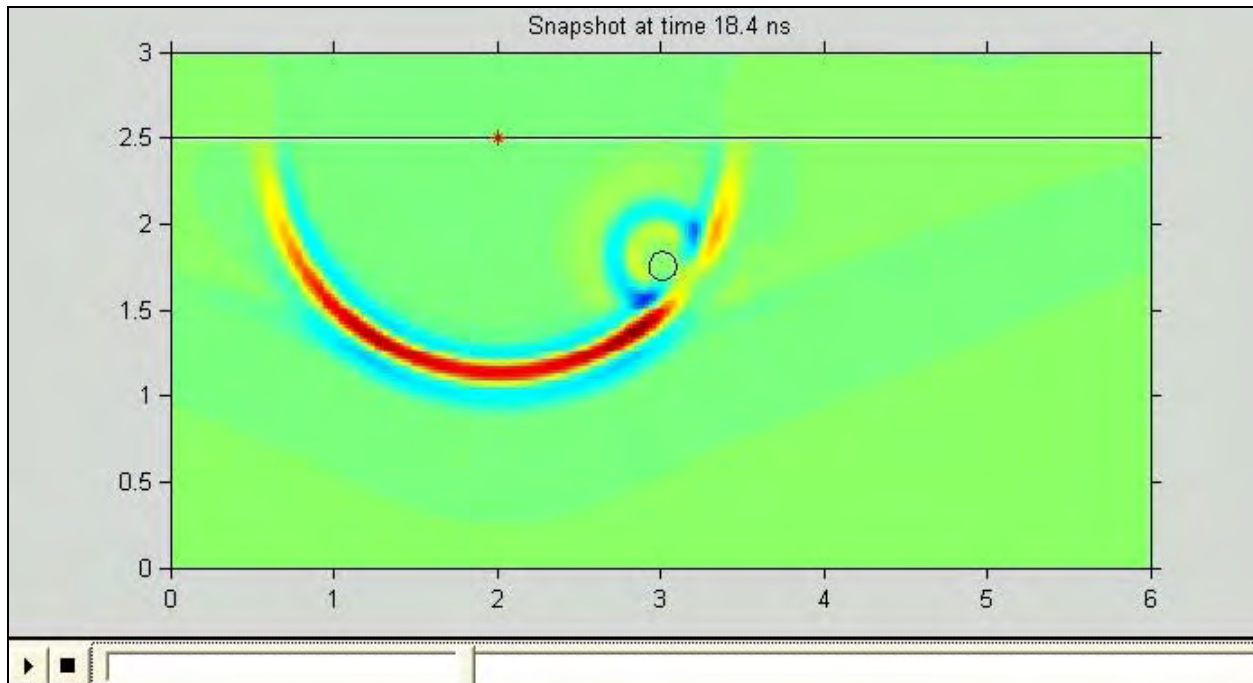


Figure 2. Single frame from an animation depicting the time snapshots of the electric field. The full animation is available on the ERDC portal. Hyperbolic response for point targets is a consequence of a detectable response from the target being recorded by the GPR sensor, both prior to reaching the actual target position and after moving past it.

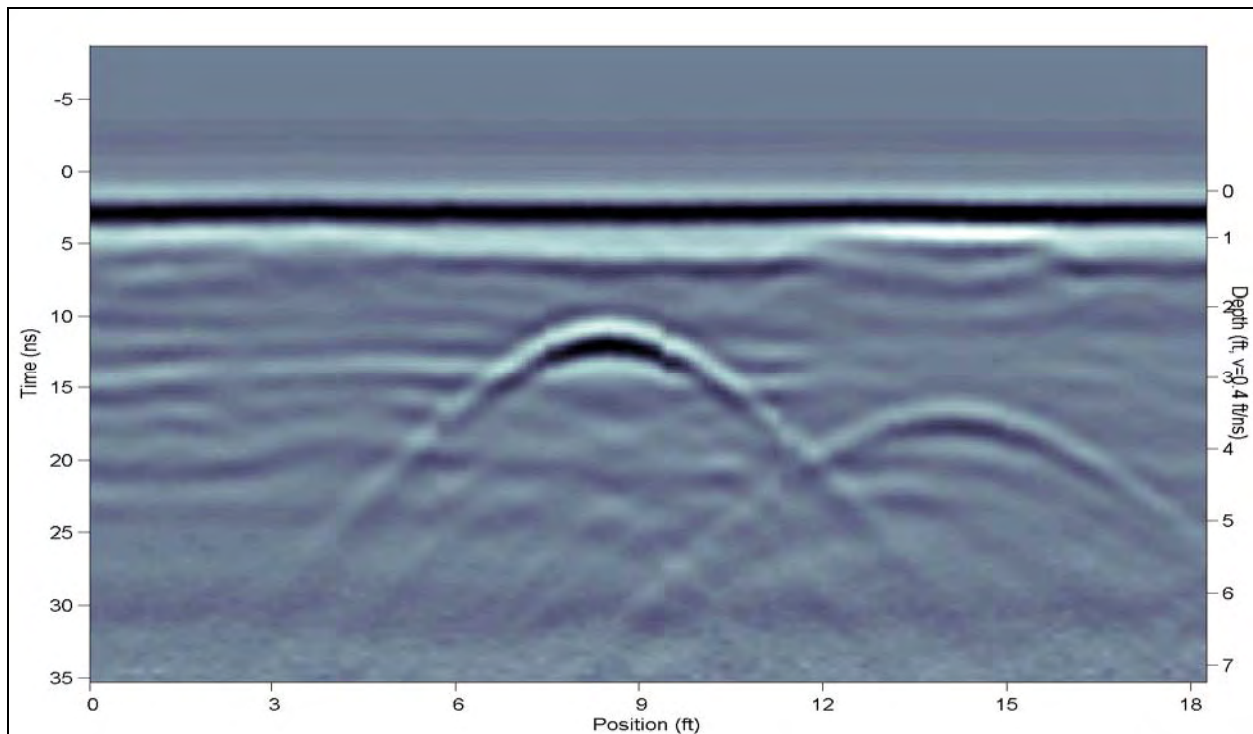


Figure 3. Hyperbolic responses are generated when crossing a linear target that is perpendicular to a survey line. The two hyperbolas in the above image represent two pipes.

The reason for this hyperbolic shape is that the beam pattern of the antenna is not simply a laser beam looking directly below the GPR sensor. It is rather better described as a cone of energy that results in an elliptical footprint that increases in size with depth (see Figure 1). Because of this fact, the GPR receiving antenna will record responses from the point target before the sensor is directly on top of the target and again as the sensor moves past the target. The responses recorded as the sensor moves toward and away from the actual target location will take longer to arrive at the receiving antenna because of the longer distance that the signal must travel. Consider the single frame from an animation depicted in Figure 2 that illustrates the wave fronts sent out at discrete position points along a survey line modeled over a metallic cylinder. Note that at the two points farthest away from the target, the signals take a longer path to return to the sensor and, therefore, occur at a later time and are attenuated more severely because of the longer travel path through the lossy medium. The peak of the hyperbola occurs when the sensor is immediately over the target and the shortest travel time occurs. For linear targets such as a pipe, the hyperbolic shape is created by crossing the target in a perpendicular fashion. Crossing the target at an oblique angle will distort the hyperbolic response.

The shape of this hyperbolic response is related to the velocity of the host material, and the velocity can be extracted by fitting a curve to the hyperbolic response. Velocity is an important concept because the GPR measures time directly and assigns depths to targets once a suitable velocity has been chosen.

Figure 3 is an example of a GPR survey line displaying hyperbolic responses. It is impossible to determine from a single line whether the targets in Figure 3 are part of a linear feature like a pipe or whether the responses are generated from a localized anomaly such as buried scrap metal, large rock, or a tree root. In order to characterize the hyperbolic responses further, a detailed survey needs to be acquired.

As mentioned earlier, the strongest response of a linear target is observed when that target is crossed in a perpendicular direction. Since the orientation of the targets is rarely known before undertaking the survey, the survey area is best characterized by collecting a series of parallel and perpendicular survey lines, as illustrated in Figure 4.

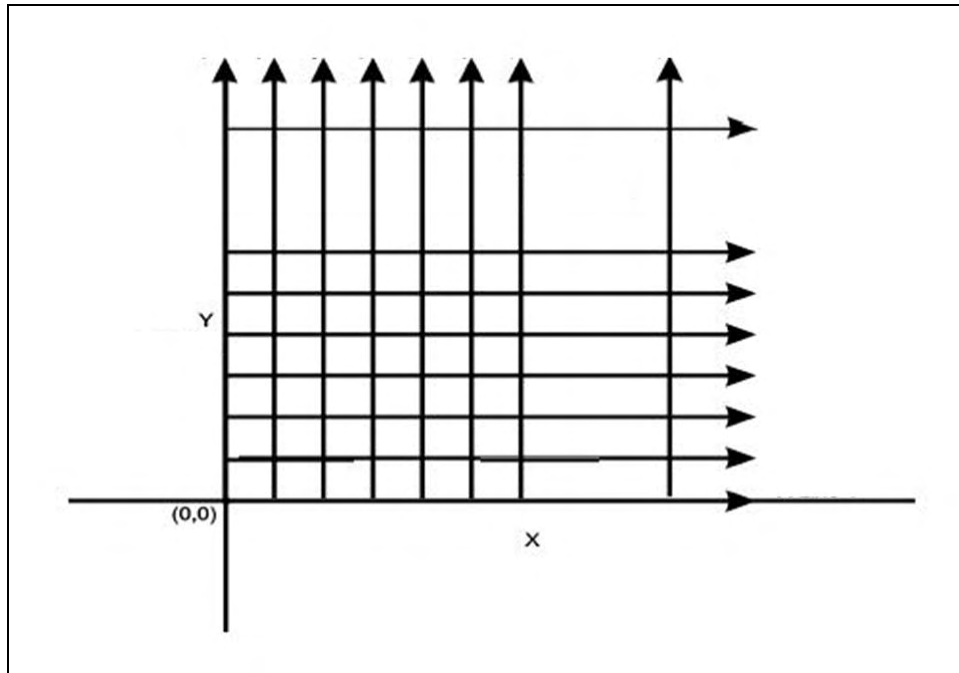


Figure 4. A series of parallel and perpendicular survey lines provides the best coverage in a GPR survey.

1.2. GPR basics – time slice images and 3-dimensional (3D) volumes

Once a series of survey lines is collected in the manner illustrated in Figure 4, trends can be identified in the lines. For example, if the two hyperbolic targets observed in Figure 3 are indeed a result of a linear target like a pipe, similar responses would also be expected on parallel collection lines. If, on the other hand, the responses came from a point target like buried rubble, there is likely to be no such hyperbolic response in parallel lines. While the inspection of individual survey lines for like responses can trace out linear features, interpretation is sometimes more intuitive via plan map views of the data. The details for this procedure are discussed for a grid of UXO data acquired at the Ashland test site later in this report (in Chapter 5, Practical Processing of GPR Data: A Case Study from the Ashland Test Site), but basic concepts of the plan map are illustrated here in Figure 5. This plan map was generated by collecting a series of lines, over the target area (approximately 18 feet [ft] \times 18 ft). The map indicated the areas of high amplitude reflectivity based on the recorded average amplitudes for a time slice between 9 and 20 nanoseconds (ns). This is no longer a cross section displaying position versus time (or depth) as shown in Figure 3, but rather a slice through the entire survey area for a specific time (or depth) range.

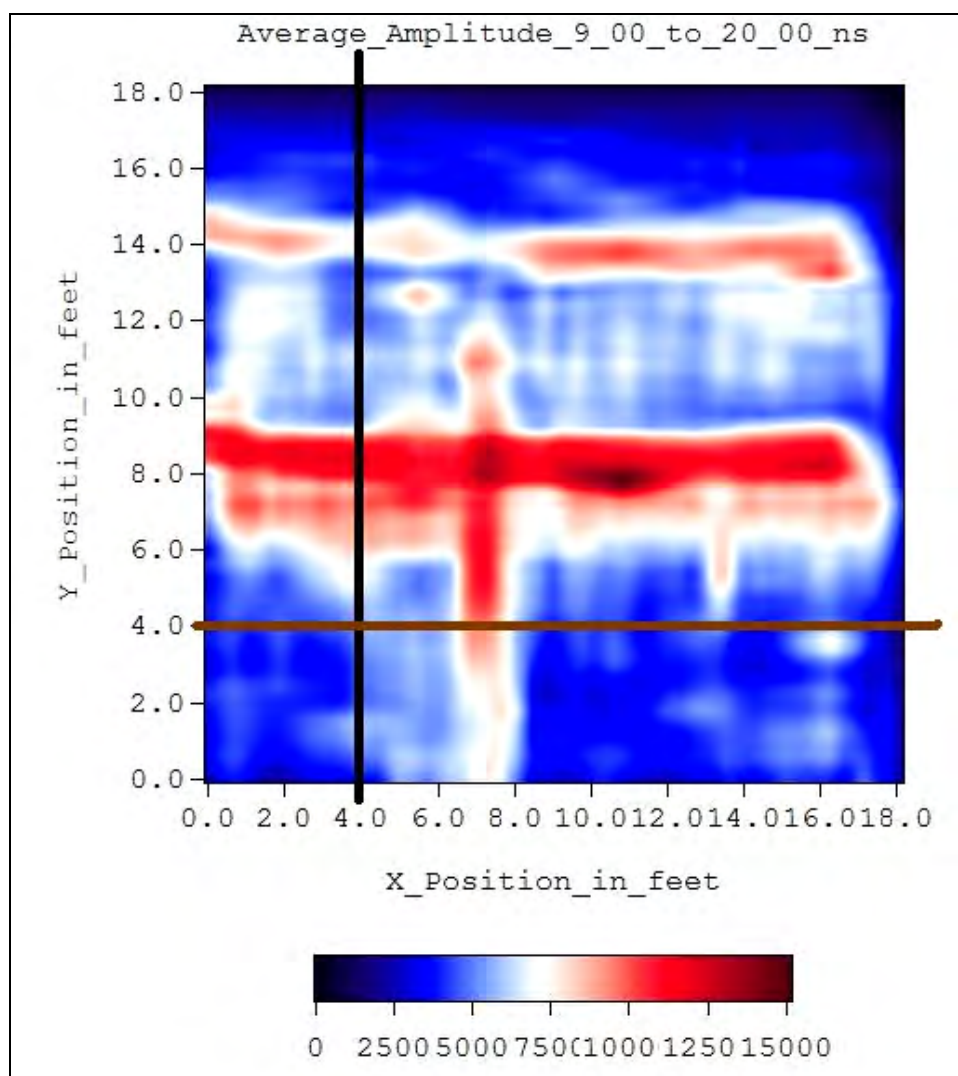


Figure 5. Plan map view of survey area depicting the average amplitude over the time interval between 9 and 20 ns. The position of the survey line depicted in Figure 3 is indicated by the solid black line, while the survey line shown in Figure 6 is represented by the solid brown line.

The solid black line in Figure 5 represents the position of the individual survey line shown in Figure 3. Two linear targets occur at approximately 9 and 14 ft along the Y axis (and run parallel to the X axis) in Figure 5. Note that these positions match the locations of the peak of the hyperbolas observed in the survey line data of Figure 3. The target occurring at 14 ft has a weaker response than the target observed at 9 ft. This again matched the observations of the Figure 3 survey line as the hyperbola at position 14 ft is deeper than the hyperbola at 9 ft and therefore the received signal is attenuated further. It is also worthy to note that there appears to be a target running perpendicular to the two targets at approximately position 7 ft along the X axis. No hyperbolic response is observed in the survey line because it did

not cross the target at a right angle, but rather it ran parallel to the target. If a survey line in the opposite direction is viewed (see Figure 6), a hyperbolic response is observed at the same position as the target that occurs at approximately 7 ft along the X axis in Figure 5.

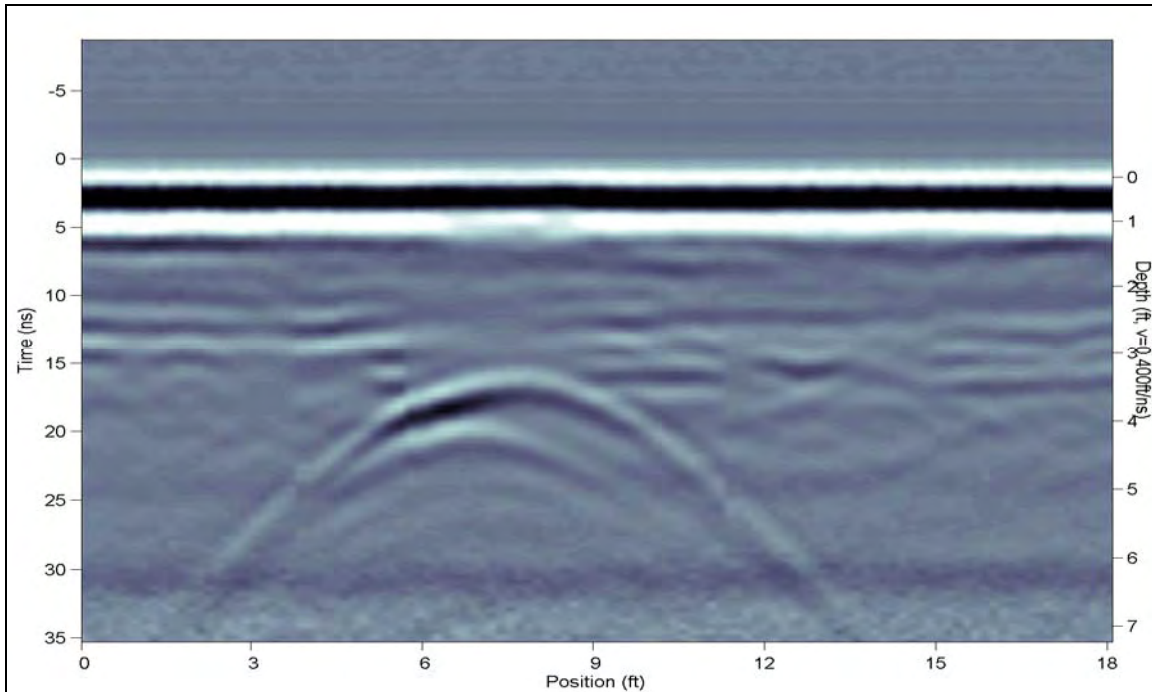


Figure 6. Hyperbolic response for single target on survey line run perpendicular to the survey line illustrated in Figure 3. Survey line location is indicated on the plan map in Figure 5 by a solid brown line.

1.3. GPR basics – extending to UXO case

Many challenges complicate the extension of the buried pipe case described above to the UXO application. In both cases GPR penetration is limited by the soil conditions of the site being surveyed and can vary significantly. The biggest distinction between the two cases is the presence of clutter. In the pipe case, hyperbolic responses generated by clutter could be readily identified as point sources if there was no linear response over multiple survey lines. The challenge in the extension of similar techniques to the UXO problem is that many of the targets will have dimensions on a similar scale as the clutter and may be indistinguishable. Clutter is likely to be site-specific and hard to predict without a test GPR survey.

The majority of UXO targets are likely to be shallow and, therefore, the use of higher frequencies may be applicable for improved resolution. Higher frequencies also become more susceptible to smaller scale clutter sizes

and, in some cases, heterogeneities in the soil and naturally occurring geology can mask the UXO target response entirely. It is also possible that the disturbance of soil horizons may be evident in GPR data in areas where targets have been buried even if there is not sufficient signal to generate a strong response from the target itself. Required line spacings are likely too small to practically survey large areas with a single channel system. GPR may be best suited to a cued-interrogation approach where a small area, high-resolution GPR grid survey is performed over an area identified via EM or magnetic measurements. Multiple-channel GPR systems that cover a wider swath may permit surveying of larger areas with the tight line spacings required in a less time-consuming manner.

2 GPR Survey Site Considerations

The most important factor in the examination of GPR for its potential role in UXO detection and discrimination is to be realistic. Like all geophysical methods, there will be environments too hostile to make useful measurements with GPR. The limitations with respect to GPR are most often a lack of penetration due to the presence of conductive (clay, silty) soils. The presence of saline water in any host soil will also lead to conductive environments that severely limit the effectiveness of GPR. When looking for single isolated targets as in the UXO case, clutter is an issue for GPR. Because GPR technology relies on differences in electrical properties of host materials and targets, it is not unusual to observe responses from nonmetallic targets such as tree roots, cobble-sized rocks, soil horizons, and other geological features. It is imperative to understand these constraints and limitations going into the investigation. GPR needs to be considered as one of several tools in the geophysical toolbox. There will be instances when GPR provides invaluable information that cannot be obtained from any other geophysical method, yet there are certain to be instances where no discernible target evidence can be elicited from GPR data.

A main goal of this study is to obtain a better understanding of environments conducive to or unfavorable to tangible GPR results. Sometimes prior information exists (Doolittle et al. 2002) that allows depth of investigation (penetration) predictions. Previous detailed site-specific geophysics (conductivity values) may exist, which further help to address the penetration issue prior to conducting a GPR survey. The type, density, and distribution of clutter will frequently remain unknown until some initial test surveying is done. There may be clutter indications (a wooded area implying the presence of tree roots, target-sized rocky outcrops visible at the surface, etc.), but in many cases the final conclusive effectiveness is obtained through an on-site test survey. The clutter issue can be addressed by applying a combination of geophysical methods. Nonmetallic false positives observed in the GPR records can be ruled out if EM and magnetic data obtained over the same target do not indicate a metallic object. GPR might also prove useful for distinguishing areas where multiple metallic targets contribute to the observed EM and magnetic responses. The ability of GPR to resolve multiple, closely spaced targets is illustrated in Figure 7.

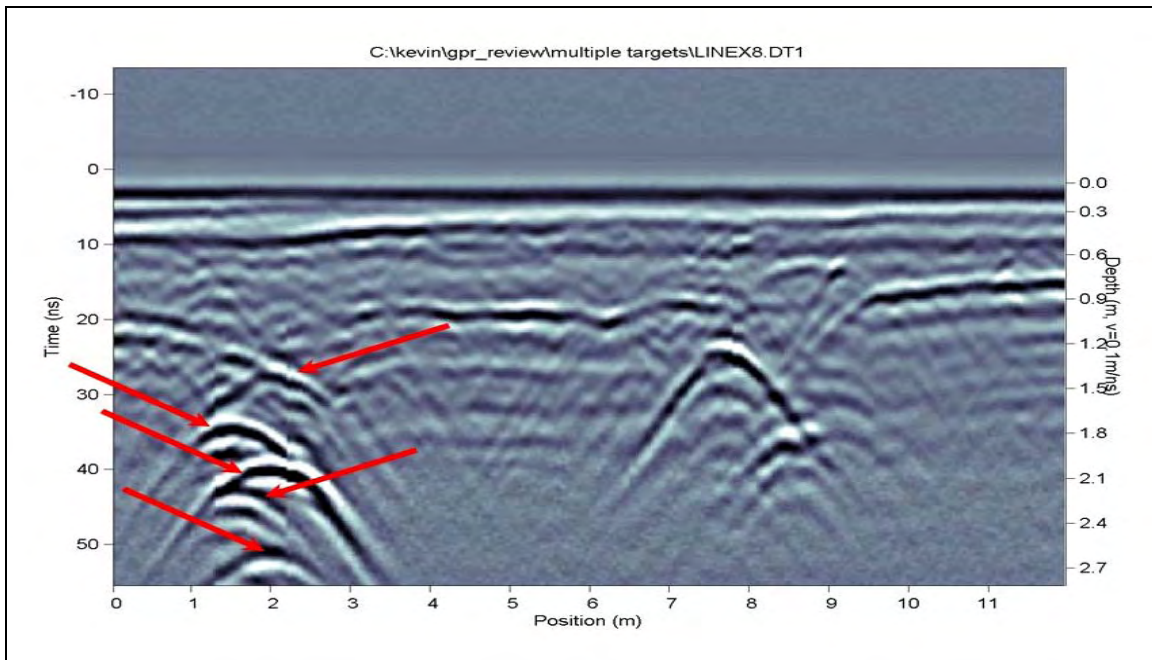


Figure 7. Detection of multiple targets in close proximity using GPR measurements. Data were collected using a 250-MHz GPR system.

The polarity of the GPR signal can also be used as a diagnostic tool for investigating clutter types. When a GPR signal is incident on a target, the reflected signal polarity is dictated by the change in impedance between the target and the host soil. In the case of a metallic target typical of a UXO, the impedance of the target is zero and the GPR reflection generated by the metallic target has a negative polarity. This polarity information can be exploited to reduce some of the GPR specific clutter (Report 7 of series).

2.1. Determining the applicability of GPR

The success of GPR for any application is largely determined by two questions:

1. Will GPR penetrate through the host environment to adequate depths and return a response from the target of interest?
2. Will the target of interest produce a distinct and detectable response that can be identified in the presence of background clutter?

More specifically, one must consider how the target's depth, geometry, and electrical properties as well as the host material properties and the survey environment will impact the results of GPR measurements of UXO targets.

2.2. Consulting the GPR suitability map

A map of the conterminous United States has been prepared by Doolittle et al. (2002), which indicates the relative suitability of soils for GPR work. Factors considered in the suitability value assigned to a particular region include clay content and electrical conductivity of the host soil. This map will serve as a useful tool for selecting sites and should be consulted early in the feasibility assessment of GPR measurements for a proposed site. Many areas which are unsuitable for deeper penetrations necessary for GPR applications involving many meters of penetration may still be viable for shallow, high-resolution surveys required for UXO work. It should also be noted that while the soil suitability map is a valuable tool in assessing the wide-scale variability in GPR suitability, the actual GPR performance in a given survey is dependent on localized site conditions, the proposed application, and the characterization of the target. This map provides a good starting point for assessing the likelihood of success when planning a GPR survey prior to considering the survey details discussed below.

2.3. Target depth

In most practical cases, the target depth will be unknown. It is crucial to understand the depth of penetration achieved, as any targets existing below the maximum depth of GPR penetration will not be detected. It is essential to determine if the intended target is at a reasonable depth for the proposed surveys. With knowledge of the electrical properties of the host soil, some insight can be gained into the expected depths of penetration for a particular environment. Simulations can be run to predict penetration for a modeled environment, but often it is quicker and more convenient to consult with the experimental results in a similar environment if available, or to conduct small-scale feasibility surveys at the actual site if practical.

2.4. Target electrical properties

A key factor in the intended target's electrical properties is that it must be distinct from the surrounding host environment. It is this contrast in electrical properties between the host soil and target that is responsible for the reflections generated and recorded by GPR. If the intended target is too similar to the host soil, the contrast may not be significant enough to generate a detectable response. Fortunately in the UXO case, targets are metallic and all energy striking the target is reflected back towards the

surface. In cases of nonmetallic targets, for example landmines, the lack of metal content means a much weaker return signal, as only a portion of the energy is reflected back towards the surface by the target.

2.5. GPR resolution

Resolution is determined by the bandwidth of the GPR system. The bandwidth determines the temporal duration of the signal, which ultimately controls the spatial extent of the excitation. GPR systems have energy spread about a center frequency. It is the center frequency that is typically given when discussing GPR antenna frequencies. The ratio of bandwidth to center frequency is normally 1 for most commercial systems. In the case of the 250-MHz Noggin system used at Ashland, energy is spread over the frequency range 125–375 MHz. Higher resolutions therefore require larger bandwidths, which translates to higher frequencies, which must come at a loss of penetration. For this reason, there is always a trade-off between resolution and penetration when using GPR. In general, resolution is typically sacrificed in favor of penetration as the added resolution is not useful if the signal cannot reach the depths of the intended targets. Resolution should not be confused with detection capability, as detectable responses can often be obtained from thin layers or small targets, while the critical dimensions of these same targets are not resolvable.

2.6. Effects of water

In addition to variations from one site to another, it is also possible that two GPR surveys over the same area collected at different times could produce differing results, particularly if the water content of the soil changes dramatically between surveys. The presence or absence of water is an important factor in determining velocities (from which target depths will be inferred) and attenuation.

In most Earth environments, water is the single largest factor in determining the bulk electrical properties. Pure water itself is not an effective conductor, but as the amount of dissolved ions in the water increases, the elevated conductivity becomes a major detriment to GPR work. The water molecule is polarizable and permittivity values for water are much higher than those of the surrounding soil. GPR signal velocity values in water are about three times slower than the velocity of the signal in a typical soil and, therefore, the presence of water in the pore space can significantly lower the GPR velocity. Water begins to absorb energy more strongly as

the frequency increases towards the water relaxation frequency of 10 gigahertz (GHz). These effects can be seen at frequencies as low as 500 MHz in otherwise low loss materials. This relaxation of the water molecule results in a loss mechanism that imposes an upper limit in the GPR frequencies for which useful measurements can be made.

The presence of water can occasionally be beneficial. In the case of buried landmines, the electrical properties of the plastic target are often similar to the electrical properties of the host soil. However when the soil is wet, the contrast between the target and its surroundings is stronger and the amplitude of the GPR response is larger.

2.7. External factors

There are numerous environmental and man-made sources of potential noise interference when collecting GPR data. Any sources transmitting in the GPR range (for the UXO case, typically 100–1500 MHz) can show up as noise in GPR recordings. Two-way radios often use a portion of this frequency band as do many analog cell phones. Initial testing at the Ashland site uncovered that the Trimble real-time kinematic global positioning system (RTK GPS) employed a radio frequency around 400 MHz to send its updates to the rover unit, which interfered with the GPR data, as indicated in Figure 8. The proliferation of radio transmitters for various broadcast formats is a good indication that this is a problem not likely to improve in the future, so caution must be taken to identify sources of external noise when making GPR measurements. External factor considerations may also include environmental conditions such as extreme heat/cold, hazardous materials, or accessibility concerns that make surveying difficult for GPR equipment or for personnel operating the equipment.

In addition to environmental limitations of the equipment, there have also been regulatory restrictions imposed by the Federal Communications Commission (FCC) in recent years. GPR is a unique ultra-wideband system in that by its very definition, it directs energy into the ground rather than into the air and is, therefore, only an unintentional emitter of weak EM waves into the air. However, in FCC modifications to Part 15.509 rules (complete rules available at www.fcc.gov/oet/info/rules), GPR was lumped in with all other ultra-wideband systems and a number of restrictions were imposed. The repercussions for GPR users are a requirement to register GPR equipment with the FCC and indicate intended areas of operation.

Manufacturers of GPR equipment are also required to meet emission standards described in the 15.509 rules. GPR equipment used in the initial Ashland surveys was FCC certified.

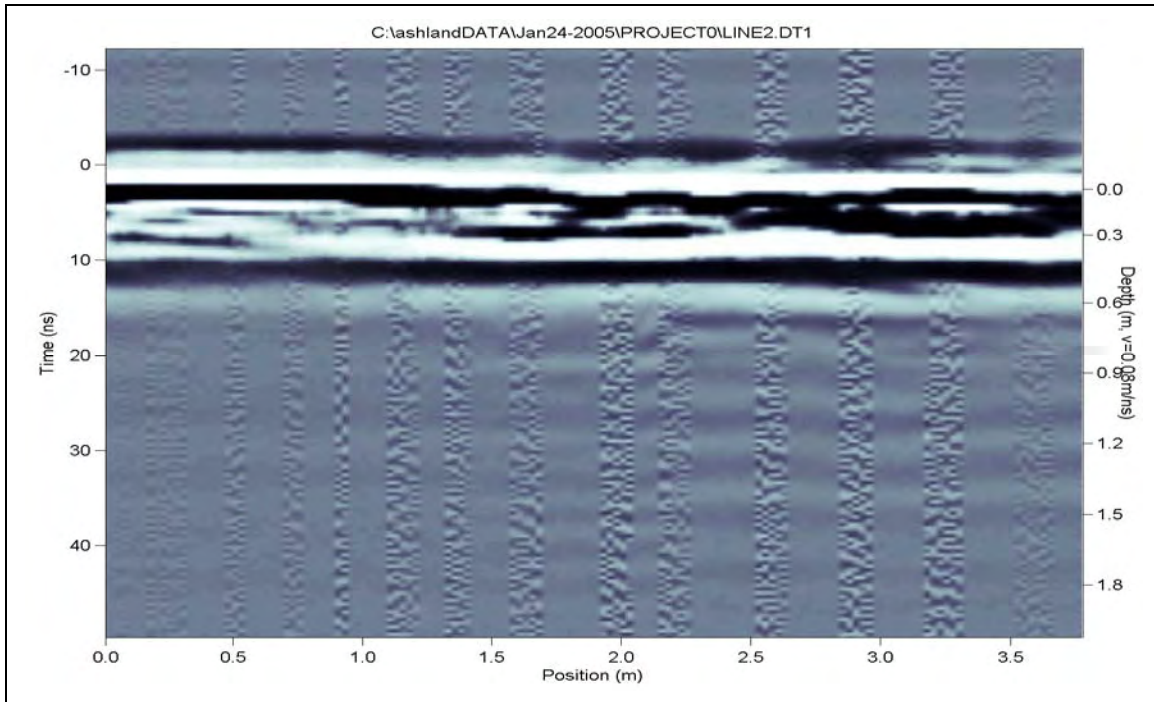


Figure 8. Vertical noise bands in the 250-MHz GPR data were observed from the Trimble RTK system transmitting real time updates using a radio frequency around 400 MHz.

3 Survey Design

If none of the factors from Chapter 2 preclude the use of GPR, the next step is to design the survey. Careful planning prior to undertaking a survey helps to ensure that the often time-consuming process of data acquisition is spent in a productive manner with the highest quality data available for post-processing.

3.1. Selecting the survey grid

There are a number of challenges that are unique to the UXO problem when planning GPR surveys. The number of survey lines required can be reduced in many GPR surveys by collecting lines that run perpendicular to the trends under investigation. In UXO surveys, that luxury is not available as anticipated targets are small, of unknown orientation, and isolated so the survey lines must be arranged such that the radar footprint provides coverage at the target depths of interest. A set of parallel and perpendicular lines as illustrated in Figure 4 is the best approach for detecting UXO targets. A significant challenge in GPR surveying for UXO applications is the sheer volume of data generated. Full coverage surveys of any substantial area at GPR frequencies can require line spacings as small as 10 centimeters (cm) and along line sampling of 2.5 cm. Such a survey is entirely impractical with a single-channel GPR system and is better suited to multi-channel GPR arrays. A single-channel GPR system is more suitable to a cued-interrogation mode of operation whereby a densely covered grid of high quality GPR data is collected over an identified anomaly.

3.2. Determining the GPR footprint

UXO targets are small enough that GPR lines must be collected at tight line spacings to ensure complete coverage of a given area. It is necessary to ensure that the footprint imaged by the GPR overlaps on adjacent lines so that complete coverage is obtained. A simplified beam pattern suggested by Annan and Cosway (1992) is helpful in determining appropriate line spacings based on the beam pattern at depth.

3.3. Antenna orientation

Most GPR antennas are dipolar and radiate with a preferred polarity. A range of common antenna orientations is illustrated in Figure 9. Most GPR surveys are conducted in an XX configuration with the antennas oriented perpendicular to the survey line direction. This results in an elliptical footprint (as indicated in Figure 1) with a minimal amount of energy resulting from off-line clutter. The XX configuration best represents a vertical slice of the ground. If off-line clutter is not a major concern, the YY orientation will result in a wider footprint and may be more appropriate for detection type surveys. The XY and YX orientations are referred to as cross polarized and the advantage of these configurations is that the direct air and ground wave signals are null coupled (although this is not always easy to achieve in practice). Numerical inversions using multicomponent GPR data (van der Kruk et al. 2003) use measurements from all four orientations to image electrical property changes. Cross-polarized measurements require the use of a GPR system with bistatic antennas.

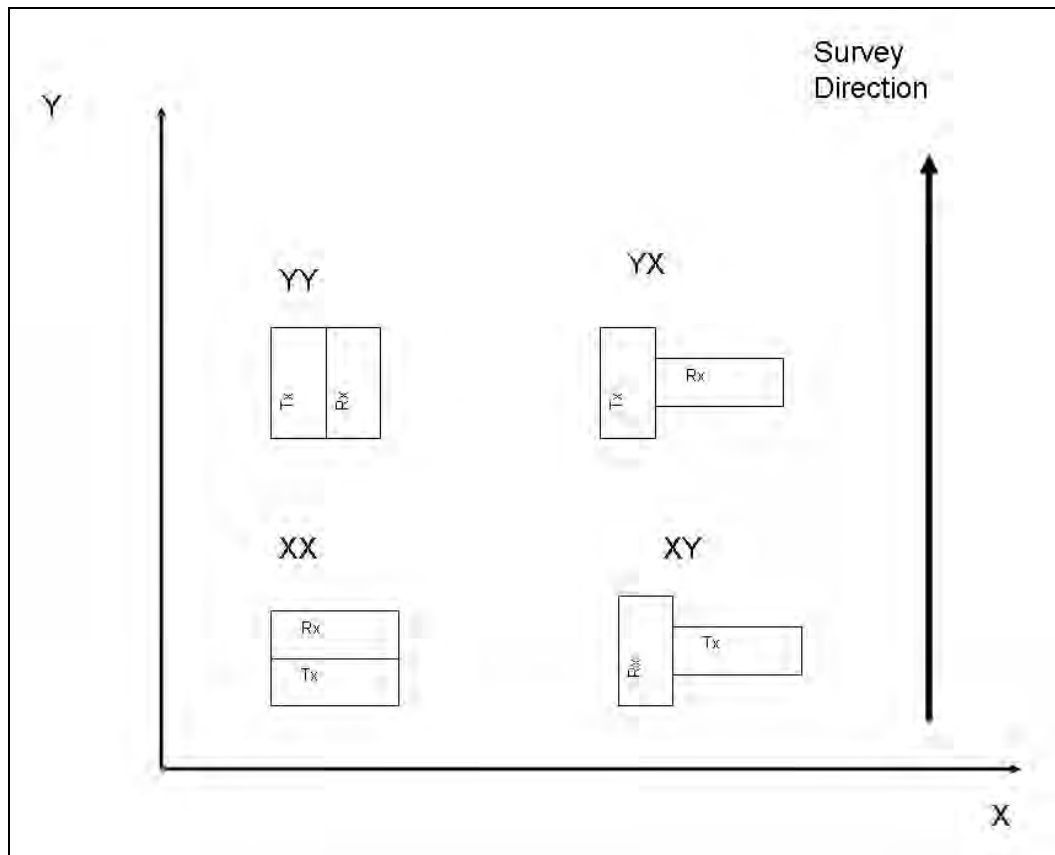


Figure 9. Possible transmit and receive antenna orientations. First letter indicates the axis parallel to the transmit antenna, while the second letter indicates the axis parallel to the receiving antenna.

3.4. Positioning

The positioning of these lines is important as the data collected are only as good as the positional data available to define the locations of targets. Tests at Ashland revealed issues using the Trimble RTK GPS system to provide positioning information (see Chapter 2, Section 2.7, External factors). Real time corrections were disabled and the data were recorded on base station and rover units independently for differential corrections post-acquisition. The GPS was not set to update as quickly as the GPR was sampling (the cart was being pushed at a normal walking speed, sampling every 2.5 cm) and as a result, multiple traces in each GPR profile wound up with identical GPS positions. Either the GPS update rate needs to be increased for future surveys or the GPS position acquired needs to be lessened from every trace in the GPR section to, e.g., every 10th trace with interpolation performed to assign positions to traces between those for which a GPS position was acquired. These same considerations are handled for magnetic and EM data sensors which sample faster than GPS updates are available, and a similar approach will be applied to future GPR surveys.

4 Modeling of Typical UXO Targets

To evaluate typical responses for UXO targets and how they will vary with the range of GPR frequencies employed in the proposed surveys, two-dimensional (2D) modeling was undertaken. Maxwell's equations relate the fundamental electromagnetic field quantities and their sources via empirical equations which govern all electromagnetic phenomena. By employing computational solutions to these governing equations, GPR responses can be modeled for a variety of settings prior to the time-consuming task of data acquisition. Comparisons can then be made between the theoretical results obtained via modeling and experimental results observed.

A suite of 2D models was run to create synthetic GPR profiles. The modeling presented here was completed using the freeware GprMax2D, which uses finite difference time-domain numerical methods (for further details on the methods used, see Giannopoulos (1997)). A range of UXO targets were chosen based on the existing inventory of surrogate targets in Sky Research's possession. Figure 10 illustrates the environment modeled in cross section. In order to model the GPR response in 2D, the geometry of the problem is invariant in the strike direction, meaning an infinitely long target is assumed in that direction. In cross section, the UXO targets are modeled as circular perfect conductors of varying diameters. Table 1 lists the position of the targets in the model space illustrated in Figure 10.

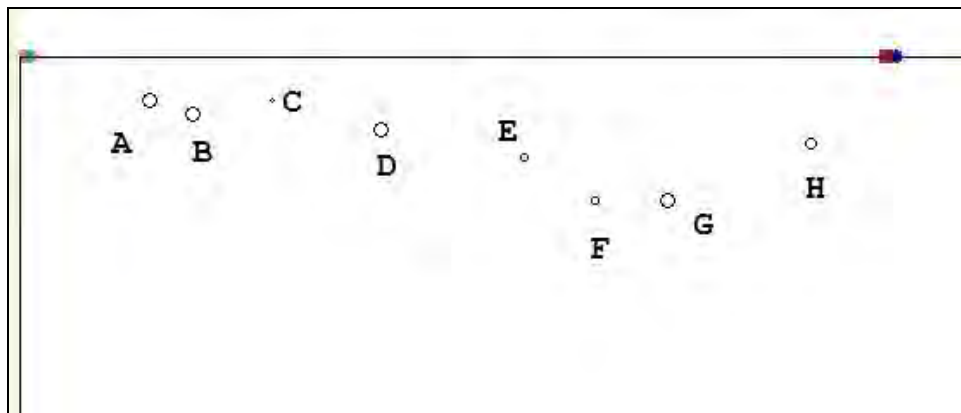


Figure 10. Cross-sectional view of the UXO targets modeled. Horizontal distance is approximately 6.5 m and the depth of the computational model is 2.5 m. Target positions and depths are described in Table 1.

Table 1. Position and size of targets included in the modeling computations.

Target	Diameter, mm	Position, m	Depth, m
A	100	0.9	0.3
B	100	1.2	0.4
C	25	1.75	0.3
D	90	2.5	0.5
E	50	3.5	0.7
F	50	4.0	1.0
G	100	4.5	1.0
H	76	5.5	0.6

Note that the letter assigned to each target in Table 1 is also used to identify the target response observed in the model output illustrated in Figures 11–12. Models were run for two distinct soil types (clay ($K_r = 15$, $\sigma = 100$ milliseconds [mS]/meter [m]), dry sand ($K_r = 9$, $\sigma = 1$ mS/m)) at three different frequencies (250, 500, and 1000 MHz). The use of higher frequencies in GPR surveys results in a higher resolution, but this comes at the consequence of less penetration over the lower frequencies. In an environment where the attenuation of GPR signals is quite strong (i.e., clay soils), it may be necessary to employ the lower 250-MHz system to achieve adequate penetration to detect targets. Conversely, in an environment where achieving desired penetration is not an issue (i.e., non-conductive dry sands), the use of higher frequencies will better resolve the targets in question. The issue of clutter must also be taken into consideration, as the higher frequencies also become more sensitive to smaller scale clutter than the lower frequencies and this may also influence which frequency of system is most applicable to a specific site. The results of the modeling are illustrated in Figures 11–12 and are summarized here.

Numerical simulations are a useful tool for examining some of the factors that affect the GPR response in detail rather than the time-consuming process exploring these parameters in the field experimentally. The model results depicted in Figures 11 and 12 illustrate the relationship between frequency and resolution and the sensitivity of the GPR response to the host soil. Results for the 1000-MHz case were the most computationally intensive and were actually run as two separate cases and then merged.

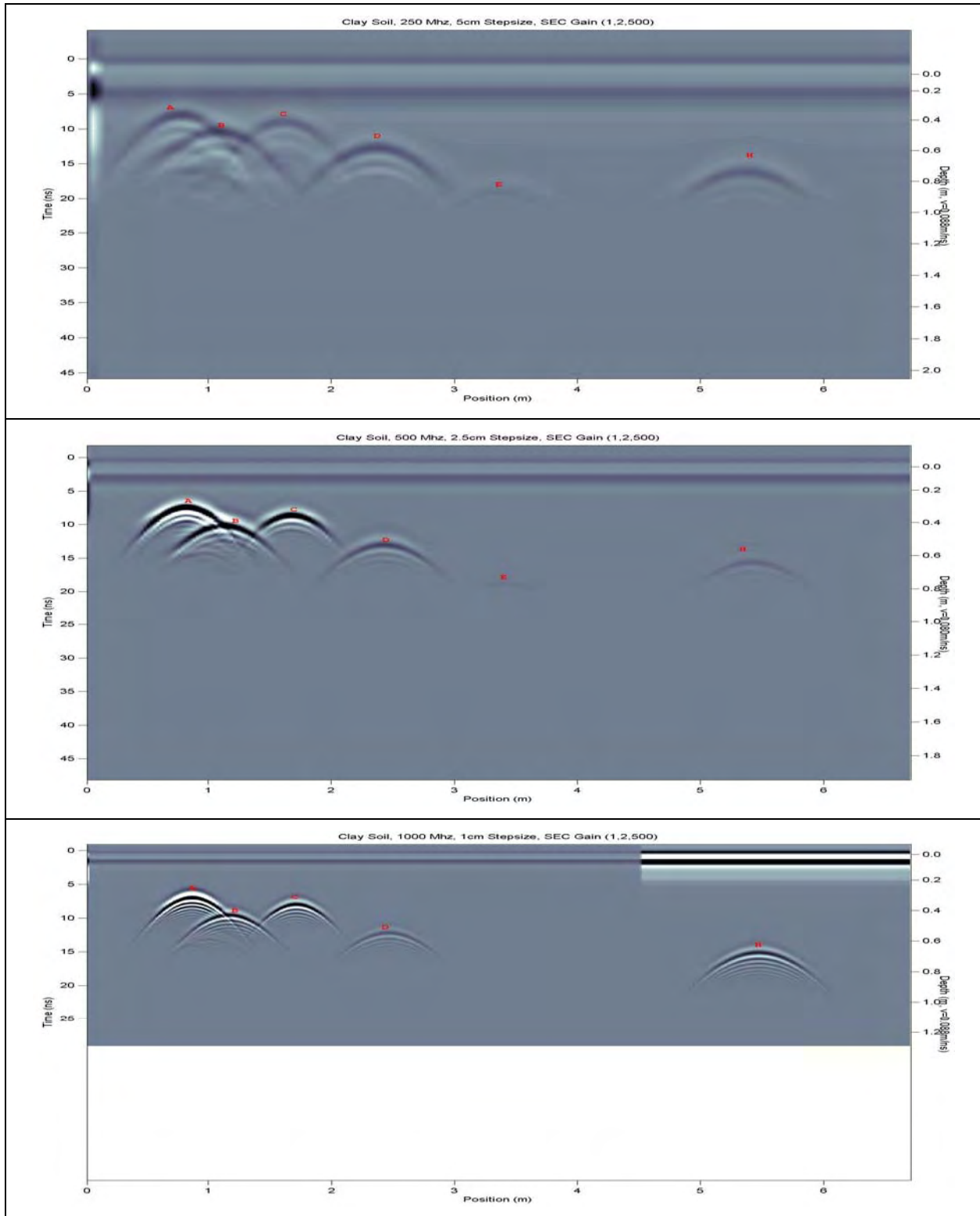


Figure 11. Modeling results for the UXO targets described in Figure 3 and Table 1 buried in a clay soil. Plots represent frequencies of 250 MHz (top), 500 MHz (middle), and 1000 MHz (bottom). All results are plotted using an SEC gain (1, 2, 500).

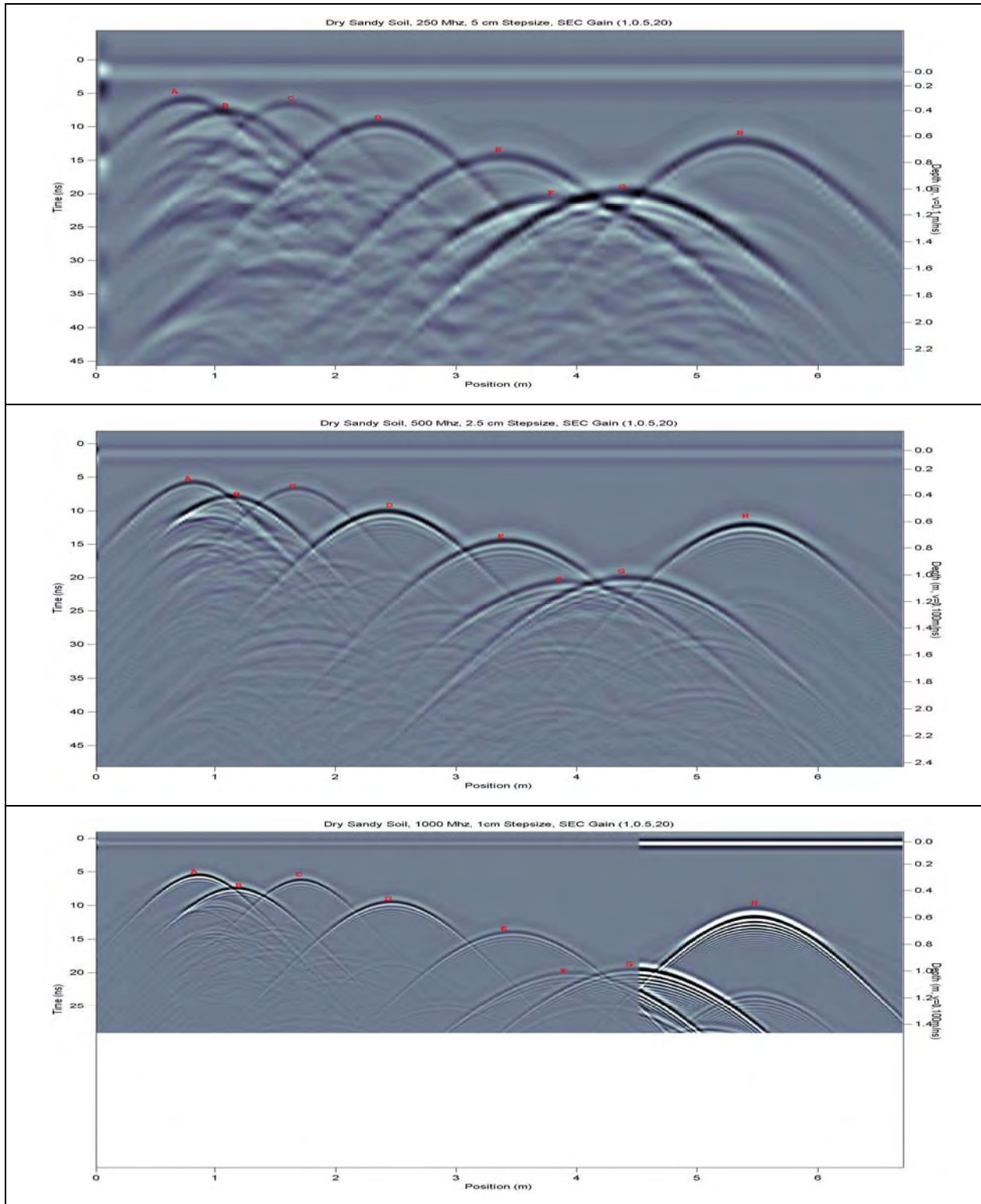


Figure 12. Modeling results for the UXO targets described in Figure 3 and Table 1 buried in a dry sandy soil. Plots represent frequencies of 250 MHz (top), 500 MHz (middle), and 1000 MHz (bottom). All results are plotted using an SEC gain (1, 0.5, 20).

That is the reason for the sudden change in the 1000-MHz image at approximately 4.5 m. The background values of the two runs were different and when they were converted to the GPR file format, the scaling was unique to each portion of the merged image. The calculations for the 1000-MHz case were also computed over a shorter time window to speed up the computation, which is why the bottom portion of the 1000-MHz results are blank in both Figures 11 and 12.

In Figure 11, modeling outputs for the clay ($K_r = 15$, $\sigma = 100$ mS/m) soil are illustrated. All results were plotted with the same SEC gain using a start value of 1, attenuation of 2, and a maximum value of 500. A discussion of the time gain parameters and their meanings can be found in Chapter 5, Section 5.4. Typically, each section would be plotted with a different gain function specific to the contained data. However, for illustration purposes, here they are all plotted with the identical gain function so that the variations in the observed results can be compared independent of the gain function applied. The same targets are detected in the 250-MHz and 500-MHz images; however, the 500-MHz image does a better job of distinguishing the three targets (A–C) placed fairly close together on the left side of the plot. In both the 250-MHz and the 500-MHz data sets, the relatively small (50-millimeter [mm] diameter) target E is barely detectable and the two deeper targets (F, G) cannot be observed in the data. Not surprisingly the 1000-MHz data provide improved resolution for the shallower targets (A–D, H) and the two deeper targets that were not visible in the lower frequency data are not evident in the 1000-MHz image either. The target that was barely seen in the 250-MHz and 500-MHz images (E) can no longer be seen in the 1000-MHz image, as the attenuation of the GPR signal for the 1000-MHz system does not provide adequate penetration to detect that target in the clay soil modeled.

Figure 12 shows how large a difference the soil type can make when the GPR profiles for the dry sandy soil ($K_r=9$, $\sigma=1$ mS/m) are considered. All the results (250, 500, and 1000 MHz) in Figure 12 were again plotted with an identical gain function, but the parameters used represented a much weaker gain than those required for the clay soil. Applying the same gain function parameters that were employed in the clay soil case would significantly over-gain the dry sand soil results. For the sandy soil results, an SEC gain (1, 0.5, 20) was used. All targets that were detectable in the clay soil are also observed in the dry sandy soil. The tails on the hyperbolic

responses generated for each UXO target are more pronounced in the dry sand case. This is a consequence of improved penetration and a detectable response recorded at greater horizontal distances prior to and past the actual target location as the sensor is moved across the surface. In addition, the two targets that were not detected with any frequency in the clay soil are readily observable over all the frequencies in the dry sandy soil case.

These modeling results help to understand some of the key issues and considerations in the GPR survey. The model is, however, a simplistic representation of the real world conditions. This is perhaps best illustrated via a comparison of the modeling results in Figures 11 and 12 with the data example illustrated in Figure 7. Note the presence of clutter in Figure 7, both in terms of horizontal geological features representing soil horizons and scattering that does not appear nearly as easily identifiable as the UXO target responses observed in the modeling results. This is the reality of GPR surveys and returns to a question discussed earlier, Will the target produce a distinct and detectable response that can be differentiated from background clutter? Because clutter is very site-specific, this question can only be answered through on-site testing. While the ultimate goal is the ability to characterize UXO targets, this cannot be accomplished without an understanding and classification of the clutter. The ability to compare results prior to the placement of UXO targets, where all observed responses can be considered clutter with those results after UXO targets are placed on the same test site, should allow for a detailed comparison of clutter and UXO target signatures.

5 Practical Processing of GPR Data: A Case Study from the Ashland Test Site

This chapter describes the manipulation of GPR data post acquisition. While surveying techniques were outlined in Chapter 1, Sections 1.1 through 1.2, the fact remains that the better the quality of the collected data, the more information that can be obtained from these data. In some instances, very minimal processing will be required, and often a target response will be observed in real time during data acquisition. In other instances, the target response may be weak and may benefit from additional processing. In many cases, all that will be required will be a simple time gain to boost signal strengths and some filtering to remove low-frequency components in the data due to antenna ground coupling. Additional processing (migration, enveloping, etc.) can be used to create 2D plan maps and 3D volumes of GPR surveys.

GPR data are typically collected as digital data along straight lines at equal intervals along that line. The process of collecting data in a straight line mimics a vertical slice through the subsurface. By collecting regularly spaced data, processing techniques originally developed for seismic data can be applied.

Many features are readily identifiable in real time in the field as anomalies become apparent on the video logger of the GPR system during the data acquisition. This is often an overlooked component of the data processing strategy but it can be crucial. Attention must be paid in the field, both to ensure the highest quality data are collected but also to provide an initial and ongoing assessment of GPR performance. For example, suppose a large-scale survey is planned that will take many hours (if not days) to acquire the data at necessary line and station intervals. Further assume that the targets of interest are several meters deep and the penetration achievable at the site is less than 1 m. Rather than blindly collecting (what will likely amount to useless) data, a better strategy would be a coarser reconnaissance survey of the proposed site to find if there are areas where adequate penetration is achieved. The finite, site-specific limitations of the GPR equipment always need to be considered so that useful data are collected and field time is optimized.

The next sections discuss the various processing operations that are routinely applied to GPR data. Details of the processing strategies can be found in numerous references (e.g., Annan 2005). Rather than focusing on the generalized GPR case, the discussion is treated more as a UXO-specific case study of GPR processing. Results are used from GPR data collected at a UXO test site in Ashland, OR.

5.1. Targets

Data were collected at the Ashland GPR test grid with a range of GPR frequencies (250, 500, 1000 MHz). A grid was collected over four targets as depicted in Figure 13. The grid was 12 by 3 m, and consisted of orthogonal sets of survey lines acquired at a line spacing of 0.2 m and a station interval of 2.5 cm. Care was taken when placing the targets in the test site to note the depth and target orientation. Digital photos were also taken of the targets prior to burial. In the grid displayed in Figure 13, the origin of the grid is the bottom left corner. X-Lines were collected parallel to the long dimension of the grid, while Y-Lines were collected parallel to the short direction of the grid. Target type and recorded depth are indicated

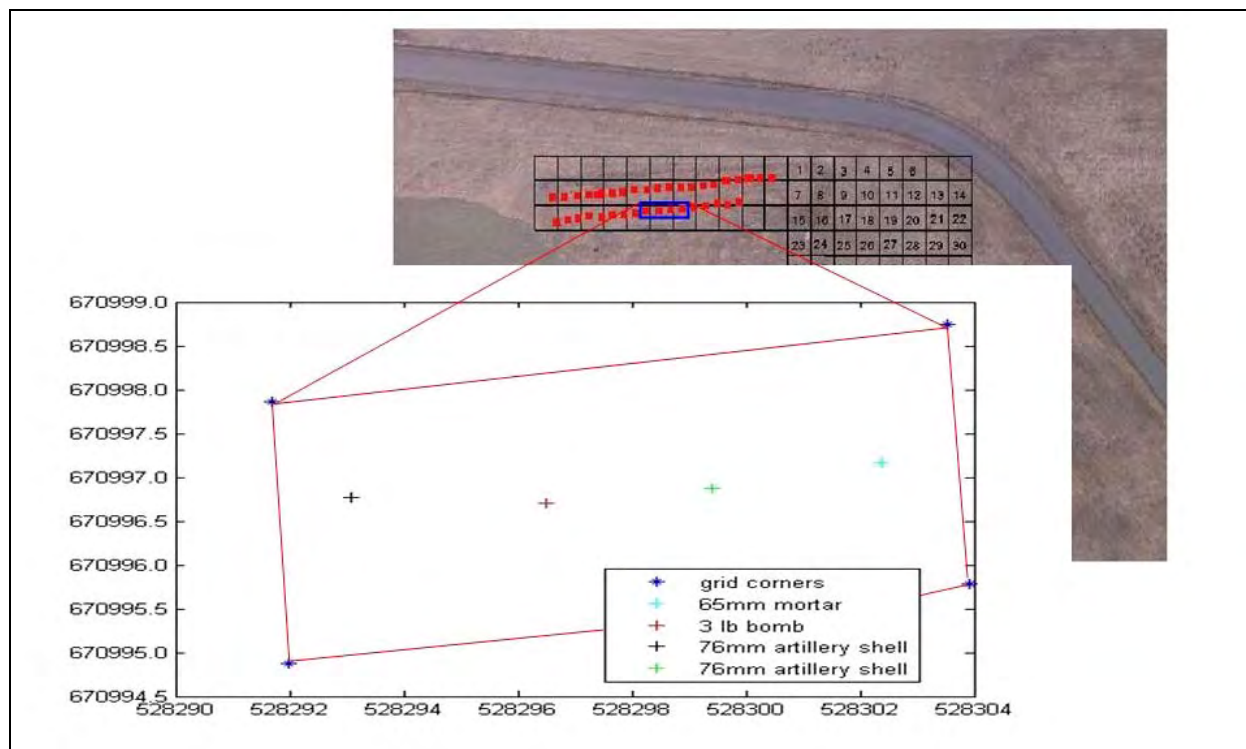


Figure 13. Targets contained in the survey grid collected at the Ashland test site and used in this section as a case study for the processing of GPR data.

in Table 2. Length and diameters were not recorded prior to burial, so values are a combination of measurements on similar targets and those obtained from ORDATA resources. Depths inferred from GPR measurements discussed in this report tend to be deeper than those reported. GPR depth estimates are dependent on an accurate estimate of the signal velocity to convert the travel times into depths. This site was particularly troublesome for assigning a representative velocity because of the varying amount of water and the air gaps that occurred over emplaced targets where the ground had subsided.

Table 2. Targets contained in the survey grid collected at the Ashland test site. Targets are listed as they appear in left to right fashion in the map view of Figure 13.

Target Type	Depth, m	Length, m	Diameter, mm
76-mm artillery shell	0.52	0.25	76
3-lb bomb	0.3	0.21	55
76-mm artillery shell	0.6	0.25	76
60-mm mortar	0.34	0.3	65

5.2. Editing data

There are often a number of tasks that need to be performed on survey data prior to applying processing. These could involve merging GPS information with the GPR data, making topographic corrections, accounting for obstacles in the field, and fixing any data glitches or problems encountered in the field.

5.3. Dewow filter

The dewow filter is a temporal filter that is nearly always applied to GPR data to remove very low-frequency components in the GPR response, commonly referred to as “wow” in the data. These low-frequency components depend on the proximity of the transmitter and receiver and the electrical properties of the ground and occur when the transmit signal induces a slowly decaying low-frequency “wow” on the recorded trace, which is superimposed on the high-frequency reflections of interest. This filter acts to remove the undesired low-frequency response while retaining the information in the high-frequency signal. Applying the dewow filter should always be the first step in the processing of GPR data.

5.4. Time gains

The signals recorded from depths by the GPR instrument are always a tiny fraction of the signal emitted into the ground. The attenuation of the signal will vary significantly with soil type and water content but responses from depth will always be weak and require some sort of time gain to visualize these weak responses. Consider, for example, the GPR section illustrated in Figure 14; these are the raw GPR data acquired with no gain or other processing applied to the section. There is little useful information that can be obtained from this image. The only features of note in Figure 14 are areas where holes were dug to place targets and the ground has since subsided slightly, generating air gaps relative to the rest of the line, which appear in the image at early times.

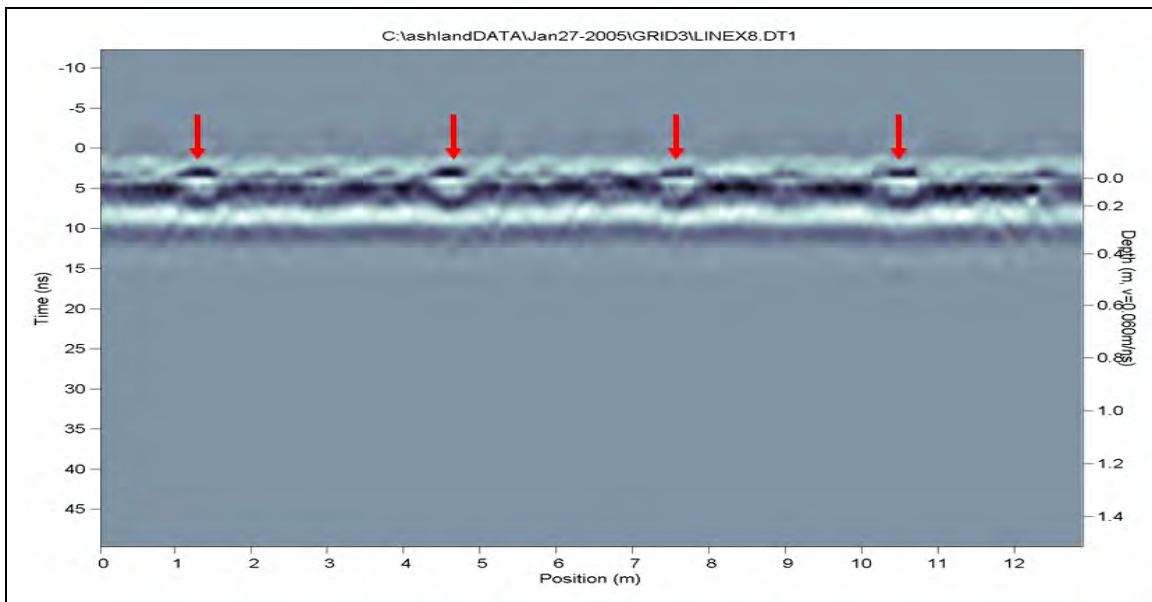


Figure 14. A GPR section with no gain or processing applied. Red arrows indicate areas where ground has subsided and air gaps are present. No UXO targets are visible.

It is only with the application of an appropriate gain function that signals from deeper depths can be observed. The simplest gain function that can be applied is a constant gain where every point in every trace is multiplied by the same factor. The same GPR section observed in Figure 14 is displayed in Figure 15, but this time with the dewow filter applied and a constant gain of 70 applied. Some of the deeper weaker targets are now evident in Figure 15 and can be identified by the hyperbolic shape of their responses. A weak target is observed at a position of approximately 1.5 m and a time of 20 ns, a strong target is centered at about 10.5 m and a time of 15 ns.

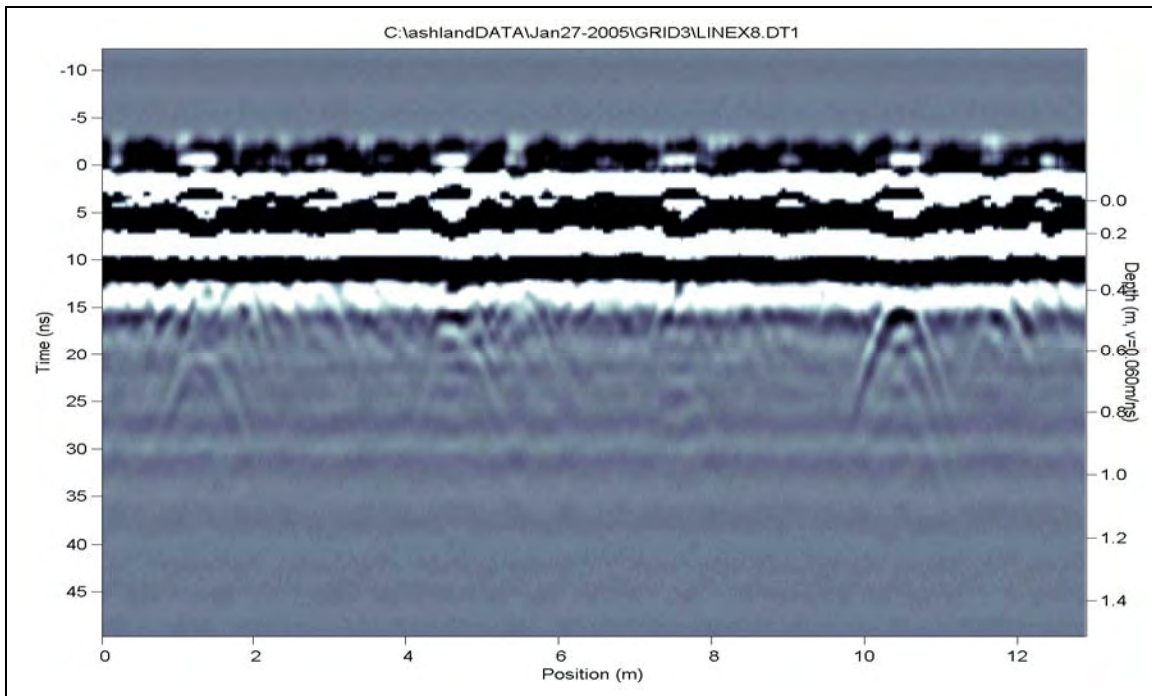


Figure 15. The same GPR section illustrated in Figure 14, but with a constant gain of 70 applied.

There is a questionable target at 4.5 m and 15 ns where there is a discernable response but the hyperbolic tails are not well defined. Although there was evidence of a hole in Figure 14 at a position of approximately 8 m, there is no observed target at depth in Figure 15. This could mean the hole was left empty, the target may be deeper than the GPR was penetrating, the target may be shallow and masked by the horizontal features between 0–15 ns, or the target may not be resolvable with the frequency of GPR employed (250 MHz). The problem with the constant gain is that while the deeper targets are detected, the stronger early time responses do not need such a strong gain function applied and they quickly become over-gained. This over-gaining makes it difficult to investigate responses from relatively shallow targets, which are particularly problematic for UXO targets, many of which can be expected at relatively shallow depths. It is desirable to define a gain function that can amplify weaker signals without saturating the observed response for stronger shallow signals.

The Automatic Gain Control (AGC) attempts to equalize all signals to the same level by applying a gain that is inversely proportional to the signal strength. The advantage of this approach is that all targets are likely to be visible in the image, and so this type of gain may be appropriate for a target detection mode; however, all relative information about amplitudes is lost in applying the AGC gain. Discriminating targets based on observed

amplitudes is not appropriate after applying an AGC gain. Figure 16 shows an AGC gain applied to the GPR section of Figure 14. The targets at 1.5 m and 10.5 m observed in Figure 15 are still both evident in the AGC image of Figure 16. The questionable target at 4.5 m does exhibit slightly more pronounced tails in the image of Figure 16. However, the observed response around 8 m is still somewhat inconclusive although a faint, deeper target at approximately 22 ns begins to emerge.

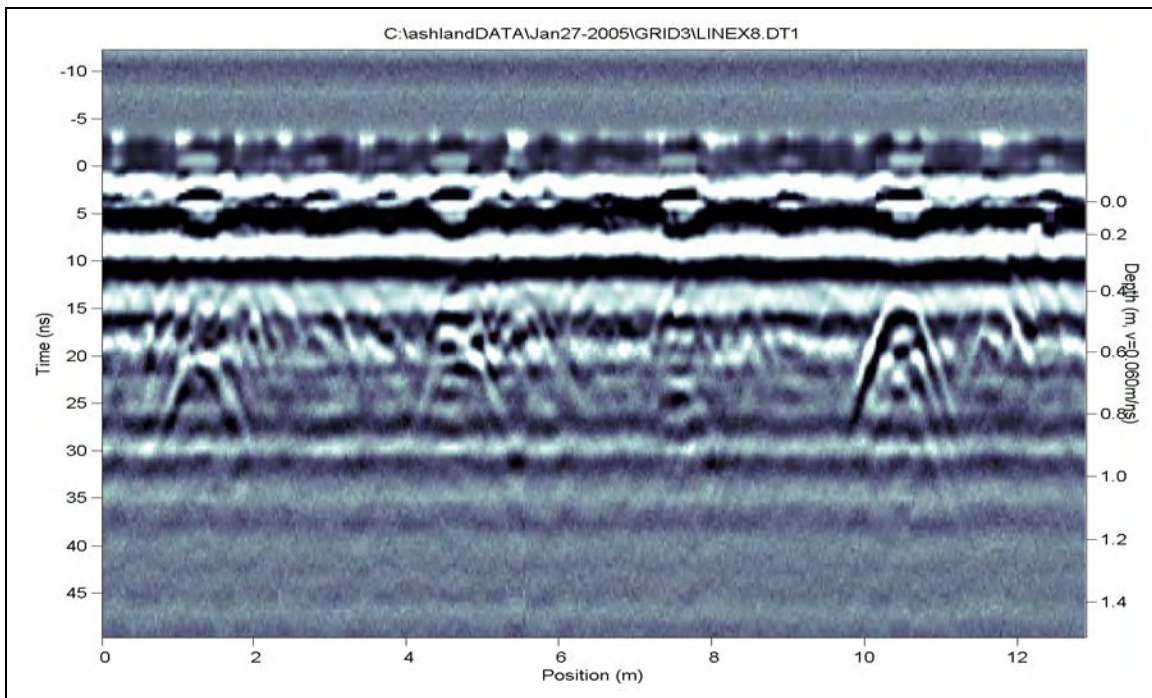


Figure 16. The same GPR section illustrated in Figure 14, but with an AGC gain using a window value of 1 pulse width (in nanoseconds) and maximum gain value of 400 applied.

The final variation on time gain, illustrated in Figure 17, is the SEC gain. This gain function attempts to account for signal losses with penetration. In this case, a start value is specified in addition to an attenuation value, which determines how rapidly the SEC (spherical and exponential compensation) gain function will increase until it reaches a user-specified maximum value. This particular gain function is able to display target responses from all four targets as illustrated in Figure 17. Because the SEC gain is based on the physical nature of the spherical spreading losses, it does a better job maintaining relative amplitude information than the AGC gain.

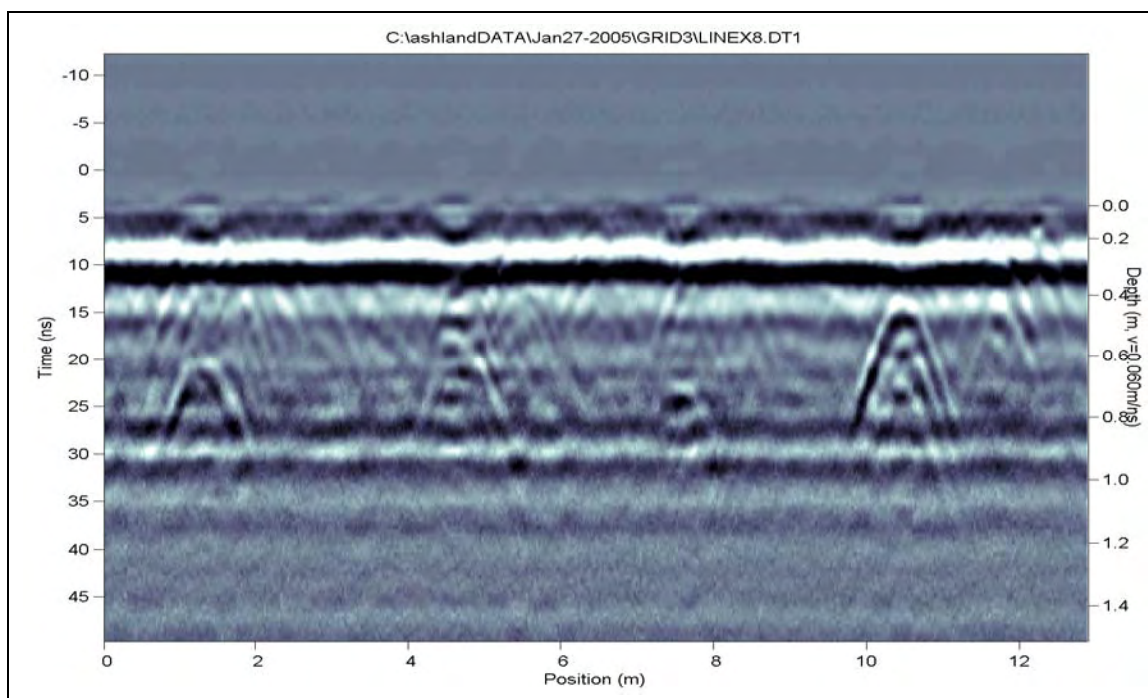


Figure 17. The same GPR section illustrated in Figure 14, but with an SEC gain using a start value of 0, attenuation of 7, and maximum value of 400 applied.

Other gain functions may work as well as or better than those presented here. The main point to emphasize is that the GPR system is recording the raw data and they are essential to apply some sort of gain function when analyzing and processing the data post acquisition. This is often an iterative and experimental approach as different soils will exhibit differing attenuations and, therefore, require unique, site-dependent gains. There is also some subjectivity of the user processing the data as to what gain function best illustrates the intended targets.

5.5. Additional processing

5.5.1. Filtering

A major challenge with the use of GPR for UXO detection is the presence of clutter. As seen in Figures 15–17, UXO targets will generally produce hyperbolic responses when a GPR transect is collected over a target. It is, therefore, not unreasonable to attempt to remove flat-lying horizontal reflectors from the GPR data. These horizontal reflectors represent soil horizons, system-specific banding, and at early times, the direct air and ground wave events. A more challenging clutter issue is the fact that localized targets such as large rocks, tree roots, pipes, etc., will also generate hyperbolic responses in the data. The ability to differentiate

legitimate UXO targets from this type of clutter will involve detailed examination of amplitudes and polarities of the observed responses and will likely require coincident EM and magnetic survey information (e.g., to rule out nonmetallic GPR false positives).

5.5.2. Background subtraction

A number of filtering techniques can be applied in an attempt to remove flat-lying reflectors while maintaining responses from steeply dipping reflectors such as the hyperbolic tails generated from the UXO targets in Figures 15–17. A high-pass spatial filter, for example, will suppress longer wavelength spatial scales while enhancing the shorter scale spatial variations. Flat reflectors can also be de-emphasized by trace differencing whereby each trace is replaced with the difference between that trace and the adjacent trace. A running average or background subtraction filter can be applied whereby a user-specified window of traces is averaged and then subtracted from the trace occupying the middle of that window. In Figure 18, an average trace was calculated over the entire section displayed in Figure 17, and that average trace was then subtracted from every trace. In comparing Figures 17 and 18, it is clear that the dominant horizontal features evident in Figure 17 have been removed in Figure 18. The air gap effects visible in the raw data of Figure 14 are more pronounced now that

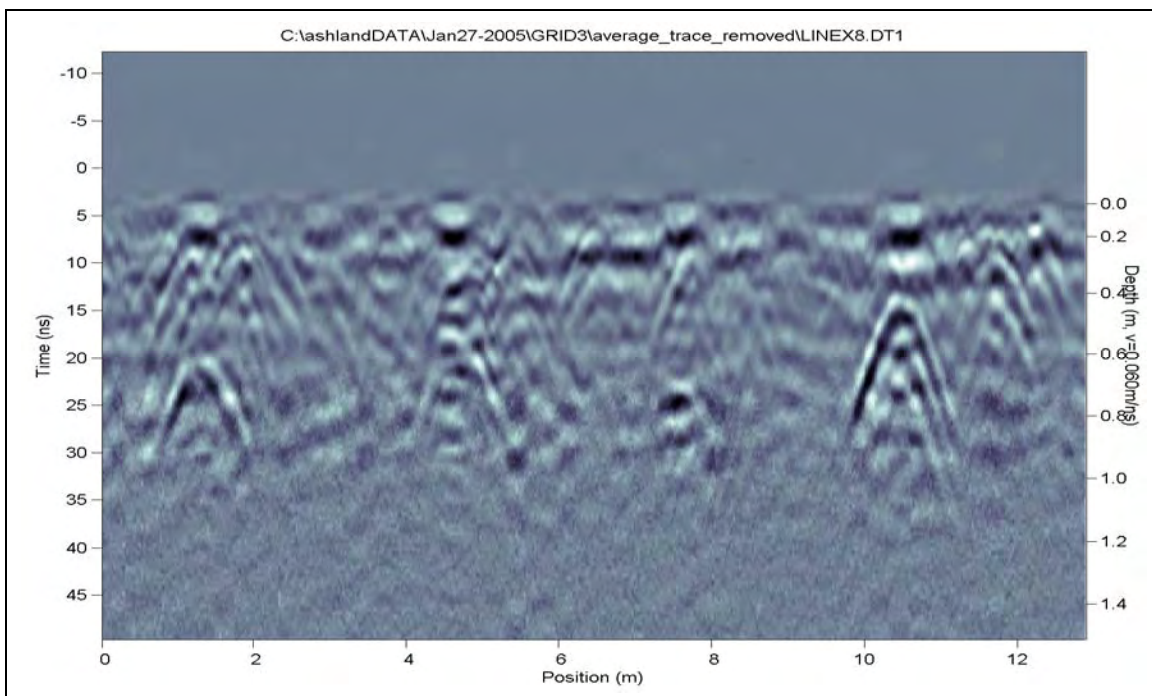


Figure 18. The same GPR section illustrated in Figure 14, but with the average trace removed and an SEC gain using a start value of 0, attenuation of 7, and maximum value of 400 applied.

the strong horizontal early arrivals are removed. The target responses themselves have not changed significantly. The importance of understanding the penetration limitations of GPR is also illustrated in Figure 18. Below 30 ns in time (or just past 1.0 m in depth), no coherent signal is observed. Any targets deeper than this will not be detectable in the GPR measurements. There is a potential target at about 25 ns and position 8 m; however, the tails are not nearly as obvious as the shallower targets as the signal has been more severely (almost entirely) attenuated at this depth.

Temporal filtering can also be applied to the GPR data. The concepts are analogous to the spatial filtering discussed above except that time filters are usually applied to a section of data one trace at a time. Time filters can often assist in the removal of high-frequency noise in GPR data.

5.5.3. Migration

When an appropriate gain function has been selected and the necessary filtering has been applied to the data, it is often useful to further manipulate the GPR data with processing steps that assist in the visual representation of the data. The migration process acts to focus energy from scattering sources back to the source point. This is a better representation of the true ground response. However, it requires knowledge of the velocity structure of the survey area. Based on the shape of the hyperbolic responses in Figure 19, velocity for the area was estimated at 0.06 m/ns.

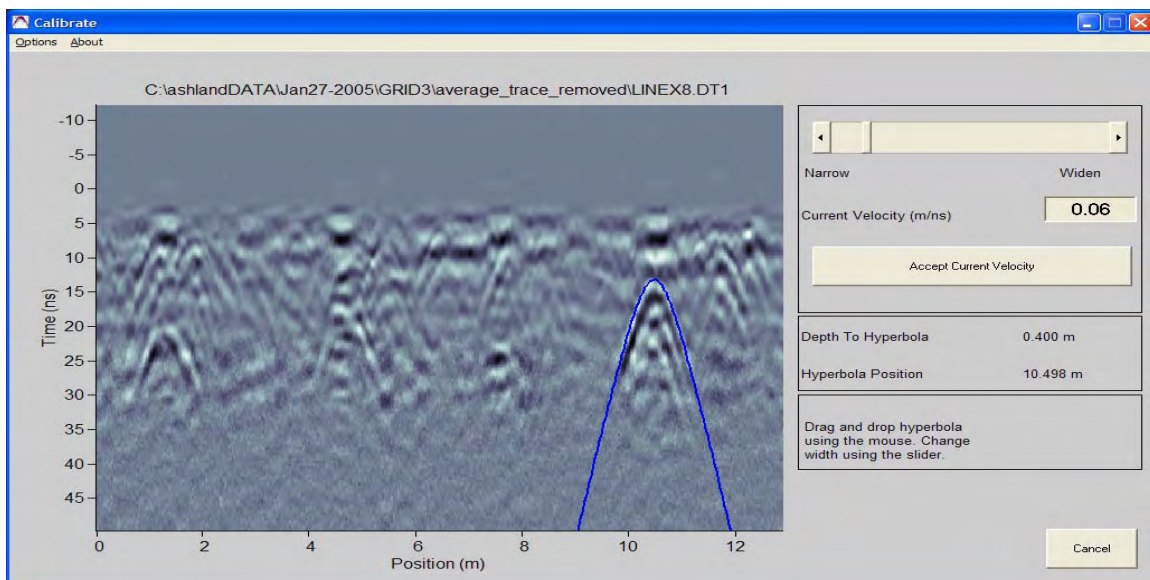


Figure 19. Calibrating a hyperbolic response to obtain a velocity estimate.

This velocity value is on the slower side of typical velocities and is an indication of the rain received at the site on the day prior to the survey. With knowledge of the velocity, migration was applied to the data shown in Figure 18 with the resulting section displayed in Figure 20. In comparing with Figure 18, it is immediately clear that the targets are not as easily identifiable without the hyperbolic tails. The target responses are indicated by the red circles. While it may be easier to identify targets without the migration applied, the migration can help to clarify the picture when creating plan maps or 3D volume visualizations. The hyperbolic tails do not spread energy over multiple time/depth slices after migration has been applied. Rather migration results in a high-amplitude event occurring over a smaller time range corresponding more closely with the actual depth of the target. The result is that the target response appears as an area of high amplitude over a relatively tight time slice interval rather than appearing to span multiple time slices. Migration is often more effective when combined with an enveloping routine.

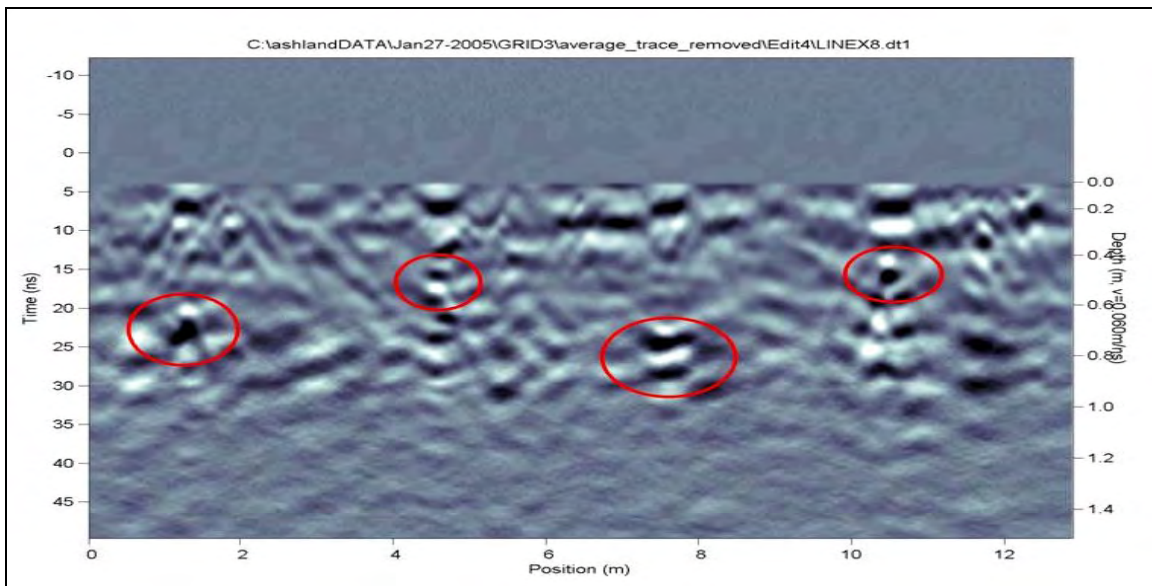


Figure 20. The same GPR section illustrated in Figure 18 (average trace removed, SEC gain 0, 7, 400), but with migration applied using a velocity of 0.06 m/ns.

5.5.4. Enveloping

Part of the difficulty in interpreting the migrated image of Figure 20 is due to the oscillatory nature of the GPR signal. The interpretation is often simplified by calculating and displaying the envelope of the data. The enveloped response is also a better representation of the actual resolution rather than the often misleading resolution inferred from the oscillatory

nature of GPR pulse. Figure 21 illustrates the migrated section illustrated in Figure 20 after enveloping via a Hilbert transform has been applied.

The enveloped image of Figure 21 is easier to interpret, particularly for the deeper targets indicated at A and C. The target at position D is not as well defined as the deeper targets, most likely as a result of an overlap between the events observed due to the ground subsidence of the target and the target response itself. Target B is also somewhat ambiguous partially due to the air gap effects of the ground subsiding, but mainly a consequence of the absence of a strong target response in the recorded data.

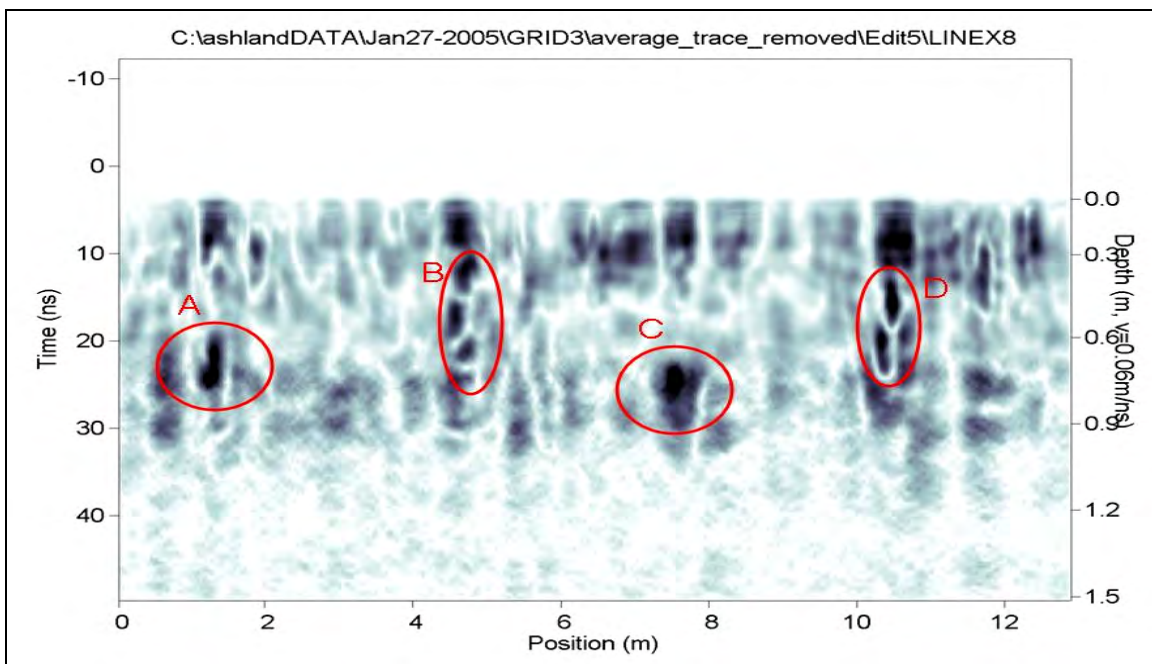


Figure 21. The same GPR section illustrated in Figure 20 with enveloping applied via a Hilbert transform.

5.6. Extending the picture: Adjacent survey lines

Up to this point, all of the processing has been applied to a single line of GPR data in an attempt to extract the maximum amount of information from that single line of data. As much as the target information has been improved by these additional processing steps, a single line of data should never be considered adequate for target identification. A survey grid needs to be defined with a series of parallel and perpendicular lines covering the area of interest. These lines should be spaced closely enough that multiple lines cross a given target. This is very much dependent on target size, orientation, and the size of the survey area, but in practice, these lines

should be spaced as closely as possible to obtain the maximum amount of information. A major challenge with using GPR for UXO detection and discrimination is that there is significant potential for the presence of clutter of the same dimensions as the target (tree roots, rocks, etc.). The more meaningful information available for the interpretation, the more insight that can be offered.

Consider for example the single survey line that appeared in various stages of processing in Figures 14–21. It is illustrated in Figure 22 (the middle image) along with the two adjacent survey lines to the right (top two images) and the left (bottom two images). Of the possible targets identified from the responses in Figures 14–21, the most prominent target, when considering the five adjacent lines in Figure 20, is the target centered at approximately 10.5 m, which appears on the first four lines at the same position and depth. With these multiple target responses, some relative characterization of the target can be estimated using the knowledge that the lines were spaced 20 cm apart. The next-most identifiable target is centered at approximately 1.5 m along lines X8–X10 in Figure 22. The deeper response with no distinct tails is also observed in three separate lines (X7–X9) at a position just less than 8 m. The weakest of the four potential targets identified in Figures 14–21 is also ambiguous over the adjacent lines; rather than a distinct target response, it appears to be just an area of disturbed soil. The ability of a target to generate detectable responses on multiple lines may prove to be an important consideration when extracting target information. There are also clutter responses in some of the adjacent lines including the shallow (about 5 ns) hyperbolic response centered just past 2 m on lines X6 and X7 and another shallow hyperbolic response in line X10 around position 3 m.

5.7. 2D plan map images

The next step in the interpretation process is to use the target information contained in adjacent lines to create 2D plan map views of the subsurface. The investigation of targets by scanning multiple profiles quickly generates large volumes of data and it becomes beneficial to define a standard processing procedure for data reduction and analysis. One such method of combining multiple profile survey lines into a single image is the creation of a plan map view. For data examined here, survey lines were separated by 20 cm and trace sampling intervals along the line were 2.5 cm.

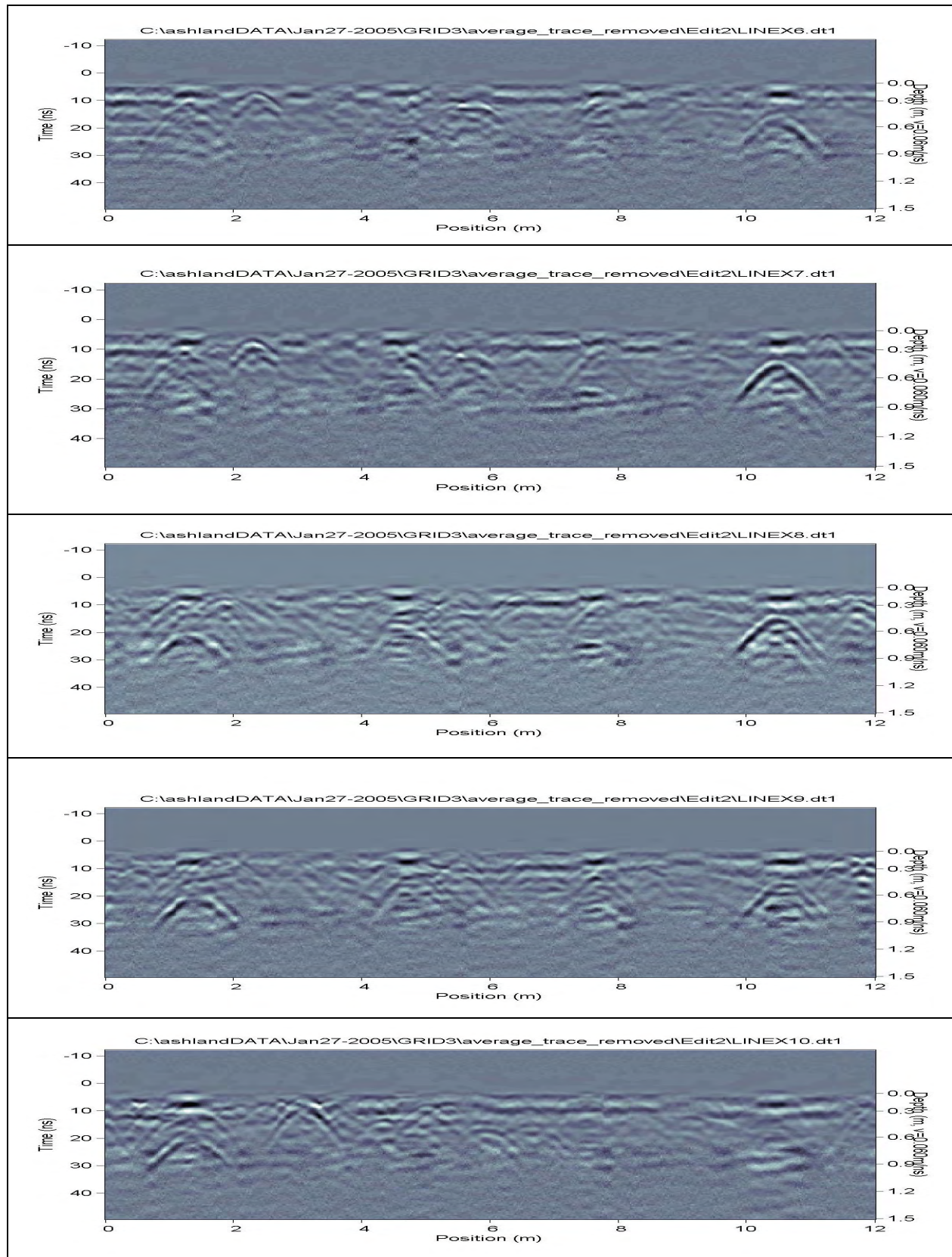


Figure 22. Adjacent survey lines (X6, X7, X8, X9, X10) from top to bottom. Lines were separated by 20 cm. Each line has dewow and SEC gain (0, 7, 400) applied.

To generate the plan map images, an average trace was calculated and removed from each survey line to minimize the direct air wave and ground wave arrivals and any flat-lying geology. A dewow filter was applied to remove unwanted ground and antenna low-frequency content from the data. Migration was applied to focus the energy from scattering hyperbolas back to the actual scattering source. A Hilbert transform is then used to calculate the energy envelope and the average rectified energy for the chosen depth slice is displayed.

An example of the types of images that can be generated is given in Figure 23, which displays the average amplitudes over the depth range between 0.3 and 0.8 m. The challenge in interpreting this image is the presence of a strong response over this depth range, which is not the result of a known target (just less than the 2-m position on the X-position axis). In fact, the amplitude of this non-known target is higher than the actual targets. These issues are examined in further detail in the following discussion of 3D volume images where the same challenge occurs. It is also possible to define a narrower depth slice and attempt to better isolate individual targets.

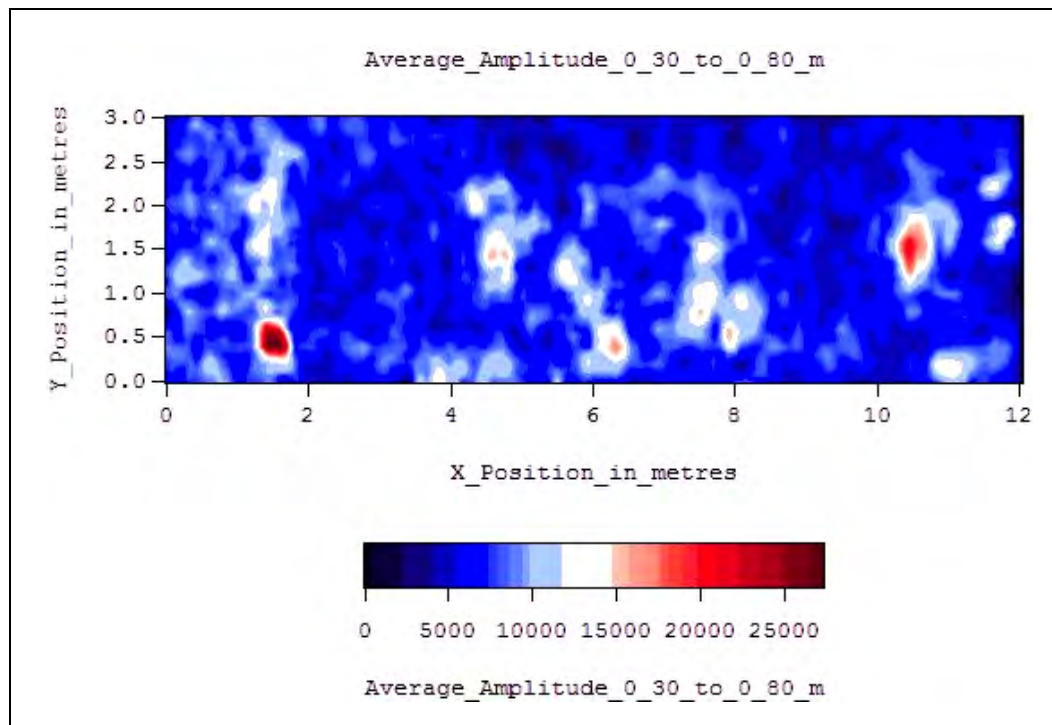


Figure 23. Plan map view of the survey area displaying the average amplitudes over the depths of 0.3 to 0.8 m.

These maps provide an indication of the reflectivity of targets in the subsurface. The scalar diffraction processing employed to arrive at these reflectivity imaging maps is based on concepts of the scalar wave equation and, hence, ignores much of the physics and vector nature of the EM wave field. Recent work has attempted to extract additional information by considering the full vector nature of the EM fields through inversion of multi-component GPR data (van der Kruk et al. 2003). The resulting processed product represents an estimate of the physical property distribution in the ground and has potential for discrimination of targets.

5.8. 3D volume images

The next step in interpretation is visualizing the data as a 3D volume. An advantage to this approach is that it is often more intuitive than a 2D time/depth slice or a single data line profile. While this method of display can visualize the entire survey data in one image, it is also possible that some of the responses observed in single profiles will be smeared out in the creation of the 3D volume. Interpretation is still a task that requires attention to detail by the person processing the data, and features observed in the 3D images should be confirmed and correlated with results from the individual survey lines.

A 3D volume for the data set which contains all of the survey lines shown in Figure 22 is illustrated in Figure 24 as an animation. In this particular animation, a volume was created that starts after the initial direct wave response and stops once the signal has faded into the noise level. The area surveyed measured 12×3 m and survey lines were collected with a line separation of 0.2 m and a station interval of 2.5 cm. Only the X-Lines were used to generate the animation (Y-Lines were omitted). This survey was conducted using a 250-MHz Noggin antenna. Prior to creating the 3D image, the following processing was applied to each survey line: average trace was removed from the profile, dewow filter, migration (using velocity of 0.06m/ns), SEC gain (1, 7, 400).

5.8.1. Interpretation of 3D animation

A first look at the starting frame of the animation depicted in Figure 24 would appear to indicate four areas of increased amplitude that correspond well with suspected target locations. However, the starting point of this animation is at the 0.2-m depth, which is far shallower than any of the targets identified in the profile images of Figure 22.

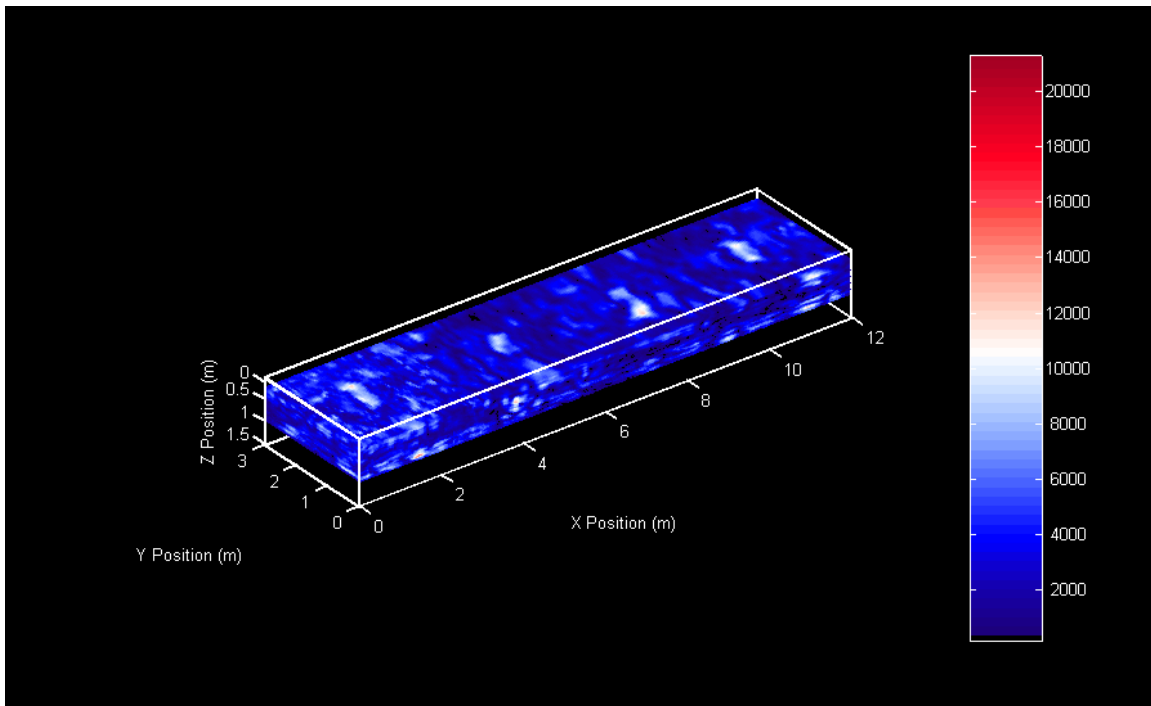


Figure 24. Single frame of 3D animation created from the survey results. Complete animation is available on the ERDC portal.

These responses are actually an indication of the areas where the ground has subsided over the emplaced targets. These responses are observed in the profile images where they extended to times that correspond to depths greater than the actual subsidence observed. The velocity used in creating the depth axis assumes the velocity inferred by measuring the hyperbolic tails on a response from a buried target. However, over the buried target subsidence the GPR signal is actually traveling through air (and therefore travels more than three times faster than the velocity assumed for soil when creating the depth axis). As a result, the effects from these air gaps appear to generate a response at depths much deeper than their actual observed depths. The responses from actual targets occur at later times (deeper) and are, unfortunately, much weaker than the early time responses generated by the ground subsidence. Based on the survey lines in Figure 22, the shallowest target occurs at a position just over 10 m along the survey lines at a depth between 0.5 and 0.6 m. Consider the 3D image truncated at a top depth of 0.49 m shown in Figure 25. There is an elevated response observed in this same region where the hyperbolic targets were observed in Figure 22, indicated by the letter A. The challenge in the interpretation is that there are similar magnitude responses (represented by circles B–E) that do not correspond to any known targets. The obvious question is Can targets and clutter be distinguished?

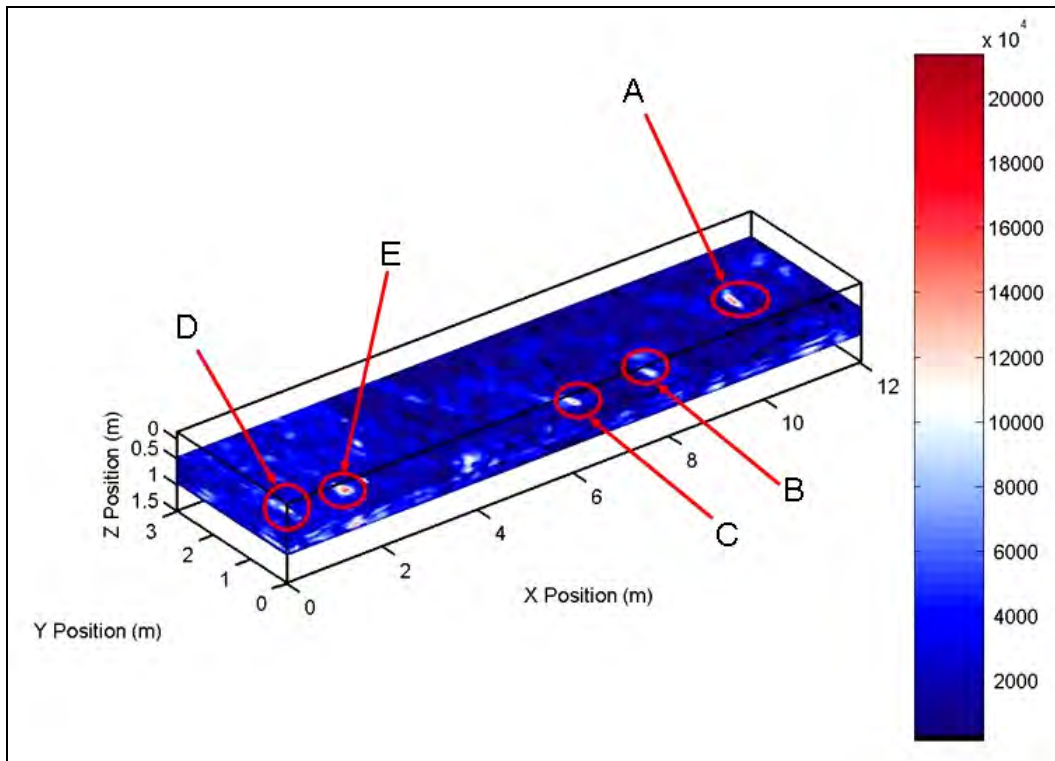


Figure 25. 3D image of the survey results truncated at 0.49-m depth. Target indicated by A corresponds to a known target location; however B–E (which represent similar amplitudes) are not relatable to any known targets and likely represent clutter.

5.8.2. Known targets versus unknown clutter

In considering responses B–E, which do not correlate with any known targets, it is useful to examine the corresponding survey line profiles to determine what type of response in the profile data generates these observed responses in the 3D image. Targets B–E all occur along similar X-Line profiles which appear to span the first 1 m along the Y Position axis. The target locations are better portrayed in the view looking down from above (i.e., the XY view) shown in Figure 26 for a constant depth of 0.49 m.

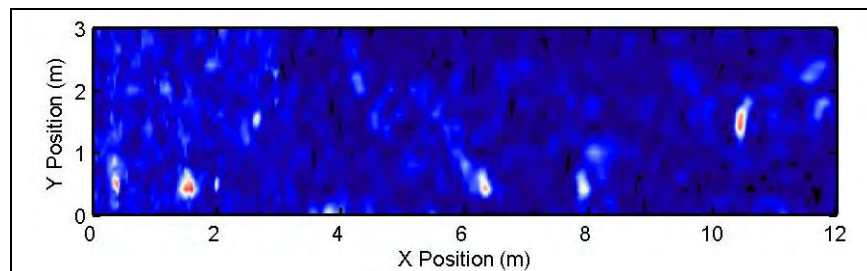


Figure 26. A plan view 3D image of Figure 25 (looking down at a depth of 0.49 m).

Further information in the responses observed in Figure 25 can be obtained from the profile views of Figure 27. Target E is a result of a strong ringing-like response at a position of approximately 1.5 m in the third and fourth lines of Figure 27. The amplitudes are very strong and the response is observed over a relatively long time window. This results in a high-amplitude bright spot occurring at this location through much of the animation represented by the single frame in Figure 24. Ringing responses in GPR data can be the result of poorly constructed shielding but they are more typically caused by a metal object placed near the antennas, or a near surface layer or reflector capable of generating return signals which bounce back and forth between the reflector and antenna multiple times. The ground will usually act to significantly dampen reverberations. However, the type of resonant response observed for target E is not uncommon when the excitation signal, target geometry, and soil properties are in agreement. This same resonant response was observed in the perpendicular survey lines LineY7 and LineY8 (shown in Figure 28) which also crossed the target. Even though this reflector does not correspond to a known target, strong enough returns on multiple lines would suggest that it should be investigated further rather than being written off as clutter. Target D is only observed as weak half diffraction tails in the first two profile lines in Figure 27; and of all the responses annotated in Figure 25, it is the most likely to be clutter, as no significant signal is observed on perpendicular survey lines.

Targets C and B are the result of weaker hyperbolic responses that are observed in both the third and fourth profiles displayed in Figure 27 at positions approximately 6.5 m and 8 m along the profiles, respectively. On the first two profiles of Figure 27, these hyperbolic responses are separated slightly further (centered around 5.5 m, 8.5 m along the line) creating a weak linear diagonal tail, which extends from C in Figures 25 and 26. While the responses do not appear as strong as those observed for known targets in Figure 22, the fact remains that they span multiple survey lines. The ability to compare these GPR results with EM and magnetic data collected over the same area could provide a great deal more insight into the nature of extraneous non-known target responses and allow for a more definitive declaration of these responses as clutter.

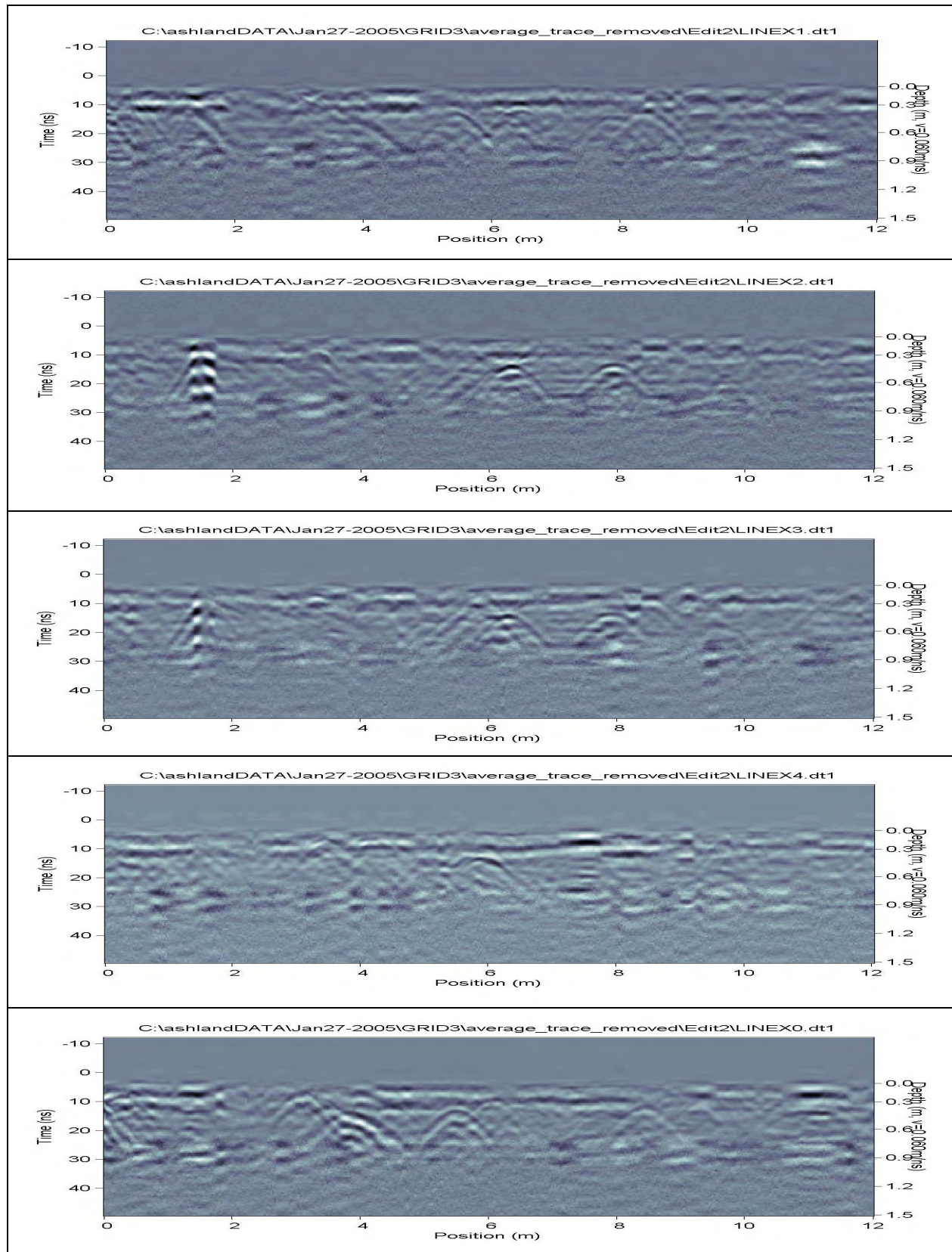


Figure 27. Adjacent survey lines (X0, X1, X2, X3, X4) from top to bottom. Lines were separated by 20 cm. Each line has dewow and SEC gain (0, 7, 400) applied.

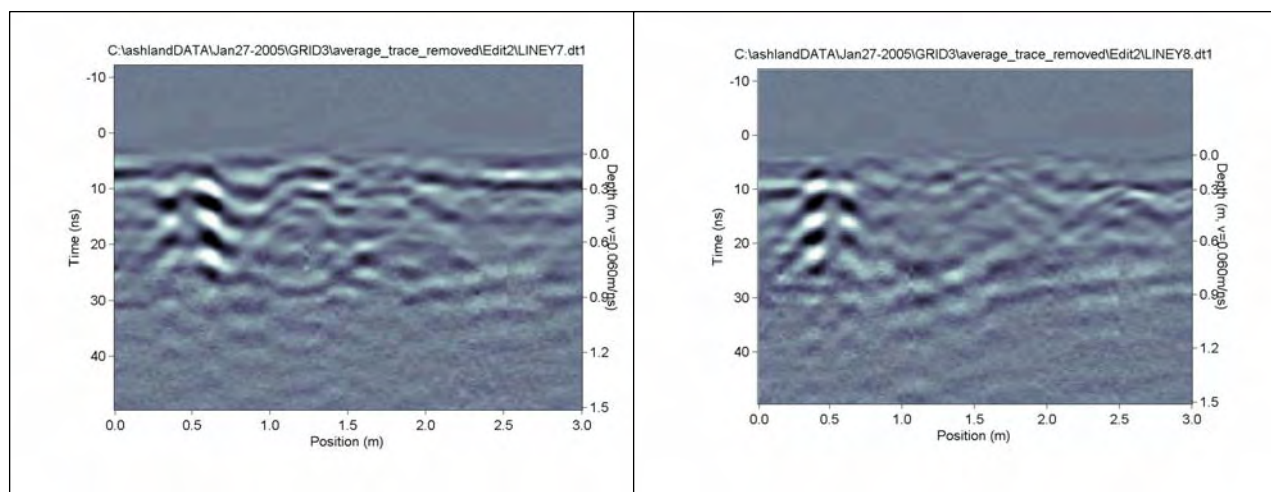


Figure 28. Lines Y7 and Y8, which cross the same resonant response (Target E) on perpendicular survey lines.

5.8.3. Deeper targets

Figure 18 indicated that the next target of interest was located at a depth between 0.6 and 0.7 m at a position of about 1.5 m along the X-position axis. Figure 29 shows the 3D volume truncated at a depth of 0.67 m. Of the areas exhibiting elevated amplitudes in Figure 29, the response annotated by G represents the same strong ringing response observed in Figure 26. Area H is likely due to some residual signal from the strong shallower target (target A in Figure 23). Circled area F is a target response corresponding to the hyperbolic targets in the bottom three profiles of Figure 22.

Deeper still, a target was observed in Figure 18 between the 0.7- and 0.8-m depth just less than position 8 m. The response itself is rather strong considering the depth, yet there are no hyperbolic tails as observed for the shallower targets. The lack of tails is most likely due to the significant signal attenuation. The signal fades out almost entirely just below this target depth. A response is observed in the 3D volume truncated at 0.77 m illustrated in Figure 30, indicated by circle J, which corresponds to this target. Examining the perpendicular survey lines (Y-Lines), which cross the target in the opposite direction to the profiles of Figure 22, it is clear that a distinct deep target is also observed in the orthogonal profiles as shown in Figure 31. The strong localized response indicated by target K is due to the strong, deep response on the second profile in Figure 8 at a position of 11 m. This particular response is not visible on multiple profiles or orthogonal survey lines and does not correspond with the position of any known targets.

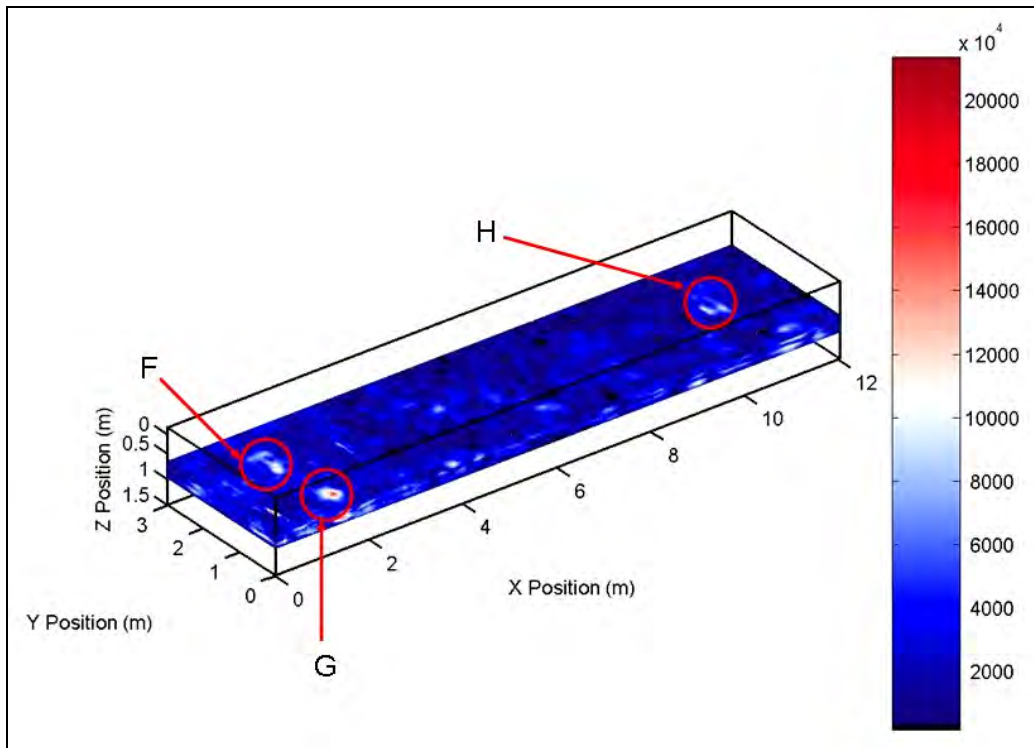


Figure 29. 3D image of the survey results truncated at 0.67-m depth. Targets indicated by F and H correspond to known target locations; however G (which represents a stronger amplitude) is not relatable to any known target and could represent clutter.

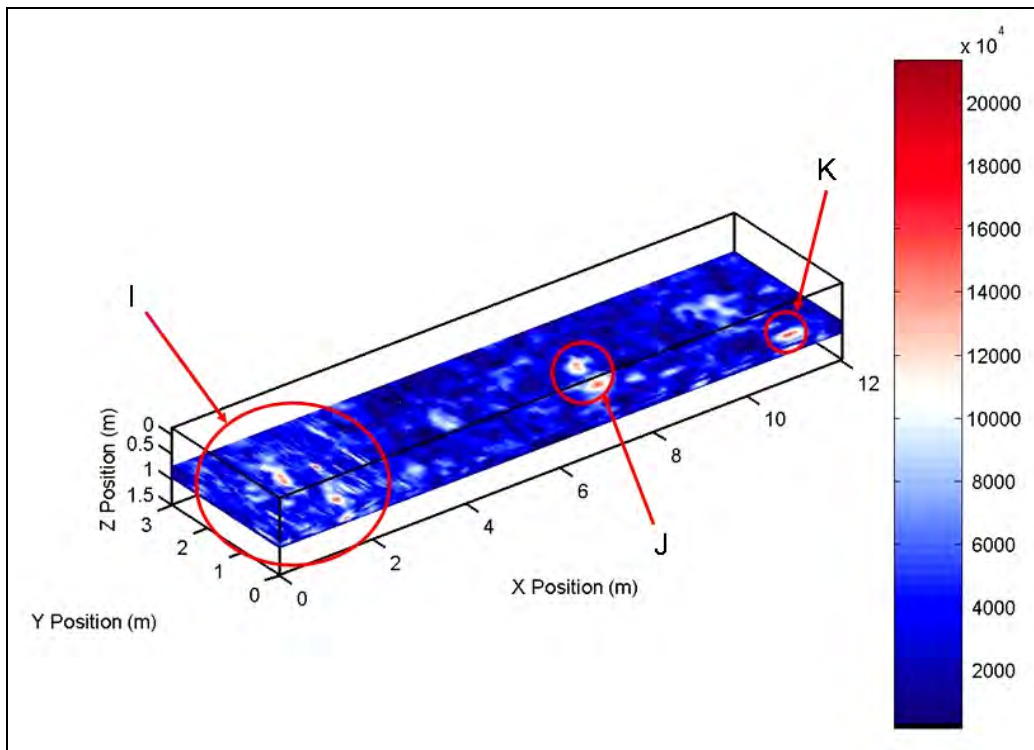


Figure 30. 3D image of the survey results truncated at 0.77-m depth. Target indicated by J corresponds to a known target location. Circle I represents an area of disturbed soil, while strong response at K is not relatable to any known target and could represent clutter.

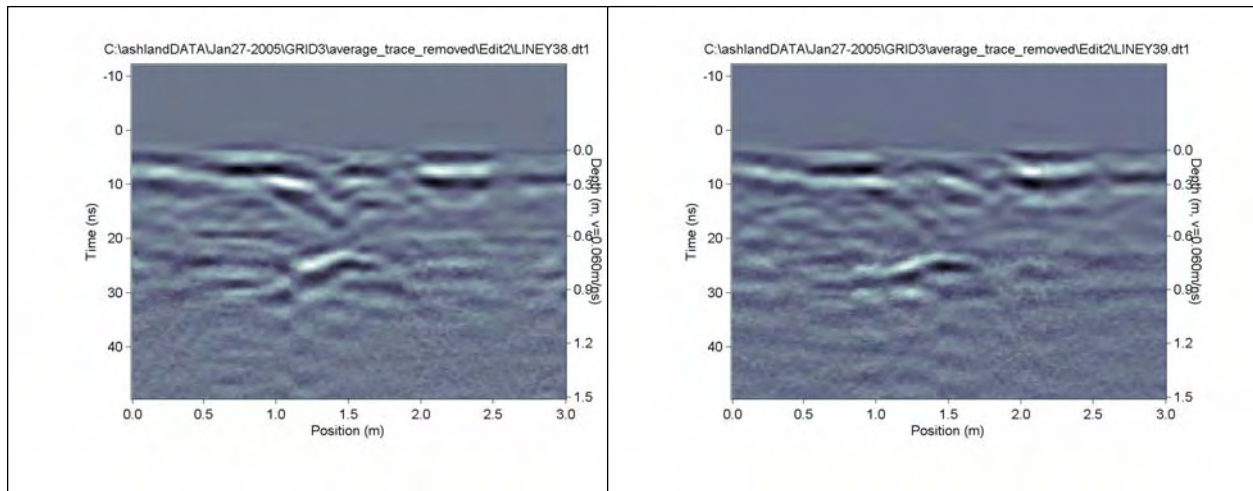


Figure 31. Lines Y38 and Y39, which cross the same deeper target response (Target J of Figure 30) on perpendicular survey lines.

5.9. Discussion

All data presented in this section were obtained with the Noggin 250-MHz system. Due to time constraints, data were not acquired over the grid with either of the higher frequencies. The higher frequencies may have been helpful in resolving some of the targets; however, the attenuation at the site may limit targets that are detectable with the higher frequencies. Line profile data were collected with all three frequencies, and processing of those data will allow for a better understanding of the applicability of higher frequencies for the Ashland test site. The Ashland test site is a realistic site with many of the associated difficulties that come with the application of GPR to UXO investigations. While known targets can be identified, the presence of clutter is a concern. Orientation of the target is also a factor and is best illustrated by the varying responses obtained for the four targets (including two identical targets, 76-mm artillery shells). Some of the known targets do not produce results that can be detected with confidence as is the case for the 3-pound (lb) bomb target.

6 Future Work

Part A focused on an introduction to some basic concepts and considerations when applying GPR methods to the UXO problem. More advanced options for interpreting GPR data need to be considered including improved imaging and inversion processes and the development of methods for combining EM, magnetic, and GPR data in a mutually beneficial manner to input the maximum amount of useful information from a site into interpretations of the subsurface. Chapters 7–10 include a literature review investigating what has been attempted in the past and what techniques hold promise for future refinements of GPR surveying of UXO targets. A range of GPR equipment options available will also be investigated for relative strengths and weaknesses and suitability to UXO investigations.

7 Overview

The following section (Part B, Chapters 8–10) is a continuation and extension of the concepts discussed in Part A (Chapters 1–6). In Part A, an overview of basic GPR functionality, data processing, and survey design considerations were discussed. Many of these concepts were illustrated using data collected from initial measurements at the Ashland test site using a 250-MHz GPR system. Part B continues in the examination of GPR data collected at the Ashland test site, but in this case, focuses on a range of frequencies (250, 500, 1000 MHz) and the comparative information that can be obtained from these respective frequencies. Discussion of the results observed from these initial measurements, limitations of the methods used, and a proposal for use of GPR in a cued-interrogation mode along with the types of information that are obtainable are presented. GPR equipment options are discussed as is some of the previous work where GPR has been employed in UXO and landmine applications.

8 GPR Equipment

GPR detects buried objects by sending out radio wave energy and recording reflections that are generated from subsurface objects, which have contrasting electrical properties relative to the host soil. The GPR signals are reflected and scattered whenever they encounter changes in the electrical properties. These scattered signals provide the means of detecting subsurface objects. Although the principle of GPR operation can be summarized quite succinctly by the previous sentences, the specifics of system design of a GPR system involve electrical engineering details beyond the scope of this report. A good overview of GPR system design considerations can be found in Annan (2005), and Daniels et al. (1988).

GPR systems exist for collecting time-domain (often referred to as impulse GPR) as well as frequency-domain data. In both cases, energy is directed into the ground and scattered energy from buried targets is measured at the surface. Conceptually, both types of systems are similar in that a transmitter generates a signal that is radiated into the ground through an antenna. The main differences between GPR systems are in how the signal is produced and radiated and the type of antenna chosen.

Most commercial GPR units (including the equipment used to acquire the GPR data at the Ashland test site described in Chapter 10) collect time-domain data. In this case, the GPR system is energized by a short pulse of electromagnetic energy (hence the name impulse radar) that covers a wide range of frequencies in the frequency domain. The bandwidth of the radiated pulse is limited by the antenna and the ratio of bandwidth to center frequency is around unity for most commercial GPR systems. An equivalent time sampling approach is typically employed via transmitter control and a variable delay time in order to sample successive points in each GPR trace. These types of systems have been in widespread use for many years and are robust, field-ready equipment.

In frequency-domain equipment, the system is energized by linearly sweeping the transmitter frequencies over a range (similar to the range of frequencies contained in the time-domain pulse). This is often referred to as swept frequency, continuous wave frequency modulation (CWFM) or chirp. The transmitter is always on, and the receiver is always listening in

contrast with the on-off pulsed nature of the time-domain system. The frequencies can also be stepped rather than continually swept. The stepped approach provides the advantage of permitting the selection of a specific frequency spectrum. However, a wider dynamic range is required, and it is often more time-consuming to collect the data.

Ideally both time and frequency-domain systems would produce the same results, but varying electronics and antenna designs mean this is not always the case. Allowing for variations between different systems based on their unique designs, the applicability of all types of GPR equipment will be constrained by the soil conditions. The penetration of GPR signal is primarily determined by the site-specific physics of EM wave propagation and scattering. These effects are illustrated in the GPR soil suitability map described by Doolittle et al. (2002). Excellent overviews of the soil properties and their effects on GPR measurements are available in Cross (1999) and Olhoeft (1998).

The platforms used for deployment of GPR sensors are highly variable. Many of the GPR sensors proposed for landmine detection are hand-held devices. GPR systems are also mounted as a single sensor on carts that use an odometer to trigger measurements at regular intervals. Array-based GPR systems extend the concept of the single cart-based GPR sensor by mounting multiple GPR sensors on a single platform, which is often vehicle mounted (Birken et al. 2002). These systems have the benefit of covering an increasingly larger area as the number of sensors in the array increases. Some of the recent sensor arrays have incorporated both electromagnetic induction (EMI) and GPR instrumentation in an effort to enhance the interpretation via data fusion from multiple sensors (Oristaglio et al. 2005).

Another consideration is the choice of antennas to be used with the GPR system. The transmit antenna must convert a supplied voltage into a predictable and repeatable field that is emitted into the ground. The receive antenna needs to detect the vector component of the electric field that is emitted by the transmit antenna and altered by the ground response. Antenna design is beyond the scope of this report, and only some of the key concerns are discussed here. Further details on antenna design for GPR systems can be found in Annan (2005); Baum (1999); and Daniels et al. (1988). Most commercial GPR system antennas (including the equipment used at the Ashland test plot) use resistively loaded dipoles. For

ground coupled systems, antennas need to be kept in close proximity to the ground surface. As these antennas are raised above the surface, GPR performance deteriorates. A large amount of signal will be reflected at the air-ground interface and will not penetrate to target depths. The direct transmitter-receiver and air-ground arrivals will also be non-time coincident and will result in strong events that reduce the target's amplitude as well as potentially masking shallow targets. Some antennas have been designed to be operated when elevated above ground. For example, in the landmine case, contact with the ground needs to be avoided for operator safety. Landmine targets are relatively shallow and penetration requirements more modest than required for deeper UXO targets.

Polarization was discussed briefly in Part A. Further details on the importance of polarization in GPR measurements can be found in Daniels et al. (2003). Because electromagnetic waves are polarized, the electric field is a vector pointed in a certain direction with the magnetic field perpendicular to the electric field and a direction of propagation perpendicular to both the electric and magnetic field directions. In the equipment used in the tests at Ashland, antennas were linearly polarized with the electric fields of the transmit and receive antennas aligned parallel to each other. Moving these antennas along survey lines perpendicular to the electric field creates a wave propagating perpendicular to the surface of the earth. This particular configuration is often referred to as parallel broadside. Crossing a horizontal target (i.e., pipe, or of more interest here, a horizontal UXO) with this electric field orientation and direction of traverse results in a hyperbolic response as the target is approached (left tail of the hyperbola), directly above (peak of the hyperbola) and traveled past (right tail of the hyperbola). If this same configuration is used, a line that passes directly on top of a horizontal target over the length of the target's long axis will appear as a flat event as the target remains a constant distance below the sensor. All of the data initially collected at the Ashland test plot were in the parallel broadside configuration, and some success was achieved inferring orientation from a number of traverses perpendicular and parallel to a slightly dipping UXO target. If bistatic antennas are used, orientations of the antennas (and the electric fields) can be altered and different target information extracted. Multiple polarization data are important for complex natural resonances (CNR) discrimination (Chen et al. 2001) as well as in full waveform inversion (van der Kruk et al. 2003).

Recent years have seen an increasing interest in GPR for a growing variety of applications, and as such there are a number of commercial GPR units available with varying levels of flexibility and complexity (further details are available at Web sites of the major commercial manufacturers: www.geophysical.com, www.malags.com, www.sensoft.ca). In addition to commercial units, there are also a number of experimental and prototype GPR systems designed to greatly increase GPR performance and drive research of GPR technology. Some systems are geared towards improving GPR performance in difficult environments (Wright et al. 2005), while other systems are designed to collect larger bandwidths and fully polarimetric data (Chen et al. 2001). Some of these systems are experimental by design and may not be suited to the rigors of rough terrain. Such systems are often the sole system built with no equivalent equipment available in case of component failure. An expert familiar with the particular instrument's operation and data may be required to collect quality data. It is unclear whether all of these experimental systems meet current FCC regulations for emission standards of Ultrawideband Devices (complete Part 15.509 rules available at www.fcc.gov/oet/info/rules). The Ashland test plot will provide an excellent opportunity to further investigate some of these more research-oriented GPR systems and compare results with those obtained using commercial GPR systems.

The goal is to use the best available systems to collect the highest quality data in order to investigate what information can be extracted from GPR measurements and determine what needs to be considered in the survey design stage to maximize target information. Initially, the procedure will be tested on smaller scales with known targets and perhaps some blind tests, but the eventual goal remains to devise a procedure that can be applied by a non-expert with adequate coverage in a cost-effective manner. This ultimately requires accurately positioned GPR data, a reproducible soil independent adaptive signal processing sequence, and an ergonomic operator response indication. ERDC intends to focus on commercially available GPR systems for proven field robustness and ease of operation that best translates into a tool that can be easily operated by a non-specialist. Initial results from testing at the Ashland test plot (see Chapter 10) indicate that useful target information can be extracted from the data obtained with the commercial GPR systems employed.

9 Previous Work

Much of the GPR work in the literature has focused specifically on the issue of landmines rather than UXO. GPR has not gained widespread acceptance as a useful tool in UXO detection and discrimination due to (1) the large number of false positives, and (2) UXO targets are typically relatively shallow with significant ferrous metal content, which leads to much more practical detection of UXO targets using magnetometry and EMI methods. Methods suited for metallic UXO targets are not effective for low-metal landmines and much effort has been made to adapt and optimize GPR methods for the landmine problem. The nature of the targets and system requirements differ enough to treat UXO and landmine work as separate cases. An earlier review of GPR-related UXO work described in Andrews et al. (1999) provides a useful overview of work in the UXO and landmine arenas.

9.1. UXO-specific work

Because the detection of UXO targets is commonly achieved via magnetometers and/or EMI systems, the most promising role for GPR is in the discrimination of UXO targets. This may include details on the depth to the target, the number of targets present, possible indications of target orientation and, in some cases, predictions of target type based on resonance responses. Areas that have high densities of UXO targets and that may produce overlapping signatures in EMI or magnetic data could benefit significantly from the additional information that GPR may be able to provide. This information can be used to constrain inversions of EMI or magnetic data. The choice of appropriate GPR frequencies is somewhat of a dichotomy. By necessity, frequencies employed need to be low enough in order to penetrate to desired UXO target depths and to minimize scattering from smaller scale features which can generate false alarms and limit penetration. This is counter-intuitive to the desire to increase resolution of the GPR images by using higher frequencies with larger bandwidths. The primary importance needs to be the penetration depth, and so the most useful GPR frequencies for eliciting useful UXO information are on the order of hundreds of megahertz rather than thousands of megahertz. At such frequencies, the wavelengths of the GPR signal will be similar to or greater than the dimensions of the intended targets and, consequently, will produce images of low resolution. However, indications of important

target details such as depth, general location, and some inferences of orientation can be obtained.

Initial tests at the Ashland test plot (see Chapter 10, Section 10.4.1) indicate that even the lowest frequency used (250 MHz) can provide insight into the target's orientation when a detailed *grid* of data is collected over a known UXO target. GPR systems measure travel times very accurately and consequently can provide accurate estimates of depths to UXO targets when the velocity of the host soil is known (and assuming the GPR signal penetrates to required target depths at the site in question). In areas with multiple targets that are too close to distinguish as individual targets via magnetometer or EMI measurements, GPR has the potential to differentiate individual targets.

Discrimination of UXO targets has also been carried out using CNR, as discussed in Chen and Peters (1997). A resonance occurs when a radar impulse illuminates a conducting target. Many UXO targets have simple geometries, and when dominant CNR are present in the data and with knowledge of the host soil conditions, classifications of UXO targets can be made based on inferred lengths and damping factors. In many types of soil, the high signal attenuation will damp any resonance, making these methods difficult to apply.

There is not an abundance of published work utilizing commercial GPR systems for UXO investigations. In Arcone et al. (2000), data were collected using a commercial system at the Jefferson Proving Grounds (JPG). Even though the soil at the site exhibited severe attenuation, some targets were identified. Responses were subtle and lacking characteristic hyperbolic tails as a result of significant attenuation of the signal by the soil. Arcone et al. also used the phase polarity of the GPR signal to identify targets. A GPR signal typically reduces to a wavelet in time with three half cycles. A positive polarity wavelet has a positive-negative-positive sequence to the phase polarity of the dominant half cycles whereas the negative polarity wavelet is negative-positive-negative. The polarity of a reflected signal is a function of the electrical properties of the target generating that reflection and the surrounding soil. Specifically, the reflection is a result of a change in the electromagnetic impedance. A reflection generated by a target of lower impedance than the surrounding soil will create a negative reflection coefficient. Since metallic targets like UXO

have an electromagnetic impedance of practically zero, they will always result in a negative reflection coefficient.

Some of the most promising applications of GPR towards the UXO problem involve the fusion of EMI and GPR data. For example, Sun et al. (2005) use information obtained from GPR measurements to compensate for a fundamental limitation of EMI measurements whereby the associated wavelengths are orders of magnitude greater than the UXO targets being imaged. The use of these longer wavelengths in EMI measurements is advantageous over the shorter GPR wavelengths as they are not as susceptible to small-scale scattering and attenuation. However, the use of these longer wavelengths in EMI measurements makes target classification problematic in cluttered sites/UXO settings where multiple targets contribute to an overlapping response. The number and location of contributing targets are difficult to discriminate from EMI measurements alone. GPR has its own challenges as a stand-alone sensor technology. False positives from nonmetallic clutter can be problematic, and there are definite site-specific limitations of penetration associated with GPR measurements. Where penetration is adequate, GPR is capable of determining depths, number of targets present (even from closely spaced targets), and can indicate approximate locations and some geometrical information. This information can be used to constrain some of the parameters in the inversion of EMI data. Conversely, the inclusion of EMI data can help to rule out many of the nonmetallic false positives in GPR data.

9.2. Landmine-specific work

GPR has been considered a potentially useful tool for landmine detection. Because it is sensitive to changes in the electrical properties, in theory GPR should be able to detect landmines with little or no metal assuming there is a significant contrast between the electrical properties of the landmine and the host soil. Landmines containing no metal are undetectable using traditional EM and magnetic measurements, which are the industry standard for metallic UXO targets, and GPR has consequently been considered the method of most promise for low-metal landmine detection.

The application of GPR to the detection of landmines remains an extremely challenging problem. Mines are physically small and the signal attenuation is large in many types of soil. Plastic mines are often similar in size and electrical properties to rocks, tree roots, and soil inhomogeneities, all of which will represent clutter in the GPR image and complicate the

target isolation and clutter suppression. Most landmines are relatively shallow, which leads to the use of higher frequencies for improved resolution. The trade-off of the shallower penetration that accompanies the use of higher frequencies is often acceptable for the landmine case, whereas UXO targets require deeper penetrations that necessitate the use of lower GPR frequencies. The sensor is elevated above the surface in landmine detection and variations in the surface topography can further complicate data interpretation. Table 3 indicates the extensive parameter space to be considered in GPR measurements of landmine targets. These variables and their respective parameters apply to GPR measurements in general and also apply specifically to GPR measurements of UXO. The UXO case is made slightly advantageous in that targets are often larger and contain significantly more metal than most landmines.

Table 3. Parameter space describing potential influences on GPR measurements of landmines. Taken from Sensors & Software (2003).

Variable	Parameters of Concern
Landmine	Size, shape, composition, structure, burial depth
GPR Sensor System	Frequency range, bandwidth, excitation antenna, receiving antenna, polarization, signal capture method
Soil	Composition, texture, water content, water chemistry, heterogeneity
Methodology	Scan, sweep, spatial sampling density, sensor elevation, sensor position
Signal Processing	Data standardization, temporal and spatial filtering, imaging operators, attribute definition, target recognition

GPR-related work with landmines is separated into two different types of sensors: handheld sensors and forward- or down-looking arrays. A handheld GPR sensor is used in a similar fashion to a simple metal locator where the sensor head is swept back and forth over the surface and the use detects anomalies whether through a visual display or an audio tone. These systems are lightweight, simple to use, and often contain both GPR and EMI sensor instrumentation in the same unit. The Handheld Standoff Mine Detection System (HSTAMIDS) engineered and manufactured by the U.S. Army incorporates both GPR and metal-detecting capabilities, as do some handheld systems developed commercially (Daniels et al. 2005).

The main challenge with the handheld system is that the area that can be covered is not very substantial. In order to cover a wider swath, arrays of sensors have been developed. In effect, these arrays can be considered

equivalent to moving a single sensor over the same area and recording the positions for multiple passes. Both down-looking and forward-looking GPR array systems are discussed in Andrews et al. (1999). In general, the down-looking array systems require close contact to the ground, whereas the forward-looking systems involve elevated antennas in a geometry designed to permit multiple looks at both targets and clutter with the intention of improved discrimination.

Discrimination of landmines from clutter items is an even more challenging task than the UXO case because the targets themselves (specifically low-metal landmines) are closer to the electrical properties of the host soil. More subtle features, such as an air gap if present in the landmine, may aid in the discrimination process. In some cases, the presence of water is beneficial to further differentiate the electrical properties of the host material and the landmine. Similar CNR techniques described above for UXO discrimination have been used to differentiate landmines from clutter items in GPR data.

9.3. Options for interpreting data

The first six chapters of this report described some of the basic options applied in the processing of GPR data and many of those same methods are applied to the data discussed in Chapter 10. Much of the processing of GPR data has relied on reflectivity imaging to enhance and display the target response based on a scalar wave equation and does not make use of the vector information contained in the electromagnetic fields. More sophisticated algorithms that make use of the full EM character of GPR data have the potential to extract additional information, and inversion routines can be employed in attempts to reconstruct physical property distributions in the ground.

From the extensive parameters listed in Table 3, an exhaustive experimental investigation of the relative effects of each parameter is not feasible. Numerical modeling allows for the exploration of these factors for those which are most relevant without the time-consuming nature of field work. Experimental work and numerical modeling should complement each other, and insights gained from one will contribute to understanding of the other. The forward model described in O'Neill (2001) is a natural complement to the experimental results discussed in Chen et al. (2001). The collection of multicomponent GPR data would also permit the application of inversion imaging routines (van der Kruk 2003).

Analyzing these results will provide insight into which GPR frequencies are likely to be most useful in detecting typical UXO targets at the Ashland test site. This particular portion of data was chosen for gauging GPR performance as it contains a number of legitimate targets, some closely spaced UXO fragments, and an emplaced non-UXO hot rock target. Detailed target information was recorded when the targets were emplaced, and the specific information for each of the indicated targets is listed in Figures 33 and 34.

All of the Ashland data presented in Part A were acquired with the 250-MHz system. This was the lowest frequency used at the Ashland site. Because the host soil was not particularly well suited for GPR surveys, the lower frequency was a necessity to obtain any type of target responses from depths greater than 30 cm. At this point, a comparison of the three frequencies used at the Ashland test site is presented to show both the increased resolution that can be obtained from higher GPR frequencies while also illustrating the diminishing depth of penetration that accompanies the transition to higher frequencies. None of the target locations were actually marked on the ground prior to GPR data acquisition. Target locations could, however, be roughly inferred from areas where the ground had subsided after target burial. The shallow holes above target locations were filled with local soil prior to surveying in an attempt to minimize air gap effects in the data over the target locations. In order to obtain some degree of repeatability between profiles collected on separate passes with the different frequencies, nylon string was laid out between end points of the collected profiles and the cart was centered over the string on each profile collected.

10.1. 250-MHz data

Consider the image of Figure 35, which shows the profile collected using the 250-MHz system on a line which is shown in relation to UXO target locations in Figure 36. Issues in the acquisition of Robotic Total Station (RTS) positioning information along the profiles resulted in no RTS positioning information being obtained for this profile. Positions in Figure 35 are obtained from the encoder of the GPR acquisition cart rather than from RTS measurements. RTS positional information was, however, collected successfully when surveying with the 500-MHz system; since both profiles followed the same path, the position of the collected survey line relative to target locations can be inferred from the positions obtained for the 500-MHz line and illustrated in Figure 36.

No.	Type	Status	X	Y	Elevation (m)	Depth (cm)	Dip	Azimuth	Origin
175	35mm projectiles	Intact	528268.772	4670999.866	575.093	24	25	180	FLBGR



No.	Type	Status	X	Y	Elevation (m)	Depth (cm)	Dip	Azimuth	Origin
12	4.2 inch mortar	Intact	528271.853	4671000.155	574.885	56	0	45 (to line)	MT



No.	Type	Status	X	Y	Elevation (m)	Depth (cm)	Dip	Azimuth	Origin
13	4.2 inch mortar	Intact	528275.047	4671000.28	575.089	37 (top)	90	NA	MT



No.	Type	Status	X	Y	Elevation (m)	Depth (cm)	Dip	Azimuth	Origin
179	Hot rock	NA	528277.969	4671000.516	575.488	10	NA	NA	MT



Figure 33. Detailed emplacement information for targets indicated in Figure 32. Easting represented by X column, northing as Y.

No.	Type	Status	X	Y	Elevation (m)	Depth (cm)	Dip	Azimuth	Origin
53	White phosphorus frag	Intact	528280.339	4671000.683	575.451	17			MT



No.	Type	Status	X	Y	Elevation (m)	Depth (cm)	Dip	Azimuth	Origin
54	White phosphorus frag	Intact	528280.853	4671000.719	575.442	18			MT



No.	Type	Status	X	Y	Elevation (m)	Depth (cm)	Dip	Azimuth	Origin
55	White phosphorus frag	Intact	528281.542	4671000.952	575.479	17			MT



No.	Type	Status	X	Y	Elevation (m)	Depth (cm)	Dip	Azimuth	Origin
80	76mm Artillery shell	Intact	528284.042	4671000.993	575.273	44	25	180	MT



Figure 34. Additional emplacement information for targets indicated in Figure 32. Easting represented by X column, northing as Y.

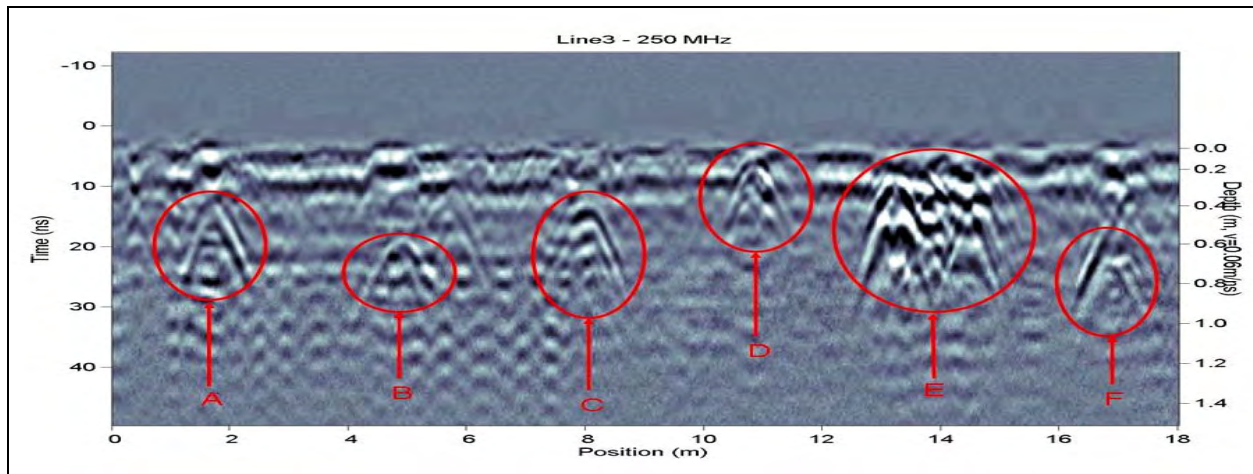


Figure 35. Target responses observed over GPR survey line indicated in Figure 32 using 250-MHz frequency system. Dewow filter was applied, an average trace was removed from the section, and an SEC gain (1, 7, 400) was applied. Approximate positions of the GPR profile relative the UXO targets are indicated in Figure 36.

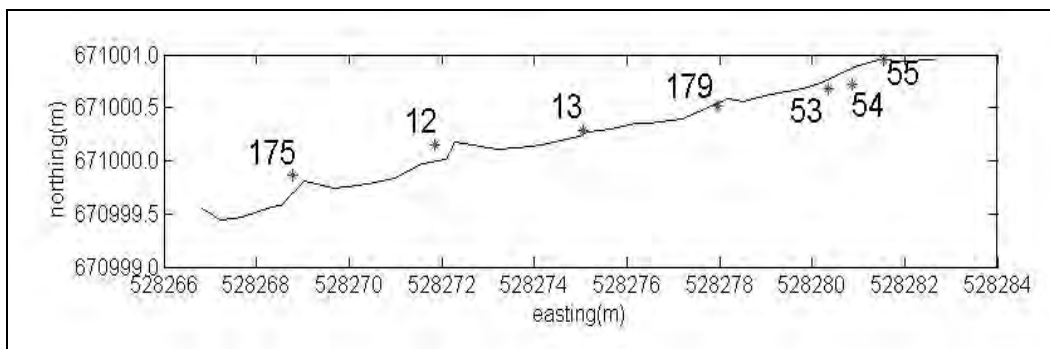


Figure 36. Approximate location of GPR survey line is represented by the solid line, while the red symbols indicate the locations of UXO targets described in Figures 32–34 and summarized in Table 4.

Targets indicated by letters A–F correspond reasonably well with the depths recorded during the placement of the targets and summarized in Table 4. Depths were calculated from the GPR data by assuming a velocity of 0.06 m/ns. This velocity was obtained by fitting a hyperbola to observed target responses. Most of the target depths determined from the GPR data in Figure 35 are in agreement with the values measured during target burial (see Table 4). Target A seems to be the only potential target with a major depth discrepancy. This could be due in part to ground subsiding and minor pooling of water above that location; the target may have been far enough off the GPR profile that while the target was still detectable, the travel time was increased over the travel time for a direct pass over the target. It is also possible that the response could be due to local clutter and not represent the UXO in question.

Table 4. Target number, type, emplaced depth and dip (measured at time of target burial) and depths of responses observed in GPR measurements interpreted as UXO targets.

Item No.	UXO Description	Emplaced Depth, m	Dip	Depth from 250-MHz GPR Measurements, m
175	35 mm projectiles	0.24	25	0.36
12	4.2 inch mortar	0.56	0	0.57
13	4.2 inch mortar	0.37	90	0.38
179	hot rock	0.10	NA	0.11
53	white phosphorus frag	0.17	NA	0.19*
54	white phosphorus frag	0.18	NA	0.19*
55	white phosphorus frag	0.17	NA	0.19*

*Indicates that individual targets were not resolvable at 250-MHz frequency, depth was taken from a combined GPR response generated by all three items.

Aside from Target A, the depths of the remaining observed GPR responses more closely match the recorded burial depths. Responses B and C in Figure 35 (Nos. 12, 13 in Figures 33, 34, 36) are both due to 4.2-in. mortar targets. Photos of the targets in place but prior to burial (see Figures 33 and 34) indicate that one of these targets (Target B, No. 12) was oriented horizontally, while the other (Target C, No. 13) was oriented vertically. In general, the horizontal target is better suited for GPR measurements as the target is more likely to span multiple survey lines. At these frequencies, the observed GPR responses appear independent of orientation. It would not be possible to infer the respective target orientations of B and C from the single survey line in Figure 35. Higher frequencies may be able to detect more subtle features and are investigated later in this report, but it may be a moot point as the penetration at higher frequencies may not be deep enough to generate tangible target responses.

The shallow response observed for Target D (No. 179), a hot rock, indicates that nonmetallic clutter items (in this case an emplaced rock) are also going to generate false alarms in GPR data. The area contained with the circle labeled E in Figure 35 is actually a combined response from multiple pieces of fragment (Nos. 53, 54, 55). This multiple target feature generates a response that is distinct from the individual targets A–D. However, individual targets in the cluster of fragments are not resolvable at the frequency employed in Figure 35 (250 MHz) but may be distinguishable at higher frequencies (500, 1000 MHz) which will be examined shortly. The final potential target circled as F in Figure 35 does not appear as

pronounced as the other circled targets as only a portion of one side of a hyperbolic response is observed. It is questionable whether or not this is an actual target response.

10.2. 500-MHz data

In Part A, all data presented were for the lowest frequency, 250 MHz. Here we look at additional information that may be available through the deployment of multiple frequencies. Consider the image of Figure 37, which illustrates the same portion of profile data displayed at 250 MHz in Figure 35, but this time the data were collected with a 500-MHz system. Targets A–C, as listed in the 250-MHz data, are no longer evident in the 500-MHz data. These deeper responses observed in the 250-MHz data were relatively weak, and it appears that the transition to the higher frequencies has come at the expense of penetration to the extent that the A–C targets of Figure 35 are no longer detectable. In the shallower targets, the improved resolution has resulted in the fragments of target area E appearing as detectable multiple targets rather than an overlapping, combined response. An additional challenge in the interpretation of the 500-MHz data compared with the 250-MHz data is the presence of banding in the data and artifacts that remain after processing data with banding present. There is a significant amount of energy between 20 and 30 ns in Figure 37.

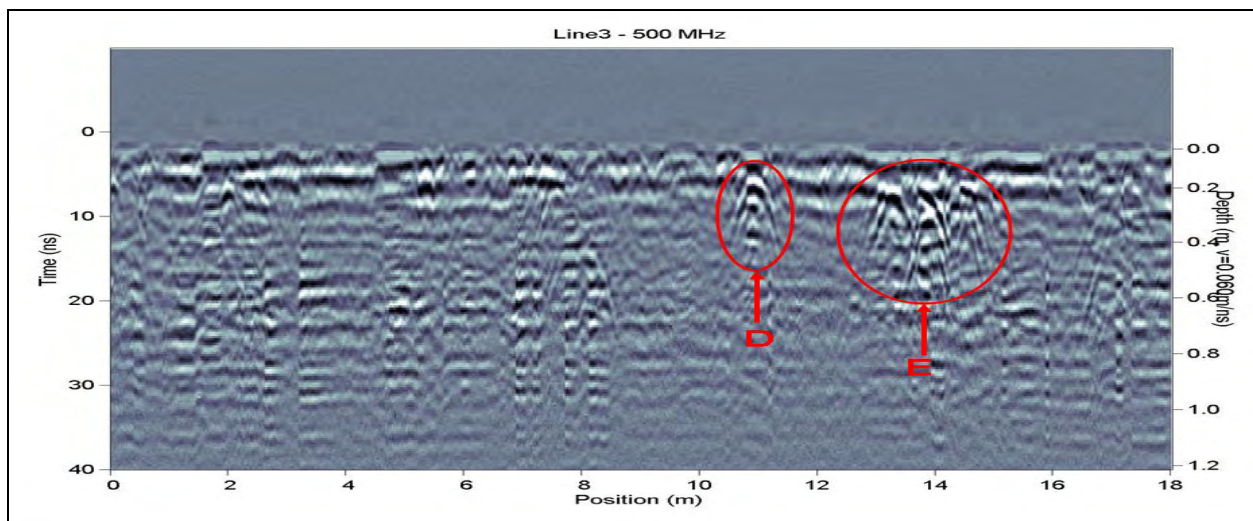


Figure 37. Target responses observed over GPR survey line indicated in Figure 32 using 500-MHz frequency system. Dewow filter applied, average trace removed, and an SEC gain (0, 3, 200) was applied. Position of the GPR profile relative to the UXO targets is indicated in Figure 36.

If energy was returned from this depth, responses would also be expected from the shallower UXO targets, especially since they were detected (targets A–C) in the lower resolution 250-MHz data of Figure 35. The responses between 20 and 30 ns in Figure 37 are actually remnants of ringing responses that were in the raw data and remained after the average trace was removed from the section. The average trace was removed to suppress flat-lying layers, particularly the direct wave and ground wave that could potentially mask shallow targets. Consider the image of Figure 38, which is the same section displayed in Figure 37 but prior to removal of the average trace. Note the strong horizontal bands in the data and the subsequent suppression of these bands after removing the average trace in Figure 37. Horizontal responses in GPR data can be attributed to legitimate horizontal targets such as geology, water table, etc.; however, the banding of Figure 38 is more typical of a resonant condition somewhere in the system, which is more often attributed to instrument design limitations or layers that partially trap the GPR signal and generate later time multiples. The horizontal responses also occur at different times between the 250-MHz and 500-MHz data, indicating that the response is probably not geologic in nature, as it would arrive at the same time assuming the feature was resolvable with both frequencies.

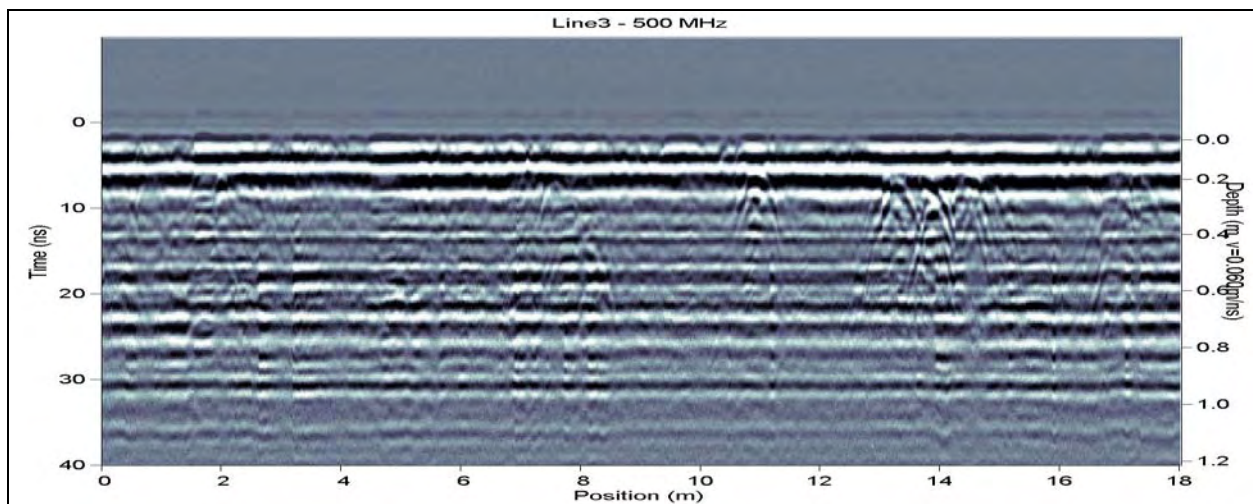


Figure 38. Target responses observed over GPR survey line indicated in Figure 32 using 500-MHz frequency system without removal of an average trace. Dewow filter and an SEC gain (0, 3, 200) were applied.

Comparison of the 500-MHz data with the lower frequency 250-MHz data indicates the classic trade-offs that are involved with selecting a GPR operating frequency. A lower frequency will penetrate further, yet a higher resolution can be achieved with higher frequencies. Generally the lower frequency is used because, as indicated in the results presented here, the

extra resolution is not particularly valuable if it comes at the expense of missing targets due to inadequate penetration. Data presented in the next section were collected over these same targets using a 1000-MHz system.

10.3. 1000-MHz data

Based on the results from the lower frequencies, it was expected that the shallower targets would be better resolved, while the deeper targets would not be detectable at 1000 MHz due to signal attenuation (Figure 39). Horizontal banding is not nearly as severe in the 1000-MHz data. The signal is attenuated strongly, and no signal penetrates deeper than approximately 12 ns (~0.4 m). This immediately rules out the possibility of detecting any of the deeper targets identified in the 250-MHz data of Figure 35. In the shallow targets that are identifiable, the results vary. As expected, the best resolution for the closely spaced clutter fragments is achieved at the highest frequency as there are three distinct targets (indicated by arrows) with target area E. The shallow rock contained in target area D is not as clear as in the lower frequency images. The tails on the hyperbolic response are no longer as well defined. Long tails on the hyperbolas mostly mean that the ground conditions were good enough to allow the signal to make it to the target and back as the target is approached and left behind. The third circle contained in Figure 39 and indicated with a question mark is a response that appears unique to the 1000-MHz data. In this case, the response originates at the surface and is most likely an area where the ground has subsided over an emplaced target and water has pooled on the surface.

10.4. Detailed grids for a single target using multiple frequencies

In order to further investigate the performance of a range of frequencies at the Ashland test site, detailed grids were collected with all three frequencies. A 2.4-m square grid was defined over a target identified on the individual profile lines. In all cases a series of perpendicular lines were collected (one set of survey lines parallel to the X axis, the other parallel to the Y axis). Lines were collected at 0.2-m spacing with a trace spacing of 2.5 cm for the 250-MHz data and at 0.1-m line spacing with 1-cm trace spacing for the 500-MHz and 1000-MHz grids. The grid is indicated in Figure 40 and additional information on the 81-mm mortar target is described in Figure 41.

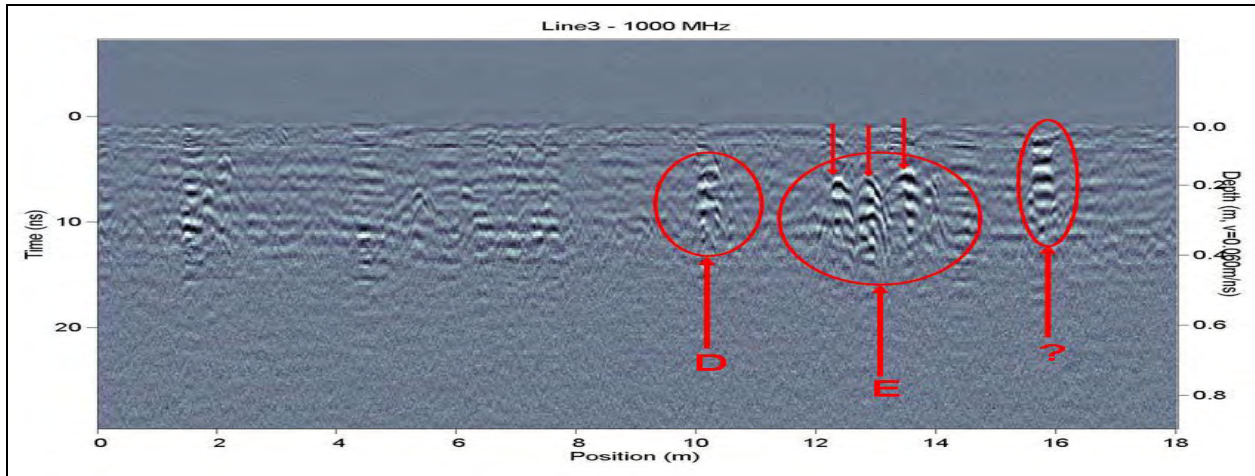


Figure 39. Target responses observed over the GPR survey line indicated in Figure 32 using a 1000-MHz frequency system. Dewow filter was applied, an average trace was removed, and SEC gains (0, 3, 300) were applied. Approximate position of the GPR profile relative the UXO targets is indicated in Figure 36.

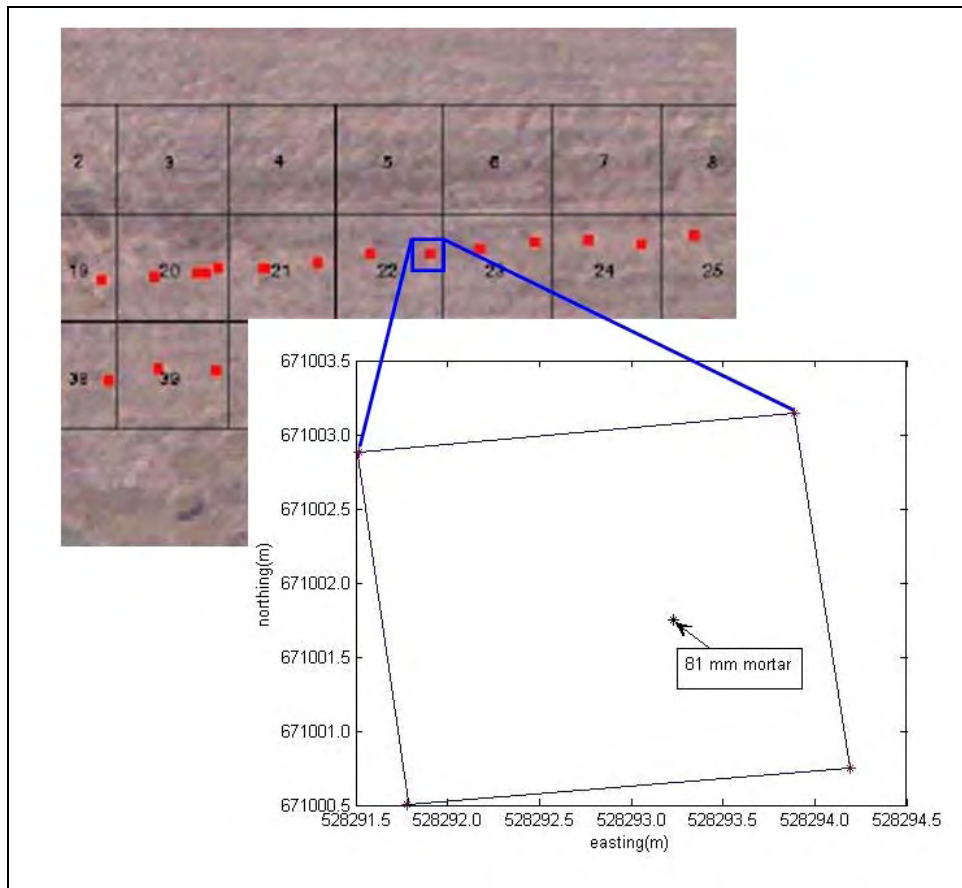


Figure 40. A detailed grid was collected over a single target with all three frequencies.



Figure 41. Single 81-mm target over which detailed grids were collected with 250-MHz, 500-MHz, and 1000-MHz GPR systems. Easting represented by X column, northing as Y.

This particular target was chosen for collecting the detailed grids, as it was shallow enough to be detectable with all three GPR frequencies. This means comparisons can be made between the relative performance of the different frequencies and some insight gained as to the types of information available from shallow targets at the Ashland site. The 3D volumes in the previous GPR paper were illustrated as animations that sliced through the volume at specific depth intervals. In the animations associated with Chapters 7–10, isosurfaces are instead displayed in a manner where all amplitudes are initially displayed, and then weaker amplitudes are progressively excluded from the image such that only the strongest amplitude responses are represented in the volume. This allows the dominant responses in the volume to be viewed.

10.4.1. 250-MHz grid data

The first data volume considered was created using the data collected with the 250-MHz system. Results from Chapter 10, Section 10.1 indicated that the best overall results were achieved with this frequency. The 250-MHz system was able to detect many of the deeper targets, which were beyond the penetration range of the 500-MHz and 1000-MHz systems. An animation of the 3D volume created for the single target scenario using the 250-MHz system was created and a single frame from that animation is depicted in Figure 42. The 250-MHz system provides a good combination of target detection with a minimal amount of clutter. In the volume created, there is a single dominant target response.

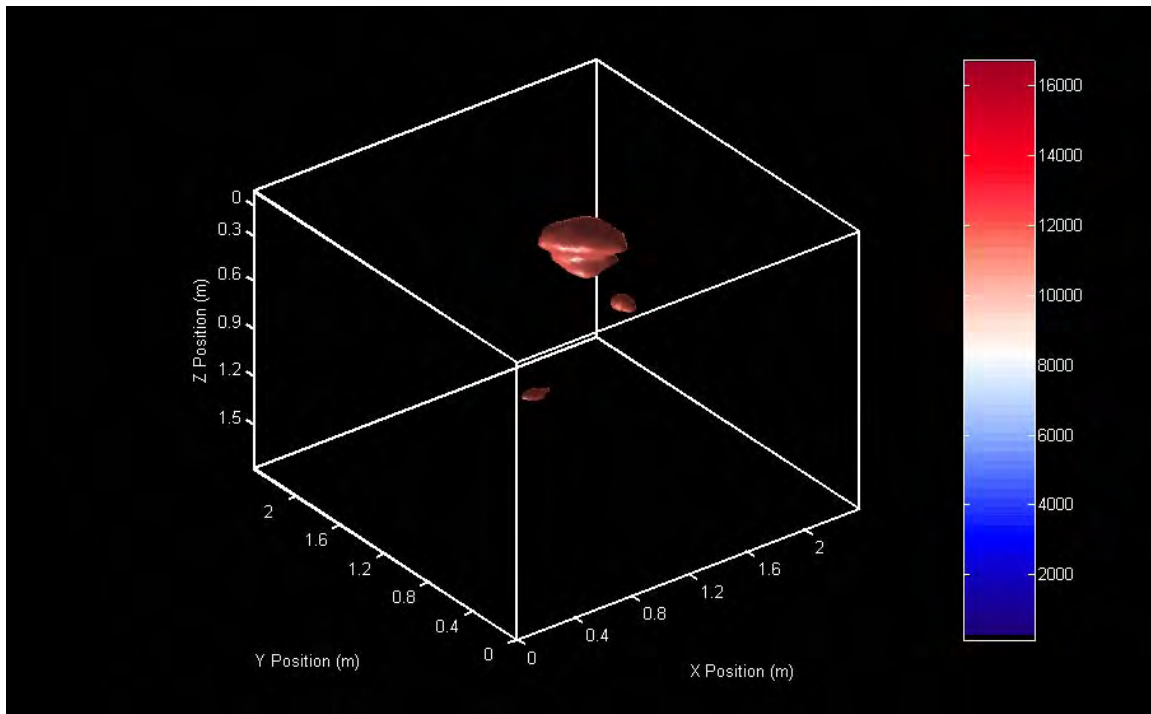


Figure 42. Isosurface view with only amplitudes greater than 70% of the maximum amplitude in the volume displayed. A single dominant response form the UXO is evident. The other two smaller responses in the current image are weaker and disappear as the amplitude threshold is increased beyond 70%. Full animation is available on the ERDC portal.

For the Ashland site, it appears that this frequency provides the best combination of deeper penetrations in a difficult environment and the ability to avoid scattering from small clutter and geology not of interest in the UXO search. It should be noted, however, that this also comes at a loss of resolution that would be available at higher frequencies. The isosurface view indicates a UXO-like target, but the frequencies used cannot resolve the target dimensions; only an indication of areas with high amplitude of the scattered response is obtained and not the actual UXO dimensions.

Consider the plan view of Figure 43, which shows the cube displayed rotated so that only the XY plane is visible and truncated at a depth of 0.25 m. The image is fuzzy and distorted, yet there are still some rough indications of the target orientation based on the shape of the high amplitude response. As Figure 41 indicates, the target is aligned with an azimuth of 180 degrees, placing it parallel to the Y axis of Figure 43.

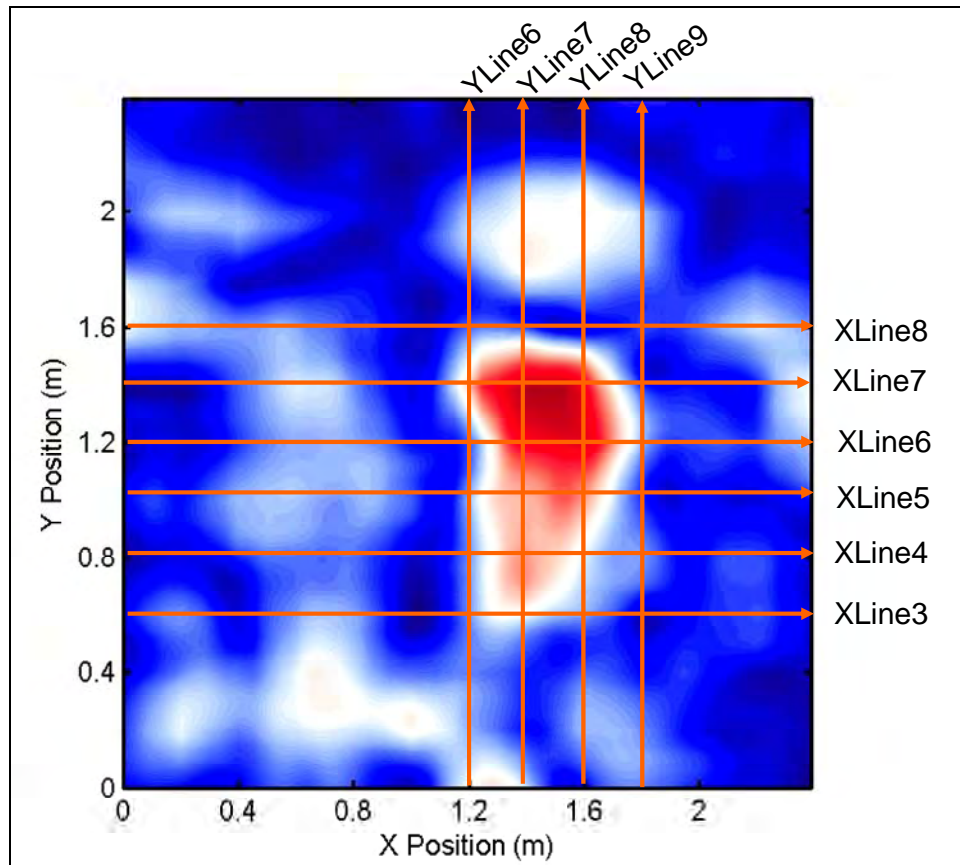


Figure 43. XY plane of volume cropped at a depth of 0.25 m. High amplitude response represents the 81-mm mortar depicted in Figure 41. Individual GPR survey lines are indicated by the orange arrows.

Rather than examining individual survey lines visually, the average amplitude versus position over a specified time interval (chosen based on the target depth of a hyperbolic response, in this case 9–15 ns) was calculated for the survey lines. The raw data had a dewow filter applied, an average trace removed, was migrated using a velocity of 0.06 m/ns, and enveloped prior to the calculation of the average amplitudes in Figures 44 and 45.

The average amplitude curves for the series of survey lines parallel to the X axis that intersect the high amplitude target area (XLine3–XLine8 of Figure 43) are indicated in Figure 44. There is a strong and identifiable single peak in the average amplitudes for the four lines crossing directly over the target (XLine4–XLine7). There are no responses on any of the lines generating similar amplitudes to the target, which could add uncertainty or ambiguity to a target designation. This very problem will be evident in the

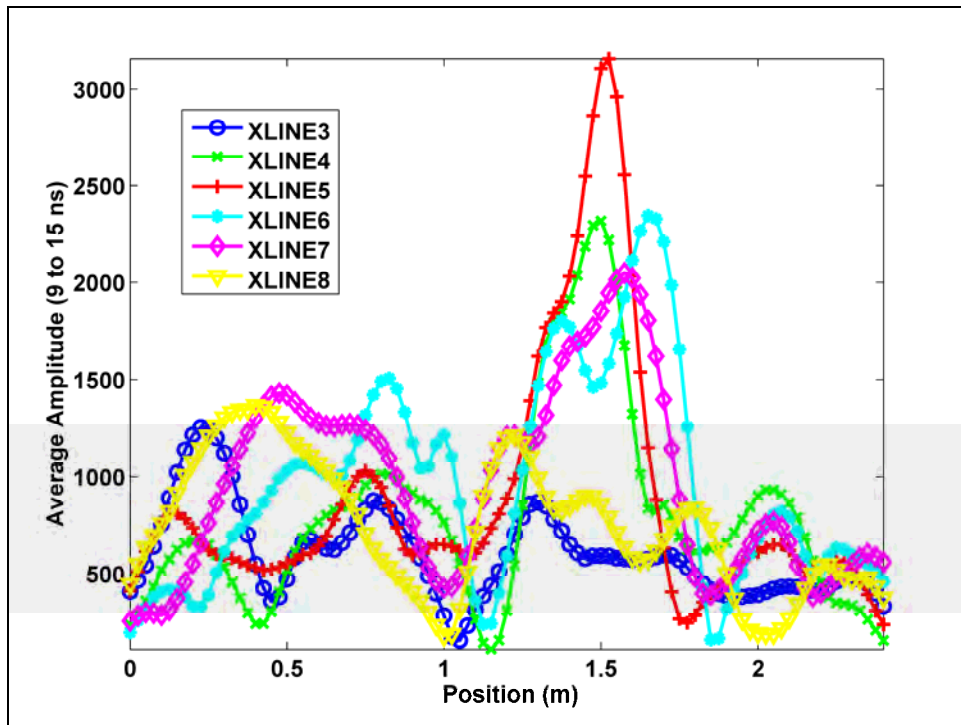


Figure 44. 250-MHz average amplitudes over the time range 9–15 ns for the XLines indicated in Figure 43. Data had dewow filter applied, an average trace removed, and was migrated ($v = 0.06$ m/ns) and enveloped.

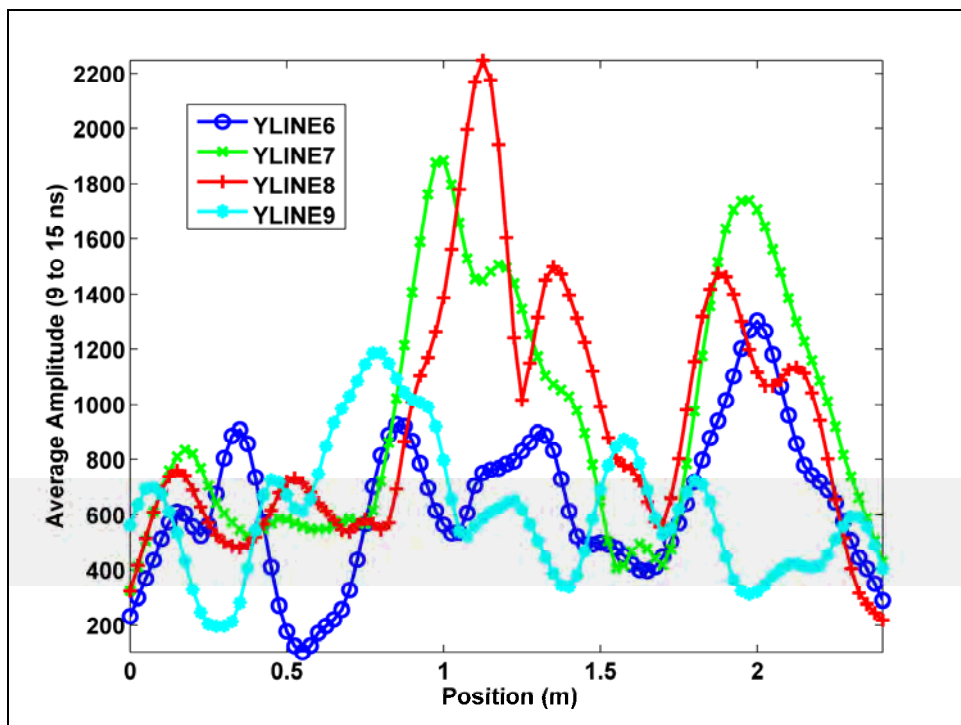


Figure 45. 250-MHz average amplitudes over the time range 9–15 ns for the YLines indicated in Figure 43. Data had dewow filter applied, an average trace removed, and was migrated ($v = 0.06$ m/ns) and enveloped.

examination of the 500-MHz data. The average amplitudes for the survey lines just beyond the high-amplitude area (XLine3, XLine8) are diminished and indicate that the respective survey lines are far enough from the target that an observable target response is minimal.

There are fewer survey lines parallel to the Y axis that intersect the high-amplitude area (YLine6–YLine9 of Figure 43), a consequence of the target oriented with its long axis parallel to the Y axis. The average amplitude plots for those survey lines are shown in Figure 45. Both lines YLine7 and YLine8 exhibit higher amplitudes, but there are two peaks rather than a single dominant peak as observed for the XLines of Figure 44. Average amplitude plots are most illustrative for a single strong response and further data are required to interpret the presence of the double peak. Some of the 500-MHz data, shown in the next section, become difficult to interpret without using knowledge gained from this 250-MHz data because there are too many similar high amplitude areas.

10.4.2. 500-MHz grid data

The 500-MHz data are not nearly as easy to interpret as the 250-MHz data. Consider for example the multitude of high-amplitude areas in the isosurface image of Figure 46. This is due in part to the higher frequency data being more susceptible to scattering from smaller scale targets. Lines were collected at 10-cm spacings for this grid, so there are twice as many lines in the 500-MHz grid as the 250-MHz grid where the line spacing was 20 cm. There is no longer a single dominant target as was the case with the 250-MHz data. From the image of Figure 46 and the associated animation, it is not feasible to select a single target using the 500-MHz data alone as there are multiple areas with similar amplitudes.

Since these data were collected over the identical grid as the 250-MHz data, further information may be elicited by examination of the survey lines, which correspond with the target locations as indicated by the 250-MHz data. Since the line spacings are 10 cm in the 500-MHz data, the nomenclature of the X and Y survey lines differs from that of the equivalent lines in the 250-MHz data. The largest responses in the average amplitude plots for the X survey lines of Figure 44 correspond to LineX8–LineX14 in the 500-MHz grid. Average amplitude plots of those responses are displayed in Figure 47, which indicates that two lines (LineX9, LineX10) exhibit substantially higher average amplitudes than the other

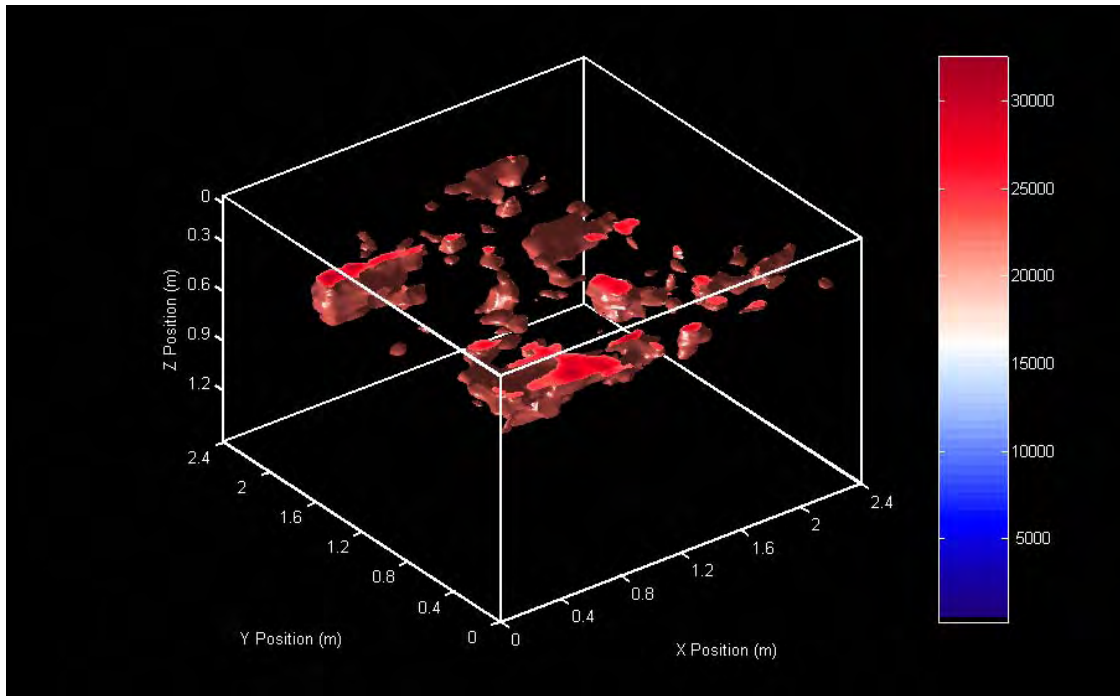


Figure 46. Isosurface view with only amplitudes greater than 70% of the maximum amplitude in the volume displayed. A single dominant response from the UXO is not evident. Scattering from smaller scale features is problematic as is system noise. Full animation is available on the ERDC portal.

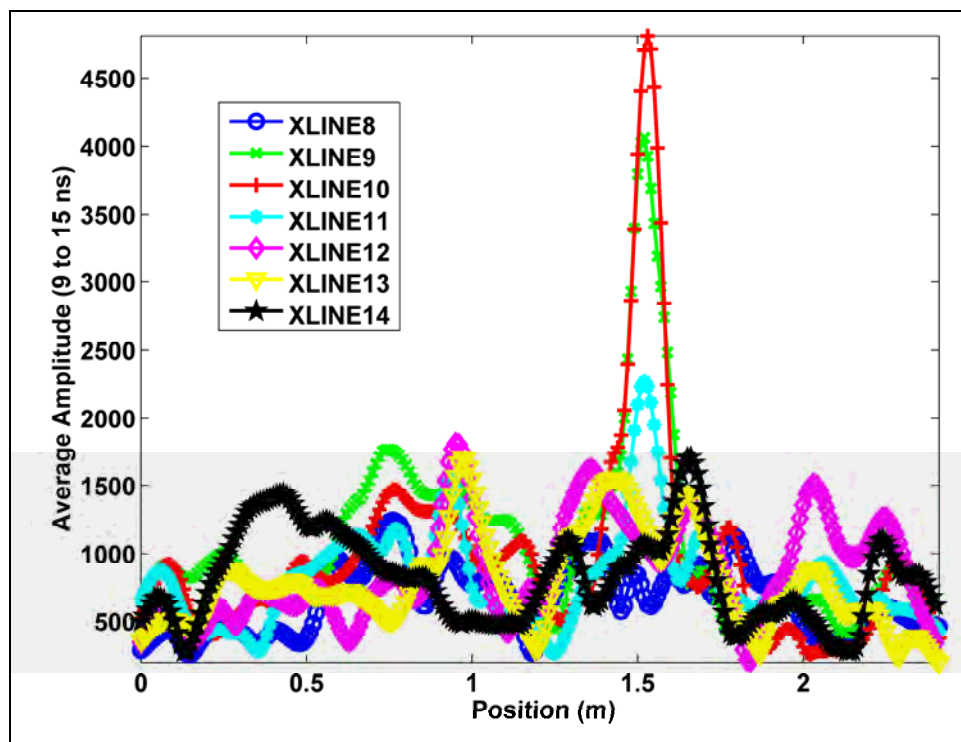


Figure 47. Average amplitudes over the time range 9–15 ns for XLines8–14 from the 500-MHz data. Data had dewow filter applied, an average trace removed, and were migrated ($v = 0.06$ m/ns) and enveloped.

lines. These high amplitudes coincide with the positions of the high-amplitude peaks in the 250-MHz average amplitude plots of Figure 44. The target is oriented in a north-south orientation, so these lines would cross the long axis of the target perpendicularly and generate a hyperbolic response, as shown in Figure 48.

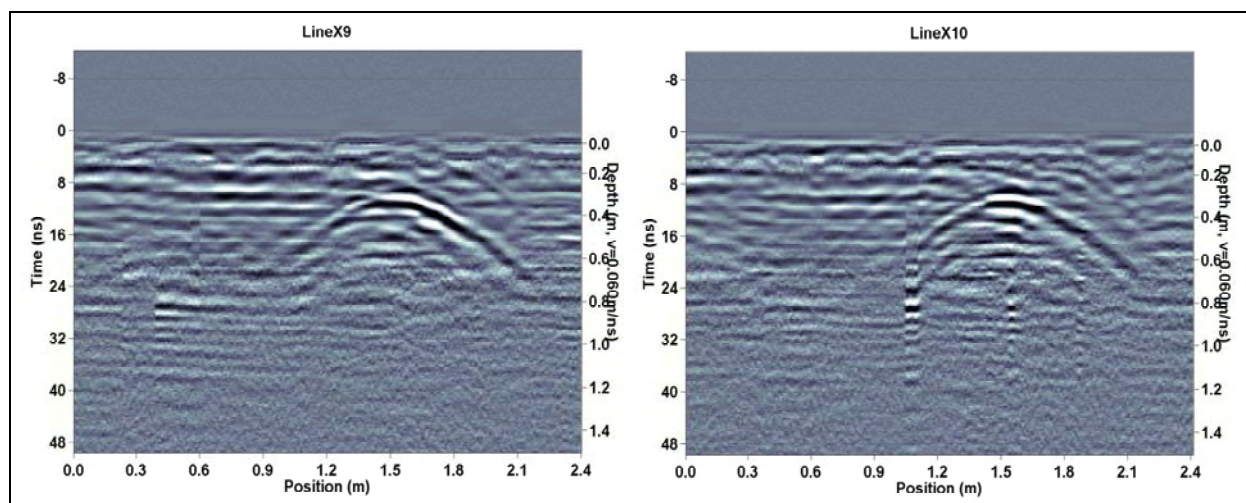


Figure 48. Survey lines XLine9 and XLine10. Both lines cross the long axis of the target perpendicularly and generate a hyperbolic response. Dewow filter was applied, an average trace was removed, and an SEC gain (1, 3.5, 400) was applied in creating the displayed images.

Applying a similar approach to the Y survey lines may help understand the target's orientation further. If the X survey lines are crossing the target perpendicularly, then the Y survey lines will be parallel to the long axis of the target. If the line spacing is such that some of the YLines run close to directly over the target, some indications of the target orientation might be obtained from variations in the travel times observed in the GPR section. Following a similar procedure discussed previously for the XLine case, the YLines in the 500-MHz data, which correspond to the strongest average amplitude peaks in the 250-MHz data of Figure 45, are YLine14–YLine16. The average amplitudes for these YLines are shown in Figure 49.

YLine15 has an average amplitude in the 9–15 ns range, much higher than that of the other two YLines. The observed response is now more of a flat reflector than a hyperbolic response as indicated by examination of the GPR section displayed in Figure 50. As the survey line runs parallel to the long direction of the target, the target remains a fixed distance from the sensor for a number of recorded traces. This differs from the perpendicular crossing of the target where the sensor approaches the target, passes directly over the target, then moves past the target, resulting

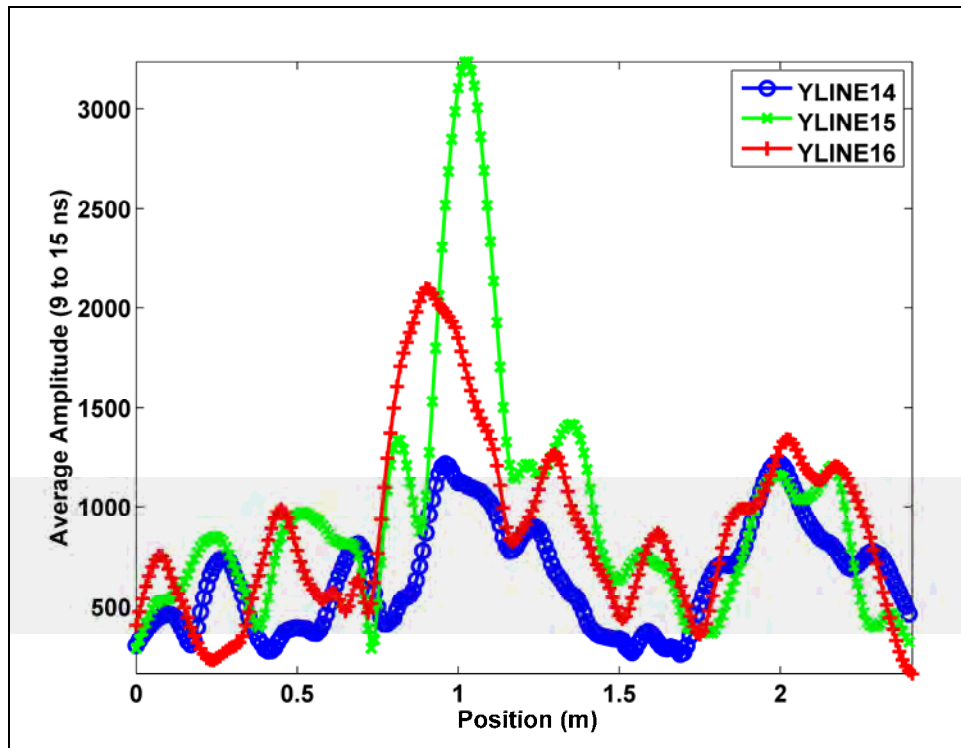


Figure 49. Average amplitudes over the time range 9–15 ns for the YLines14–16 from the 500-MHz data. Data had dewow filter applied, an average trace removed, and were migrated ($v = 0.06$ m/ns) and enveloped.

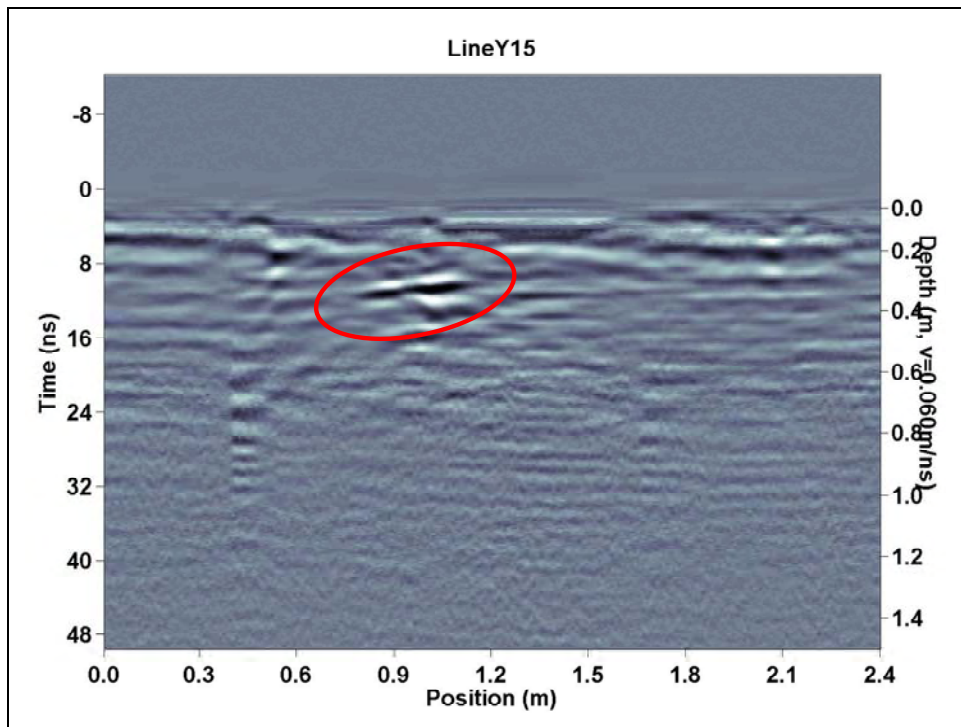


Figure 50. Survey line YLine15 runs parallel to the long axis of the target and generates a flat response rather than a hyperbolic response in the 500-MHz data. Dewow filter was applied, an average trace removed, and an SEC gain (0, 3, 200) was applied in creating the displayed image.

in increased travel times when the sensor is physically further from the target and the hyperbolic-shaped response results. For a horizontal target perfectly parallel to a flat surface, the response would appear in the data as a flat-lying reflector if a survey line were collected directly on top of the target's long axis. In this case, the target has a slight dip (see Figure 51), which is perceptible in the image of Figure 50 as the travel times are slightly longer at the left edge of the target response than they are at the right end.

10.4.3. 1000-MHz grid data

The 1000-MHz data are an improvement in terms of ease of interpretation over the 500-MHz data. Similar to the 250-MHz data of Figure 42, a strong response is observed in the vicinity of the known UXO target. At first it may seem puzzling as to why the 500-MHz data exhibits more scattering from smaller-scale objects than both the 250-MHz and 1000-MHz data. One may expect that the higher frequency should be susceptible to smaller-scale variations. Much of the strong target obscuring responses in the 500-MHz data occur at depths between 0.3 and 0.6 m, which is below the depth of penetration of the 1000-MHz data.

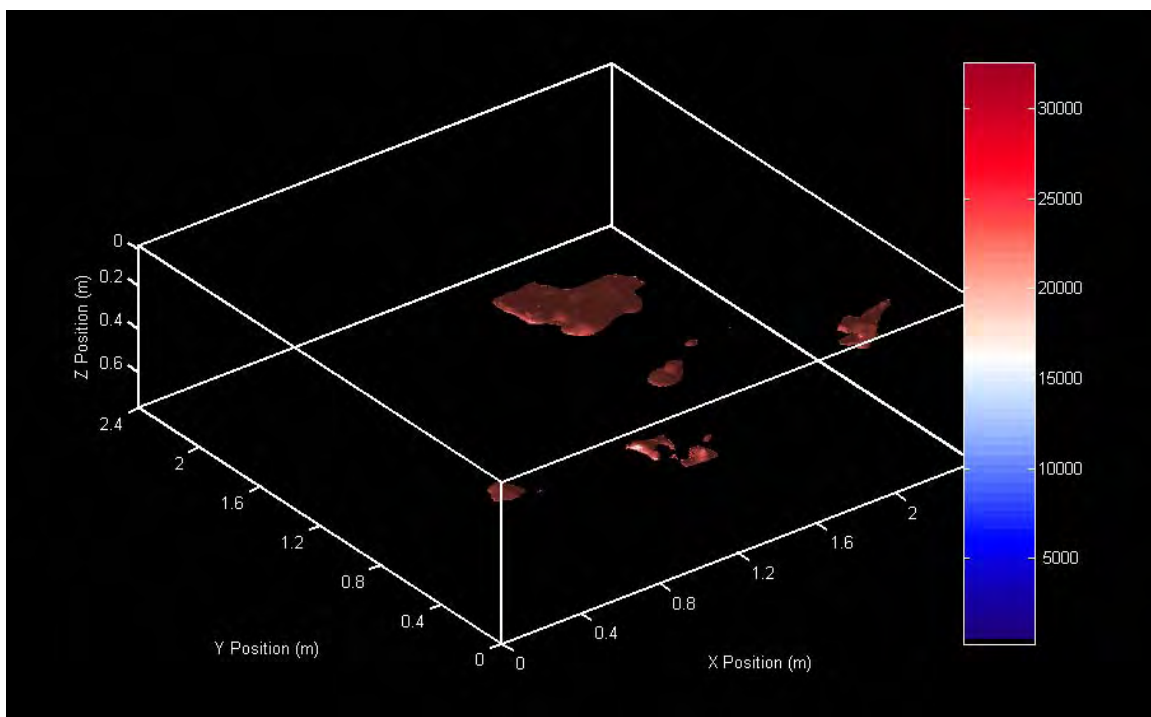


Figure 51. Isosurface view with only amplitudes greater than 70% of the maximum amplitude in the volume displayed. A single dominant response from the UXO is evident. The other smaller responses in the current image are weaker and disappear as the amplitude threshold is increased beyond 70%. Full animation is available on the ERDC portal.

The process of consulting the average amplitude plots for indications of individual survey lines was helpful in the previous case of the 500-MHz data, which contained significant clutter that masked the target. Clutter is less of an issue in the 1000-MHz data, yet a similar approach is employed to further investigate indications of target orientation that may be drawn from these high-frequency measurements. The same survey lines were chosen to extract average amplitudes as the 500-MHz data (the 1000-MHz grid was collected over the identical grid and at the same line spacings). Consider the X survey lines displayed in Figure 52. The main difference from the average amplitude plots of the 250-MHz and 500-MHz data is that the amplitude values are considerably smaller, an indication that the 1000MHz signal is very weak over the range considered (9–15 ns) and has been attenuated more severely than the lower frequencies. Even though the amplitudes are relatively weak, there is still a distinct elevated response in the 1000-MHz average amplitude plots of Figure 52, which occurs at the same position observed in the 250-MHz and 500-MHz data.

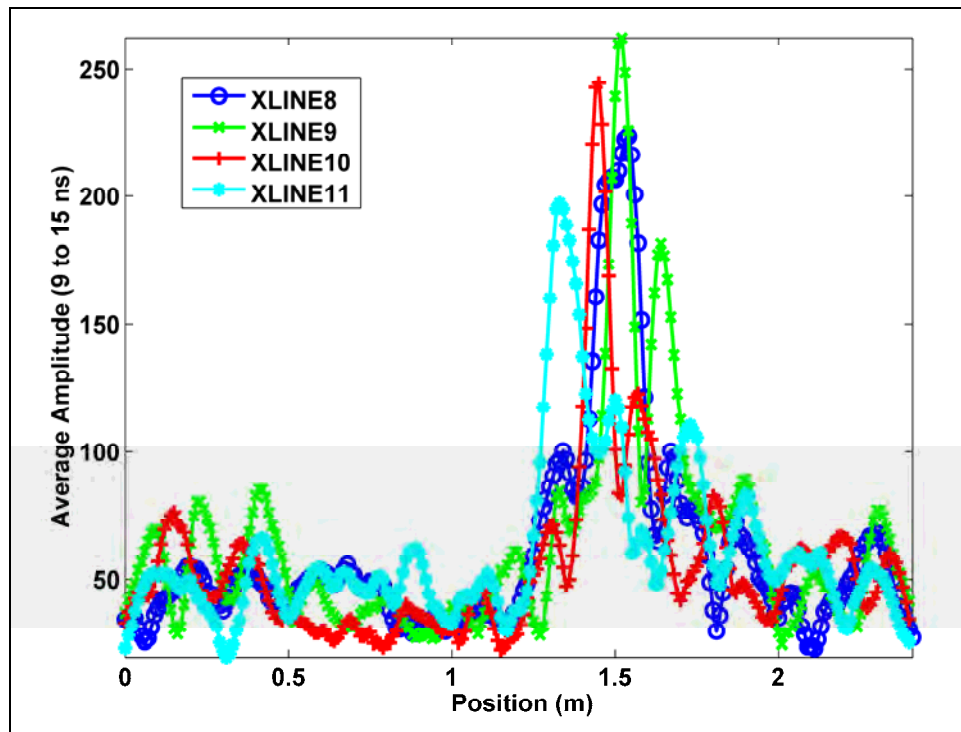


Figure 52. Average amplitudes over the time range 9–15 ns for XLines8–11 from the 1000-MHz data. Data had dewow filter applied, an average trace removed, and were migrated ($v = 0.06$ m/ns) and enveloped.

The X survey lines displayed in Figure 53 indicate that even though a detectable response is observed in all four survey lines, the characteristic tails on the hyperbolic response are not nearly as evident as those observed in the hyperbolas in the 500-MHz data (see Figure 48). The signal is more severely attenuated at the higher frequency, and consequently, the tails of the hyperbola are suppressed.

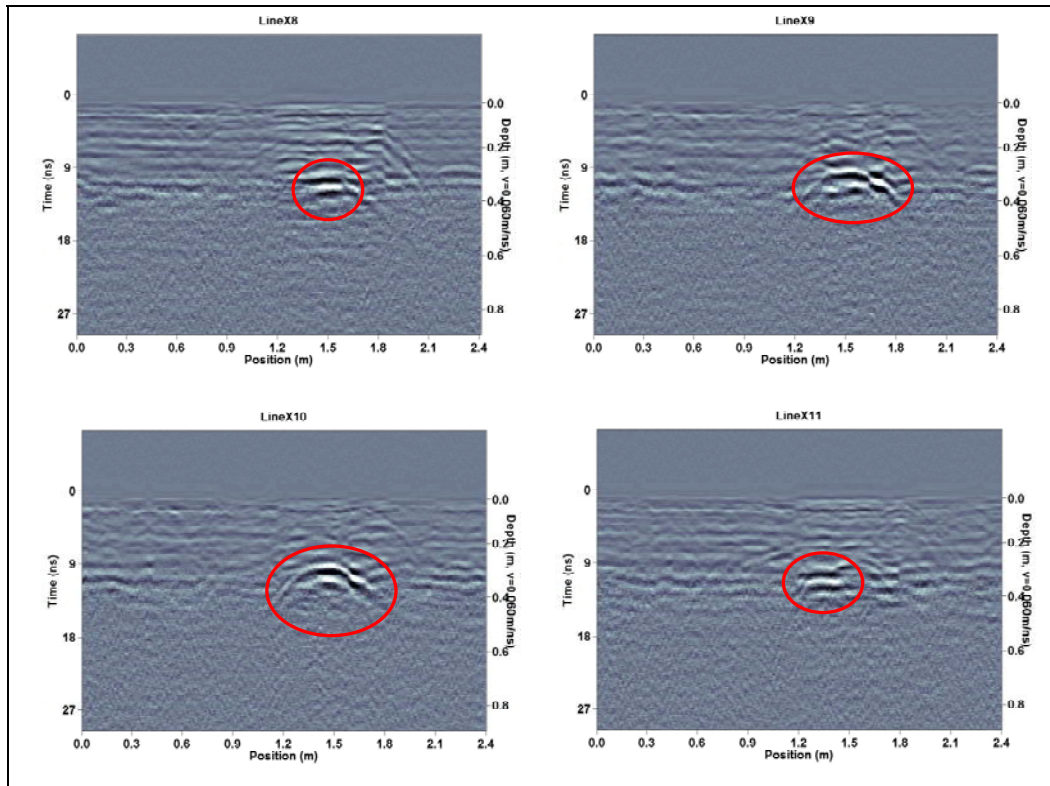


Figure 53. Survey lines XLine8 to XLine11 for the 1000-MHz data. All lines cross the long axis of the target but do not generate a hyperbolic response with pronounced tails because the signal is strongly attenuated. Dewow filter was applied, an average trace was removed, and an SEC gain (0, 3, 300) was applied in creating the displayed images.

The average amplitudes for the Y survey lines are shown in Figure 54. Results are similar to the observations in the YLines that were part of the 500-MHz data. A strong peak is observed in the average amplitude for YLine15 at a position of approximately 1 m along the line. The YLine15 section view is displayed in Figure 55 and, just as in the 500-MHz image of Figure 50, there is evidence of target dip.

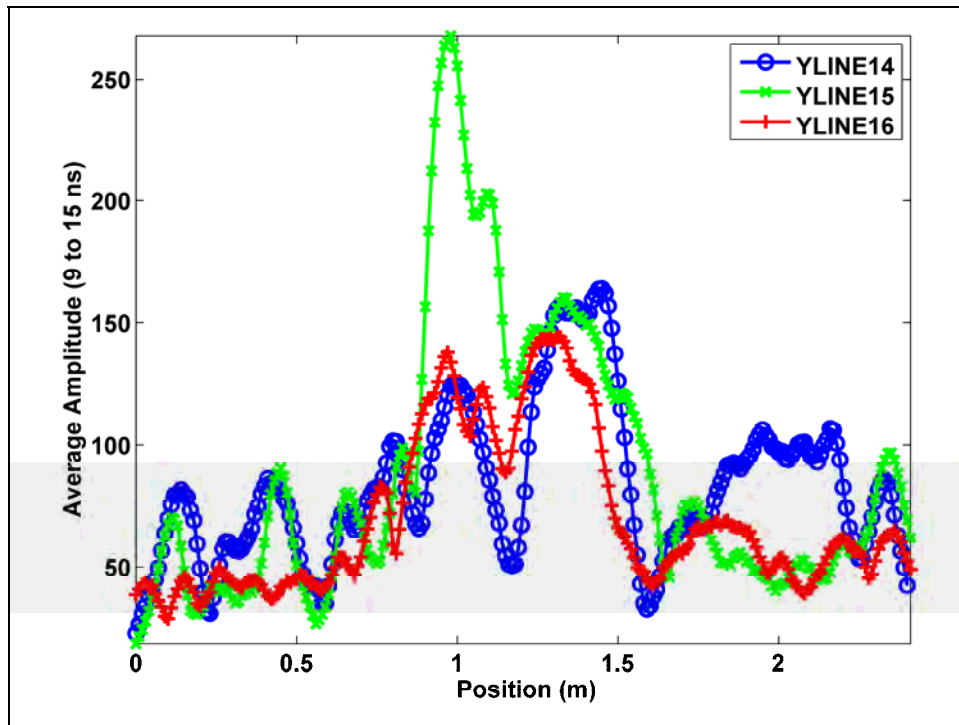


Figure 54. Average amplitudes over the time range 9–15 ns for YLines14–16 from the 1000-MHz data. Data had dewow filter applied, an average trace removed, and were migrated ($v=0.06$ m/ns) and enveloped.

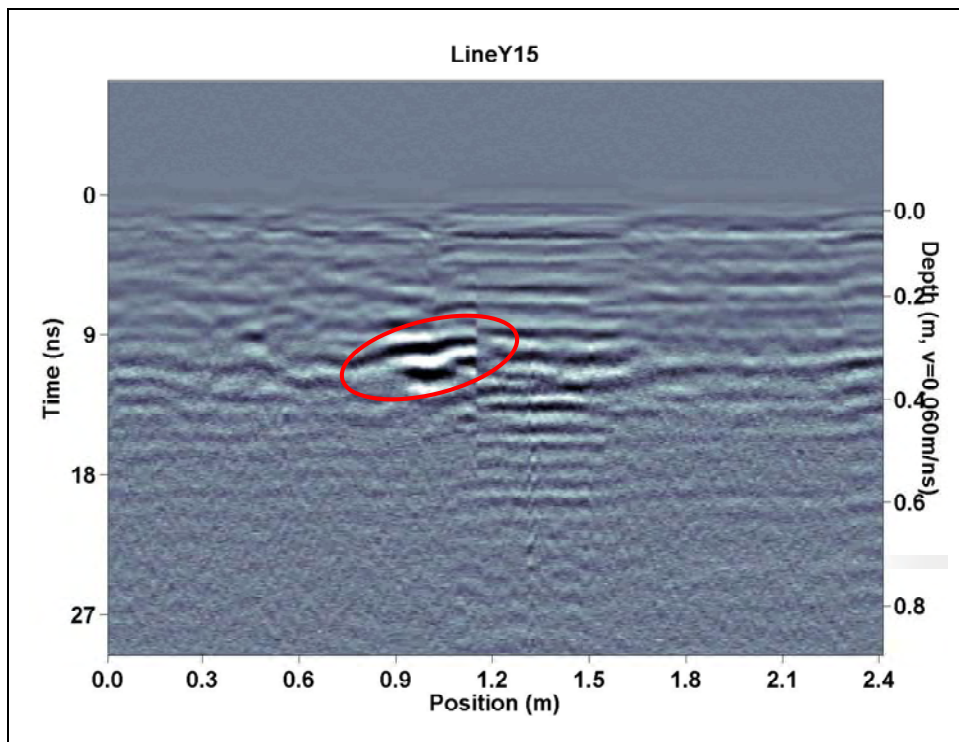


Figure 55. Survey line YLine15 in the 1000-MHz data. Dewow filter, average trace removal, and an SEC gain (0, 3, 300) were applied in creating the displayed image.

11 Conclusions and Caveats

The observations in this report are based on a single grid over a known target. Further data need to be collected over a wider variety of targets and orientations to determine the universal applicability of these methods. Many of the objects that will be emplaced in the Ashland test plot will permit further investigation and, in particular, the multi-object scenarios will permit the extension of these techniques from a single target to attempts to discriminate multiple targets in close proximity.

The examination of average amplitude plots over a specified time window was helpful in identifying where the strongest responses were observed for a series of survey lines. This choice of time window was based on a strong hyperbolic response observed in the 250-MHz data. If no such clear response exists in the data, a broader time window corresponding to the expected range of target depths needs to be considered, which increases the likelihood of responses from clutter.

Although target responses were observed for all frequencies, the most accurate target information is obtained by considering data from all three frequencies. The 250-MHz data give a clear indication of target location with minimal clutter. Clutter is problematic for the 500-MHz data and without prior knowledge of target location from the 250-MHz data, it would be impossible to differentiate clutter and target. If EM and magnetic data did not show corresponding anomalies in these areas, it might be possible to rule out some of the responses as GPR-specific clutter. However, using the location inferred from the 250-MHz data, and with the smaller line spacing used at 500-MHz, improved resolution gives a better indication of the target orientation. At 1000 MHz, results are similar to the 500-MHz data, but clutter is less problematic as the signals fade into the noise level just below the target of interest. Using a combination of all three frequencies with varying levels of clutter provides the optimal interpretation, but it also means a significant increase in the time required for data acquisition, data processing, and interpretation.

The data volume is also a function of how dense the data collected for each particular frequency needs to be. The results for both the 500-MHz and 1000-MHz frequencies were collected using a line spacing of 10 cm. This

spacing was sufficient to obtain both hyperbolic responses as the long direction of the target was crossed perpendicularly as well as flatter-lying responses when the survey line runs parallel to the long direction of the target. The line spacings cannot be increased beyond 10 cm if this type of orientation information is to be obtained. The task becomes even more daunting as the target is rotated from a horizontal towards a vertical orientation where survey lines no longer have a long axis to cross perpendicularly. Smaller UXO targets or those without a clear long axis direction will not permit use of these techniques. To this point, data had been collected as a grid of perpendicular lines. Creating 3D volume images and plan map views requires collection of closely spaced orthogonal lines in such a grid. While 3D volumes can be generated from a grid of single orientation survey lines, it will not always be possible to deduce target orientation. This method provides the best coverage of the area of interest. However, as illustrated in the test data presented here, target information can be inferred from individual survey lines extracted from the complete grid. Future work at the Ashland test plot will investigate the feasibility of determining target depth and orientation with some carefully chosen survey lines rather than a complete grid and compare the results and time required for both methods.

While these methods appear to give some useful target information, there is just not adequate resolution to make any reliable discrimination decisions on particular target types and sizes. These methods, however, show potential to be useful for estimates of depths to targets, some target geometries, and differentiating multiple targets in close proximity. Discrimination of target types may be possible with more sophisticated techniques. Complex natural resonances have been exploited to estimate linear factors from which discriminations are made (Chen et al. 2001). Discrimination between targets and some clutter can be inferred by the polarity of the reflections from the target (Arcone et al. 2000) and inversion of multi-component GPR data (van der Kruk et al. 2003) could provide estimates of conductivity and permittivity properties of the targets.

12 Strategy for Ashland Test Plot

Because most UXO targets contain significant amounts of ferrous metal, EM and magnetic measurements have become the standard detection methods. GPR is not likely to compete with these sensors as a primary detection method, largely because of its susceptibility to false positives. The intended use of GPR is rather in a cued-interrogation mode. In order to achieve adequate penetration to generate returns from UXO targets, lower GPR frequencies are necessary. These lower frequencies are less susceptible to small-scale variations and soil inhomogeneities that appear as clutter in GPR data acquired with higher frequencies. Tests on the Ashland test plot have demonstrated the ability to obtain accurate estimates of depth and some indications of orientation for targets with an elongated axis. Additional data sets and experimentation are required to investigate this further.

The tendency when planning GPR surveys is to attempt to achieve the highest possible resolution. Increased resolution is typically sought by transitioning to higher GPR frequencies. The resolution gained by the use of higher frequencies is often more than offset by the loss of the penetration that accompanies the use of higher frequencies. For the majority of UXO targets, items can be expected to be buried within the first meter. In many soil types, the use of higher GPR frequencies (>1 GHz) results in a severely attenuated signal that will not adequately penetrate the host soil. The data collected at the Ashland test plot indicate that lower GPR frequencies hold more promise for cued interrogation of UXO objects.

It is not practical to survey an entire area at the line spacings that the Ashland results indicate are required. With a single-channel system, such as the one used at the Ashland site, it is a question of data acquisition being far too time-consuming to acquire sufficient data for complete coverage with GPR measurements. While there are array-based systems that make the coverage of large areas a more realistic possibility, there are two main issues with this approach in a practical sense. Many of the array-based systems are designed for landmine detection where targets are expected to be smaller, possibly nonmetallic, and shallower than many UXO scenarios. This leads to systems that employ higher frequencies to achieve greater resolution at the cost of penetration, which will not be

adequate for detecting deeper UXO in many types of soil. The array-based systems provide a greater coverage; however, the instrumentation, which incorporates multiple array elements, is by necessity much larger than the single-channel system and may be difficult to deploy in realistic field conditions with uneven ground conditions and obstacles. There are also extreme field scenarios where even a single-channel cart system cannot be practically deployed and a handheld device may be more practical. If deeper penetration is required than handheld system capabilities, a traditional bistatic GPR system may be required to methodically step along in extreme field situations.

Even more troublesome than the accessibility issue for array-based systems is the issue of false alarms. Of all instrumentation applied to the UXO problem, GPR is uniquely sensitive to false alarms, as responses will be observed in the data not only for UXO, but also for tree roots, large rocks, soil inhomogeneities, and any other targets of UXO-like dimensions that differ electrically from the host soils. The array-based system will be more efficient at collecting large volumes of data to adequately cover the survey area, but unfortunately this could also mean large numbers of false alarms to sift through in the interpretation stage. False alarms from non-UXO clutter will certainly be location-dependent and be more of an issue in some areas than others. One method of addressing GPR-specific clutter (i.e., differentiating nonmetallic clutter) would be to incorporate the data obtained from EM and magnetic surveys over the same areas. Since these methods are not susceptible to the same nonmetallic clutter as GPR methods, many GPR false positives may be ruled out as potential UXO targets via this approach. Some array-based GPR sensors also incorporate EMI sensors (Oristaglio 2005).

For all of the above reasons, the authors intend to use GPR in a cued-interrogation mode. Initial EM and magnetic surveys will be performed over the entire survey areas, and potential targets will be identified from these surveys. GPR will be deployed in areas where there is some ambiguity in the target response from the previous two methods. For example, GPR will be used to determine if an observed response is the result of a single target or closely spaced multiple targets, which may be contributing a combined response in EM/magnetic data that is really the superposition of multiple target responses. In soils that are favorable for GPR work, it is also possible that GPR may be able to penetrate and detect targets at depths beyond the limits of EM measurements. The Ashland test plot was

designed with many of the above ideas and scenarios in mind and will provide a unique opportunity to test and refine a multi-sensor measurement procedure for extracting maximum target information.

References

- Andrews, A., J. Ralston, and M. Tuley, M. 1999. *Research of ground penetrating radar for detection of mines and unexploded ordnance: Current status and research strategy*. Institute for Defense Analyses, D-2416, Log: H 99-002922.
- Annan, A. P. 2005. *Ground penetrating radar principles, procedures and operations*. Sensors & Software Inc. Short Course Notes.
- Annan, A. P., and S. W. Cosway. 1992. Simplified GPR beam model for survey design. *Extended abstract of 62nd Annual International Meeting of the Society of Exploration Geophysicists, New Orleans, 1992*.
- Arcone, S. A., K. O'Neill, A. J. Delaney, and P. V. Sellmann. 2000. UXO detection at Jefferson Proving Ground using ground-penetrating radar. ERDC/CRREL TR-00-5. Hanover, NH: U.S. Army Engineer Research and Development Center.
- Baum, C. E. 1999. *Detection and identification of visually obscured targets*. Taylor and Francis.
- Birken, R., D. Miller, M. Burns, P. Albats, R. Casadonte, R. Deming, T. DeRubeis, T. Hansen, and M. Oristaglio. 2002. Efficient large-scale underground utility mapping in New York City using a multi-channel ground-penetrating imaging radar system. *Proceedings, SPIE* 4758:186–191.
- Chen, C. C., and L. Peters. 1997. Buried unexploded ordnance identification via complex natural resonances. In *IEEE Transactions on Antennas and Propagation*, 42:1645–1654.
- Chen, C. C., M. B. Higgins, K. O'Neill, and R. Detsch. 2001. Ultrawide-bandwidth fully-polarimetric ground penetrating radar classification of subsurface unexploded ordnance. *IEEE Transactions on Geoscience and Remote Sensing*, 39:1221–1230.
- Cross, G. 1999. *Soil properties and GPR detection of landmines - A basis for forecasting and evaluation of GPR performance*. Contract Report: DRES CR 2000-091.
- Daniels, D. J., R. Amin, J. Dittmer, P. Curtis, and N. Hunt. 2005. MINETECT production development. In *Proceedings, SPIE, Detection and Remediation Technologies for Mines and Minelike Targets X*, March 28-April 1, 2005., 5794.
- Daniels, D. J., D. J. Gunton, and H. F. Scott. 1988. Introduction to subsurface radar. In *IEEE Proceedings* 135(4):278–320.
- Daniels, J. J., L. Wielopolski, S. Radzevicius, and J. Bookshar. 2003. 3D GPR polarization analysis for imaging complex objects. In *Proceedings. SAGEEP*, San Antonio, TX, February 2003. 686–697.

- Doolittle, J. A., F. E. Minzenmayer, S. W. Waltman, and S. W. Banham. 2002. Ground-penetrating radar soil suitability map of the conterminous United States, Ninth International Conference on Ground Penetrating Radar, ed. S. K. Koppenjan and H. Lee. In *Proceedings, SPIE 4758*:7–12.
- Giannopoulos, A. 1997. The investigation of transmission-line matrix and finite-difference time-domain methods for the forward problem of ground probing radar. Ph D diss., Department of Electronics, University of York, UK.
- Olhoeft, G. R. 1998. Electrical, magnetic and geometric properties that determine ground penetrating radar performance. In *Proceedings of GPR'98, Seventh International Conference on Ground Penetrating Radar, May 27–30, 1998*. Lawrence, KS: The University of Kansas, 177–182.
- O'Neill, K. 2001. Discrimination of UXO in soil using broadband polarimetric GPR backscatter. In *IEEE Transactions on Geoscience and Remote Sensing*, 39:356–367.
- Oristaglio, M., R. Birken, T. Hansen, R. Deming, S. MacIntosh, and Q. Zhu. 2005. Efficient large-scale utility mapping with radar and induction arrays. In *Proceedings, SAGEEP'05, April 3–7, 2005, Atlanta, GA*, 31–43.
- Sensors & Software Ltd. 2003. *Evaluation of hand-held GPR System for AP landmine detection*. Final report. Contract Report: W7702-00R801/001/EDM.
- Sky Research, Inc. 2005. *UXO standardized test site: Soil sampling program*. Ashland, OR. Unpublished Report.
- Sun, K., K. O'Neil, C. C. Chen, H. Young, F. Shubitidze, I. Shamatava, and K. Paulse. 2005. Highly contaminated UXO sites: Combination of GPR and EMI for discrimination of clustered scatterers. In *Proceedings, SAGEEP'05, April 3–7, 2005, Atlanta, GA*, 1156–1165.
- van der Kruk, J., C. P. A. Wapenaar, J. T. Fokkema, and P. M. van den Berg. 2003. Three-dimensional imaging of multi component ground-penetrating radar data. *Geophysics* 68(4):1241–1254.
- Wright, D., C. Oden, M. Powers, C. Moulton, S. R. Hutton, J. Kibler, and G. Olhoeft. 2005. A ground penetrating radar system for high loss environments. In *Proceedings, SAGEEP'05, April 3–7, 2005, Atlanta, GA*, 1156–1165.

REPORT DOCUMENTATION PAGE

Form Approved
OMB No. 0704-0188

Public reporting burden for this collection of information is estimated to average 1 hour per response, including the time for reviewing instructions, searching existing data sources, gathering and maintaining the data needed, and completing and reviewing this collection of information. Send comments regarding this burden estimate or any other aspect of this collection of information, including suggestions for reducing this burden to Department of Defense, Washington Headquarters Services, Directorate for Information Operations and Reports (0704-0188), 1215 Jefferson Davis Highway, Suite 1204, Arlington, VA 22202-4302. Respondents should be aware that notwithstanding any other provision of law, no person shall be subject to any penalty for failing to comply with a collection of information if it does not display a currently valid OMB control number. **PLEASE DO NOT RETURN YOUR FORM TO THE ABOVE ADDRESS.**

1. REPORT DATE (DD-MM-YYYY) September 2008		2. REPORT TYPE Report 2 of 9		3. DATES COVERED (From - To)	
4. TITLE AND SUBTITLE UXO Characterization: Comparing Cued Surveying to Standard Detection and Discrimination Approaches: Report 2 of 9 – Ground Penetrating Radar for Unexploded Ordnance Characterization; Fundamentals				5a. CONTRACT NUMBER	
				5b. GRANT NUMBER	
				5c. PROGRAM ELEMENT NUMBER	
6. AUTHOR(S) Stephen D. Billings and Kevin Kingdon				5d. PROJECT NUMBER W912HZ-04-C-0039	
				5e. TASK NUMBER	
				5f. WORK UNIT NUMBER	
7. PERFORMING ORGANIZATION NAME(S) AND ADDRESS(ES) Sky Research, Inc. 445 Dead Indian Memorial Road Ashland, OR 97520-9706				8. PERFORMING ORGANIZATION REPORT ERDC/EL TR-08-33	
9. SPONSORING / MONITORING AGENCY NAME(S) AND ADDRESS(ES) Headquarters, U.S. Army Corps of Engineers Washington, DC 20314-1000 U.S. Army Engineer Research and Development Center Environmental Laboratory 3909 Halls Ferry Road, Vicksburg, MS 39180-6199				10. SPONSOR/MONITOR'S ACRONYM(S)	
				11. SPONSOR/MONITOR'S REPORT NUMBER(S)	
12. DISTRIBUTION / AVAILABILITY STATEMENT Approved for public release; distribution is unlimited.					
13. SUPPLEMENTARY NOTES					
14. ABSTRACT The objective of project W912HZ-04-C-0039, "UXO Characterization: Comparison of Cued Surveying to Standard Detection and Standard Discrimination Approaches," was to research, develop, optimize, and evaluate the efficiencies of different modes of unexploded ordnance (UXO) characterization and remediation as a function of the density of UXO and associated clutter. This report, one of nine written for the project, focused on an overview of the fundamentals of ground penetrating radar (GPR) with specific emphasis on the detection and discrimination potential of the technology. Part A (Chapters 1–6) includes a brief overview of general GPR concepts, data, and survey procedures. Factors that determine the site-specific applicability of GPR are identified and existing tools for assessing the applicability of GPR to a particular site are reviewed. Part B (Chapters 7–10) describes the types of GPR instrumentation and reviews previous UXO and landmine specific work involving GPR. In both Parts A and B, GPR concepts introduced are discussed and illustrated with data acquired at the Sky Research Ashland (Oregon) test plot using commercial off the shelf (COTS) GPR sensors. In Part A, single GPR profiles over a row of emplaced UXO targets acquired using a single-channel 250-megahertz (MHz) COTS GPR system are displayed. Further examples illustrate how multiple survey lines collected in a grid can be combined to create two-dimensional (2D) and three-dimensional (3D) visualizations of the subsurface and the targets contained therein. In Part B, examination of GPR data collected at the Ashland test site continues, but in this case, focuses on a range of frequencies (250, 500, 1000 MHz) and the comparative information that can be obtained from these respective frequencies. Discussion of the results observed from these initial measurements, limitations of the methods used, and a proposal for use of GPR in a cued-interrogation mode along with the types of information that are obtainable are presented.					
15. SUBJECT TERMS					
EMI sensors		Ground penetrating radar		Unexploded ordnance (UXO)	
Frequency-domain electromagnetic induction (FEM)		Time-domain electromagnetic induction (TEM)		UXO discrimination	
		Total-field magnetics			
16. SECURITY CLASSIFICATION OF:			17. LIMITATION OF ABSTRACT	18. NUMBER OF PAGES	19a. NAME OF RESPONSIBLE PERSON
a. REPORT UNCLASSIFIED	b. ABSTRACT UNCLASSIFIED	c. THIS PAGE UNCLASSIFIED			99